Elucidating the Impact of Inhaled Micro-, Nanoplastics from Surgical Face Masks *in vitro*

MSc by Research: Medical and Healthcare Studies

2023

Lewis James Hodgetts

[redacted]

Prof Martin J. D. Clift, Dr Stephanie Wright, Prof Shareen H. Doak

I, Lewis James Hodgetts, declare that:

This thesis has not been previously accepted in substance for any degree and is not being concurrently submitted in candidature for any degree.

Signed (Candidate) Lewis James Hodgetts..... on 04/07/2024.

Statement 1

This thesis is the result of my own independent investigations, except where otherwise stated and that other sources are acknowledged by footnotes giving explicit references and a detailed bibliography appended.

Signed (Candidate) Lewis James Hodgetts..... on 04/07/2024.

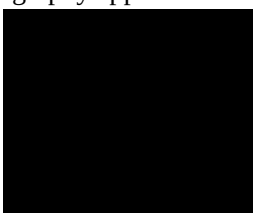

Statement 2

I hereby give consent for my thesis, if accepted, to be available for photocopying and for inter-library loan, and for the title and summary to be made available to outside organisations, from 00:00 on the 1st July 2025.

Signed (Candidate) Lewis James Hodgetts..... on 04/07/2024.

Acknowledgements

Swansea University – *in vitro* Toxicology Group, UK

Martin J.D. Clift

Shareen H. Doak

Kirsty Meldrum

Stephen J. Evans

Michael J. Burgum

Gillian E. Conway

Demi Pritchard

Ryan Bigham

Joshua W.P. Bateman

Katie Marchant

Olivia Whittle-Wright

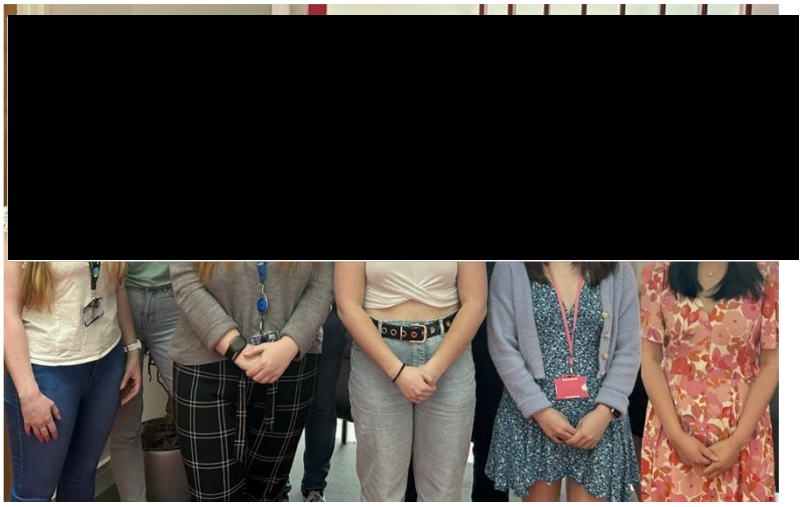

Swansea University – *in vitro* Toxicology Group

Imperial College London – Environmental Research Group, UK

Stephanie Wright

Joseph Levermore

Eric Auyang

National Research Centre for the Working Environment, Denmark

Ulla Vogel

Abstract

The use of surgical face masks is commonplace throughout medical and occupational settings, but their use was extended to the public during the COVID-19 pandemic, resulting in an influx of manufacture and wastage. These masks are predominantly synthesised from polypropylene (PP), but the complete material list is unknown, and their exact composition varies between suppliers. These single-use masks are known to shed micro,-nanoplastic (MNP) debris directly into the respiratory system, and into the environment upon improper disposal. Plastics in the environment degrade into MNPs over time *via* several processes, eventually gaining the potential to become airborne. The scenarios of how these mask MNPs could be inhaled, were represented in this project by the use of the innermost layer of mask only (white), and the indirect environmental route; an amalgam of all three mask layers (blue). Despite much focus on the environmental impact of MNPs, the effects these particles could have to human health following inhalation, is largely unknown. Therefore, the aim of this project was to determine the toxicity of PP MNPs, and MNPs derived from face masks representative of two different inhalation exposure scenarios, using an advanced *in vitro* approach. All synthesized MNPs used a top-down approach; the cryogenic milling of commercial PP powder, 55-75 μm in diameter (purchased from Goonvean Fibres Ltd.), into particles ≤5 μm in diameter. Surgical masks MNPs were synthesized *via* repeated cryotome slicing. All MNP were characterised *via* pyrolysis-GC-MS, dynamic light scattering and zeta potential, and further by SEM and STEM-EDX following aerosolisation. NCI-H441 type-II alveolar epithelial cells were cultured at the air-liquid interface, and were exposed to 0.5, 1.0 or 2.0 μg/cm^2 of each MNP type for 24 hours. Carbon black (Printex 90) was used as positive particle control. Endpoint analyses of cell death (trypan blue exclusion), barrier integrity (dextran blue), pro-inflammatory response (IL-1β/IL-6/IL-8) and genotoxicity (mononucleate micronucleus) were conducted, alongside Confocal LSM microscopy. STEM-EDX presented each MNP sample to consist predominantly of sodium and chlorine, with lesser expression of carbon, oxygen and titanium. Pyrolysis-GC-MS confirmed dominance of PP content in the tested MNPs, alongside the presence of additives, although this requires further investigation. Both mask MNPs presented significant concentration-dependent increases to IL-8 production and mononucleated micronucleus formation, peaking at 1.0 μg/cm^2, but then decreasing at 2.0 μg/cm^2 across all respirable MNP samples. Respirable PP MNPs also displayed similar trends to the mask MNPs, but these were not statistically significant findings. Current data therefore suggests that inhalation of MNPs do have the potential to produce hazardous responses to alveolar models *in vitro*. Future developments should improve on the realism of the model by the incorporation of immune cell co-culturing. To improve endpoint analysis, the introduction of oxidative stress evaluation and gene expression is necessary, in addition to the validation of a suitable genotoxic assay protocol for NCI-H441 cells.

Contents

List of Figures

List of Tables

Abbreviations

Abbreviation	Meaning
MNPs	Micro-, Nanoplastics
PM	Particulate Matter
PP	Polypropylene
ENPs	Engineered Nanomaterials
CH_4	Methane
CO_2	Carbon dioxide
N_2O	Dinitrogen oxide
NOx	Nitrous oxide(s)
NH_3	Ammonia
SO_2	Sulphur dioxide
NMVOCs	Non-Methane Volatile Organic Compounds
DAQI	Daily Air Quality Index
O_3	Ozone
COMEAP	Committee on the Medical Effects of Air Pollutants
GSS	Gilbert Skill Score
FPA-µFTIR	Engineered Nanomaterials
CNT	Carbon Nanotubes
SWCNT	Single-walled Carbon Nanotubes
MWCNT	Multi-Walled Carbon Nanotubes
SWCNH	Single-walled Carbon Nanohorns
TiO_2	Titanium dioxide
WIPO	World Intellectual Property Organisation
ISO	International Organisation for Standardisation
ASTM	American Society for Testing and Chemicals
NIOSH	National Institute for Occupational Safety and Health
SOP	Standard Operating Procedure
FFP2	Filtering Facepiece 2
PPE	Personal Protective Equipment
pO_2	Partial Pressure of Oxygen
pCO_2	Partial Pressure of Carbon dioxide
TCA Cycle	Tricarboxylic acid Cycle
ATP	Adenosine triphosphate
ALI	Air-Liquid Interface
PS	Polystyrene
Vitrocell	Vitrocell Cloud 12 Aerosol Exposure System
RPMI	Roswell Park Memorial Institute
PBS	Phosphate Buffered Saline
P/S	Penicillin/Streptomycin
EDTA	Ethylenediaminetetraacetic Acid
FBS	Foetal Bovine Serum
NaCl	Sodium Chloride
BSA	Bovine Serum Albumin
PFA	Paraformaldehyde
DMSO	Dimethyl Sulfoxide
EtOH	Ethanol
DPX	Dibutylphthalate Polystyrene Xylene
Tris	tris(hydroxymethyl)aminomethane
IL-	Interleukin-
CB	Carbon black
C-PP	Commercial, not milled, non-respirable PP MNPs
R-PP	Commercial, milled, respirable-PP MNPs
PDI	Polydispersity Index
Pyro-GC-MS	Pyrolysis-Gas-Chromatography Mass-Spectrometry
DLS	Dynamic Light Scattering

NIST	National Institute of Standards and Technology
ddH_2O	Double-distilled water
ATCC	American Type Culture Collection
CCM	Cell Culture Medium
SEM	Scanning Electron Microscopy
QCM	Quartz crystal microbalance
TEM	Transmission Electron Microscopy
HAADF	High-Angle Annular Dark-Field
STEM-EDX	Scanning-Transmisson electron Microscopy-Energy Dispersive X-ray
LSM	Laser Scanning Microscopy
TBE	Trypan Blue Exclusion
ELISA	Enzyme-Linked Immunosorbent Assay
PAMP	Pathogen Associated Molecular Pattern
TNF-α	Tumour Necrosis Factor-α
OECD	Organisation for Economic Cooperation and Development
CBPI	Cytokinesis-Block Proliferation Index
MMS	Methyl methanesulfonate
ANOVA	Analysis of Variance
PET	Polyethylene terephthalate
LN	Liquid Nitrogen
Mono/MN	Mononucleated Micronucleus
MMAD	Median Mass Aerodynamic Diameter
DNA	Deoxyribose nucleic acid

Chapter 1 – General Introduction

Single-use surgical face masks are routinely used throughout medical practice and industry, they are intended to be single use, but are known to shed inhaled debris of various sizes and morphologies (Han & He, 2021). There is also growing evidence of adverse effects occurring when used for extending periods (Klimek, et al., 2020). Their use was widely extended to the public throughout the duration of the Covid-19 pandemic as a means to reduce the rate of transmission across the population. Due to the sudden increase in demand for the masks, their manufacture across the world greatly increased, and therefore their wastage. The influx of mask wastage resulted in an increase to masks not being correctly disposed of, leading to them infiltrating into bodies of water and landfill, where they will degrade and form Micro-, Nanoplastics (MNPs) with the potential to become airborne (Mbachu, *et al*., 2020), contributing to air pollution as particulate matter (PM). These masks are primarily constructed from polypropylene (PP), but the remaining materials are not fully understood. Chapter 1 will discuss what is currently known and unknown about MNPs, with a focus on PP where applicable, the anatomy and physiology of the lungs and how both of these areas can be translated into *in vitro* experimentation.

1.1 The Lower Respiratory Tract

1.1.1 Mechanism of Breathing

The primary function of the respiratory system is to facilitate the intake of oxygen (part of gaseous exchange) for its delivery *via* erythrocytes (by binding to haemoglobin) to somatic cells and gametes, to allow them to perform their specialised functions, alongside growth, mitosis, and meiosis (Tidy, 2021). Some secondary functions of the respiratory system include protection from potentially harmful substances, facilitated by ciliated epithelial cells, mucous production, and mechanical reactions such as coughing, and sneezing (Bourouiba., *et al*, 2014). Gaseous exchange also describes the expiration of carbon dioxide (CO_2), a product of oxidative phosphorylation, conducted by the mitochondria, which are found in the cytoplasm of cells, in turn regulating the pH of blood (de Goede, *et al*., 2018).

Inhalation and exhalation are controlled primarily by two muscles, the diaphragm and the intercoastal muscles, but sternoclastoid and scalene muscles are additionally recruited when an individual is in respiratory distress. Collectively, these muscles mechanise airflow, by decreasing and increasing the pressure inside the thorax (by increasing and decreasing volume, respectively), in comparison to the air pressure outside of the thorax (Chaudhry & Bordoni, 2021), as depicted in figure 1.1.

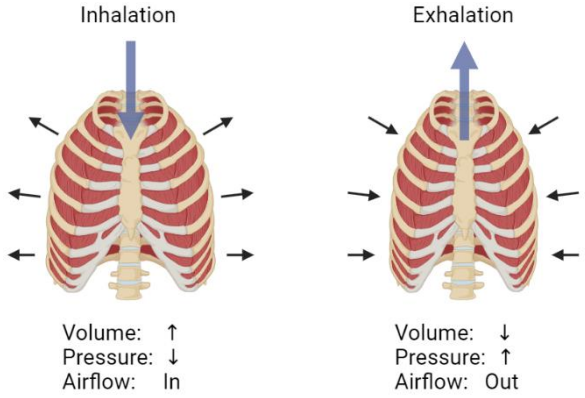

Figure 1.1 - Inhalation and exhalation mechanics (created by myself, using Biorender.com)

During inhalation, the diaphragm contracts, flattening and pulling downwards, simultaneously, the intercostal muscles contract, pulling the ribs upwards. Together, the volume of the thorax increases, decreasing pressure and expanding the lungs, and drawing air inwards, ultimately to

the alveoli, where gaseous exchange occurs. The inverse occurs during exhalation, where an increase to thorax pressure forces air out of the lungs, and consists of a greater proportion of carbon dioxide, which is a product of aerobic respiration (Dugdale, 2020).

1.1.2 Pathway of Respiratory System

There are several organs and structures included within the respiratory system, which can be divided into two different groups based upon either functionality or anatomy. Grouped by function, the structures are divided into the conducting zone (nose and mouth to the bronchioles) which forms the path for inhaled gases to travel to the respiratory zone, and the respiratory zone (alveolar ducts to the alveoli), where gaseous exchange occurs. In terms of anatomy, the structures are grouped into the upper respiratory tract (outside/above thorax), containing the nose/mouth > pharynx > larynx, and the lower respiratory tract, which is depicted in figure 1.2 (Taylor, 2021).

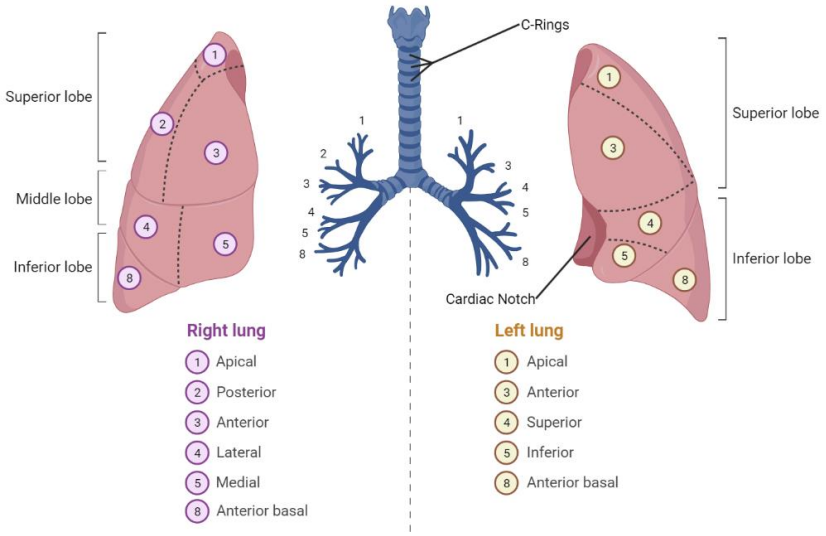

Figure 1.2 - Structure of the lower respiratory tract (pre-made template on Biorender.com)

Both of the lungs are anatomically similar, but structurally different (Betts *et al*., 2022). The right lung consists of three lobes, separated by a horizontal fissure and an oblique fissure, whereas the left lung only contains two lobes, divided by a single, oblique fissure. Additionally, the left lung houses an indent, called the cardiac notch, where the heart resides (Chaudhry & Bordoni, 2021).

Using computerised tomography of lungs and alveoli, it is possible to determine the total volume of the lungs, which is usually around 4000-6000 cm^3 (Yuan *et al*., 2010). This can also be calculated by adding together the values of tidal volume (volume of air inhaled and exhaled in one breath cycle), inspiratory reserve volume (volume of air forcibly inhaled after tidal volume), expiratory reserve volume (volume of air forcibly exhaled after tidal volume), and residual volume (volume of air in lungs after maximal exhalation) (Kutz & Grotberg, 2021).

The trachea is the largest pathway for air into the lungs, usually between 10 cm to 13 cm in length in adult humans, with walls 3mm thick and an external diameter between 1.8 cm to 2.3 cm. The length of the trachea is lined with 18-22 cartilage C-rings, which retain the structural integrity of the trachea during the changes to pressure, preventing it from collapsing. The opening of the C-rings is lined with the trachealis muscle, a smooth muscle, which allows the diameter of the trachea to temporarily decrease during events such as coughing or swallowing (Furlow & Mathisen, 2018, and Mieczkowski & Seavey, 2021). The trachea splits into the two bronchi at the base, called the carina, each bronchus enters the respective lung at the hilum

(root of the lung) (Furlow & Mathisen, 2018, and Chaudhry & Bordoni, 2021). The bronchi follow a similar structure to the trachea, but are smaller, with the right bronchus having a slightly larger diameter than the left (Ball *et al*., 2021). Both the trachea and the bronchi are inner-most lined with ciliated epithelial cells and goblet cells (Kia'i & Bajaj, 2021). Ciliated epithelial cells have cilia on their apical surface, inwards to the trachea, which 'beat' to move mucous and debris out of the respiratory tract and out of the body through the mouth or nose, or into the digestive tract for destruction in the stomach (Yaghi & Dolovich, 2016). Goblet cells produce mucous, which entraps debris and pathogens that enter the respiratory tract. The viscosity and trapping-ability of mucous is due to the rich presence of mucin glycoproteins (Lillehoj & Kim, 2002).

Bronchioles are not supported by cartilage rings, are significantly narrower, do not consist of any mucous-producing cells and gradient towards columnar epithelial cells, as they go deeper into the lung and branch further (Ball *et al*., 2021). Each lung contains an average of between 22,300 (McDonough *et al*., 2011) and 17,427 (Verleden *et al*., 2014) bronchioles and are 1mm in diameter on average (Vasilescu *et al*., 2020). The end of terminal bronchi present the alveoli, small air sacs which account for around 140 m^2 of the surface area of the lung and are the site of gaseous exchange.

1.1.3 Cellular Structure of the Alveoli and Their Function

The alveoli primarily facilitate the passing of oxygen and carbon dioxide across themselves into and out of the bloodstream respectively. There are two cell types which form the structure of alveoli, type I epithelial cells and type II epithelial cells. Type-I squamous epithelial cells can form up to 85%-95% of the surface of the alveoli, with the cuboidal type-II epithelial cells, not usually at a surface, and are notable by their presence of lamellar bodies (Knudsen & Ochs, 2018). Sometimes individual cells may constitute multiple alveoli, with multiple of its surfaces fronting alveolar lumina, which may contribute to the structural integrity of the alveoli and is a feature which had not yet been incorporated into *in vitro* models of the air-blood barrier. The layers of epithelial cells between the alveoli and the encompassing endothelial capillary cells (diffusion barrier) are only around 2 μm in total (Knudsen & Ochs, 2018) and collectively form the air-blood barrier (Ball *et al*., 2021).

Type-II alveolar epithelial cells constitute only 5-15% of the total alveolar surface, but up to 60% of the total alveolar epithelial cells and 10-15% of total lung cells (Castranova *et al*., 1988). These cells secrete pulmonary surfactant, containing the main active lipids of dipalmitoylphosphatidylcholine and phosphatidylglycerol, but they also secrete the proteins SP-A, SP-B, SP-C, and SP-D (Rooney *et al*., 1994. Batenburg and Haagsman, 1998) which are imperative to maintain function of the lungs, as the surfactant reduces surface tension of the air-liquid interface in the alveoli (Veldhuizen & Haagsman, 2000). These surfactants are released form the cells *via* exocytosis from lamellar vesicles (Ryan *et al*., 1975), and can similarly be returned into the cell *via* endocytosis, where its degradation products can be used to reconstitute vesicles (Williams, 1984. Hallman and Teramo, 1981. Chander *et al*., 1987). Type-I epithelial cells indirectly trigger the secretion of pulmonary surfactant by the stimulation of caveolae, mechanical sensors activated by plasma membrane stress (Diem *et al*., 2020). Type-II cells are considered stem cells, as they have proven to differentiate into Type-I

cells (Mason *et al*., 1997. Griffiths *et al*., 2005. Reynolds *et al*., 2004. Gomperts and Strieter, 2007. Uhal, 1997. Weiss *et al*., 2006) to repopulate the alveolae in both *in vivo* (Liu *et al*., 2006) and *in vitro* studies (Brody and Williams, 1992. Danto *et al*., 1992. Dobbs *et al*., 1988. Kikkawa and Yoneda, 1974. Paine *et al*., 1988. Paine and Simon, 1996).

The alveoli, and more specifically type-I and type-II alveolar epithelial cells, are the location at which gaseous exchange occurs, this is also the primary site at which inhaled nanomaterials could translocate into the circulatory system due to this region being the shortest path of traversal, and impact secondary organ systems (Sultana *et al*., 2013). Furthermore, if the rate of intake of inhaled particles is greater than their clearance, they will accumulate within compartments of the lung, depending on the particle characteristics such as size, as previously discussed, and is termed particle overload (Pauluhn, 2011). The overloading accumulation of insoluble particles such as coal dust, TiO_2 and diesel soot, in the lungs of rats, presented prolonged inflammation, tumour formation and fibrosis (Olin, 2000).

The exchange of gases between the alveoli and the encapsulating venous capillaries relies on gradients of gas partial pressures. The partial pressure of oxygen (pO_2) is much greater in the alveoli than the capillary blood, as the haemoglobin returning to the lungs *via* the pulmonary artery, has been deoxygenated after supplying the rest of the body with oxygen and will therefore diffuse into the blood from the alveoli (Ahmed *et al*., 2020).

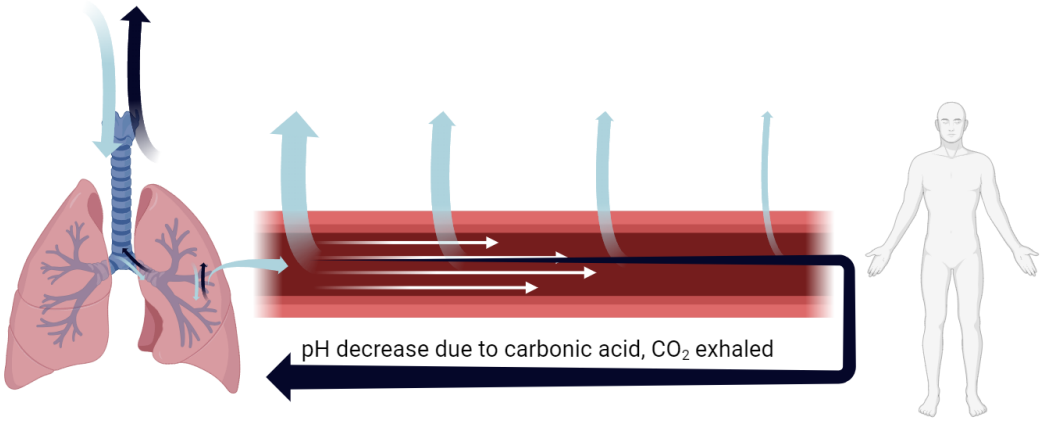

Figure 1.3 - Process of Gaseous Exchange. The size of arrow indicates the decrease of diffusion of each gas as the haemoglobin becomes more O_2 saturated, and less CO_2 saturated. (created by myself, using Biorender.com)

The diffusion of carbon dioxide also relies of a gradient of partial pressure (pCO_2); however, the gradient runs in the opposite direction (Petersson & Glenny, 2014) (Figure 1.3). CO_2 is a product of the tricarboxylic acid cycle (TCA cycle; a cyclic process which is part of aerobic respiration, to synthesise adenosine triphosphate, ATP, for a vast array of functions) (Hopkins *et al*., 2021). CO_2 is transported unbound to proteins, dissolving in the water component of blood to form carbonic acid, which acidifies the pH of blood (Alabduladhem & Bordoni, 2021). Excessive acidity increase (exacerbated after exercise and other events increasing CO_2 production), is detected by three mechanisms, chemoreflexes, central command and neural feedback from muscles. Ultimately, these mechanisms aim to reduce blood acidosis from carbonic acid, by increasing breathing rate and tidal volume temporarily (Guyenet & Bayliss, 2015).

1.2 The Atmosphere and Air Pollution

1.2.1 Particulate Matter and Air Pollution

The definition of air pollution according to the World Health Organisation is the presence of chemical, biological, or physical agents which contaminate the natural characteristics of the atmosphere of the indoor or outdoor environment (World Health Organisation, 2021a).

Air pollution typically consists as gaseous pollutants and PM, which are solid or liquid particles floating in ambient air (Zhu, *et al*., 2021). Besides the physical state of the particles, either solid or liquid, all airborne matter which falls into these size categories is included, regardless of origin or material. The consistency of PM can vary depending on the location, for example salt-based PM is more prevalent on the coasts, from aerosolised seawater, or higher prevalence of metal-based PM in underground-rail systems, which tend to be enclosed, poorly ventilated systems (Loxham & Nieuwenhuijsen, 2019). The most prominent and well-known air pollutants include the 'Greenhouse Gases', which consists of Methane (CH_4), Carbon Dioxide (CO_2), and Nitrous Oxide (N_2O), which are commonly associated with the escalation of climate change (Pytlak, et al., 2021).

Microparticles define 3-dimensional objects within the size range of 1 μm to 1000 μm in diameter (Boholm & Arvidsson, 2016), in contrast to nanoparticles which concern 3-dimensional objects within the nanoscale range of 1 nm – 100 nm (Boholm & Arvidsson, 2016). Particulate matter PM defines particles typically present in the ambient air, which can sediment onto the earth as a result of gravity. PM is classified into the aerodynamic diameter of particle and are usually monitored in classifications of PM_{10} (<10 μm in diameter, coarse), $PM_{2.5}$ (<2.5 μm in diameter, fine), PM_1 (<1 μm in diameter, very fine) and $PM_{0.1}$ (nanoscale particles <0.1 μm in diameter, ultrafine particles) (figure 1.4). PM_{10} and $PM_{2.5}$ are known to be two of the most significant contributors to air pollution and human health, but research into PM is problematic due to the vast heterogeneity of the materials within classifications (World Health Organisation, 2021b).

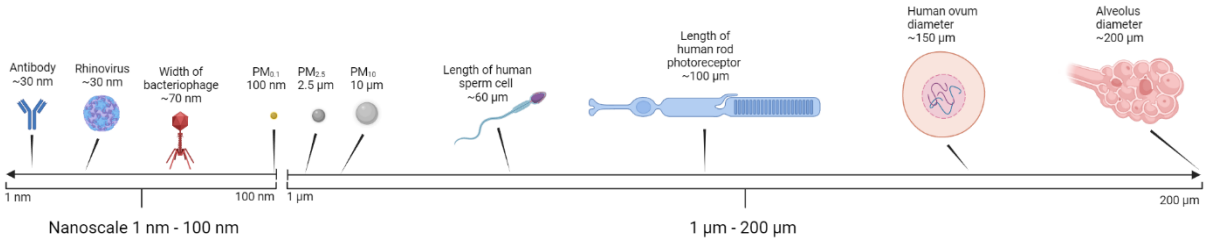

Figure 1.4 - Scales of biological structures and relevant PM aerodynamic size categories (created by myself, using Biorender.com)

Contribution to air pollution can originate from both natural and manufactured processes. In nature, spontaneous wildfires, and volcanic eruptions are some of the natural events which release pollutants into the air, however due to the spontaneity and frequency of these events, their overall contribution to air pollution is less consistent than industrial processes. Industrialisation is a main contributor to air pollution, primarily concerning the burning of fossil fuels in all forms and applications. Some of the most common methods of fossil fuel uses being combustion engines and power stations (Bai *et al*, 2018). The distribution of PM origins are depicted in figure 1.5.

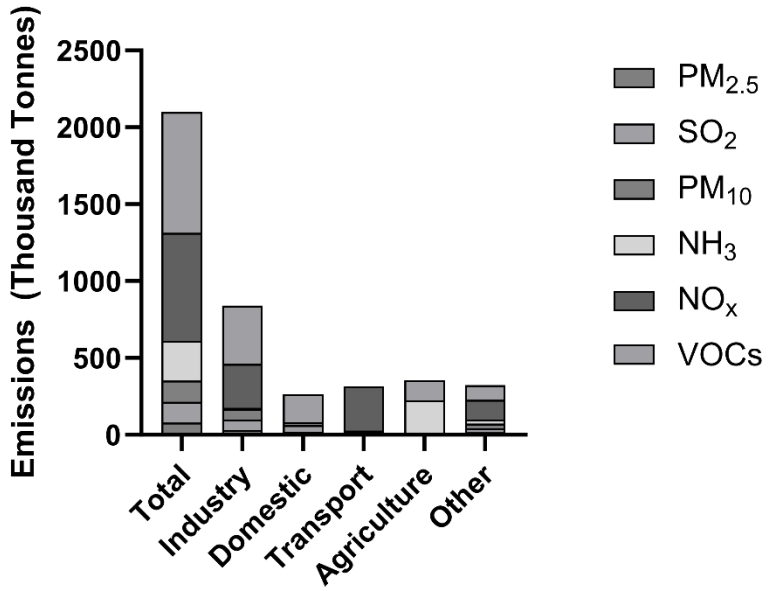

Figure 1.5 - Emission and distribution of air pollutants in the UK in 2020 (UK Government - Department for Environment, Food and Rural Affairs, 2022)

1.2.2 History and Progression of Anthropogenic Pollutant Emission

The production of anthropogenic air pollution would have originated from the discovery of fire, but to a much larger scale from the development of civilisations, from the mass burning of fuels for light sources, forges, breweries, furnaces and in cooking, as early as the Sumerian civilization from 4500 B.C. - 1900 B.C., Ancient Egyptian from 3100 B.C. - 30 B.C. Ancient Greek from 1100 B.C. - A.D. 140 and The Ancient Romans from 750 B.C. – A.D. 470 (Jacobson, 2012. Walters, 2021).

Additionally, the progression of mining ushered the release of pollutants and PM into the atmosphere, with some mined minerals, such as coal releasing PM and methane gas, is also feeding into air pollution generated by coal used for combustion (U.S EPA, 2003). The mining and use of coal rapidly accelerated during the Industrial Revolution between A.D. 1733 and 1913 and demanded the introduction of UK regulations to limit the release of pollutants into the atmosphere such as the Railway Clauses Act (1845), the Smoke Nuisance Abatement Acct (1853) and the Alkali Act (1863). Despite these legislations, London, and several other UK cities developed a lingering smog (portmanteau of smoke and fog); a term introduced in 1905 by Harold Antoine des Voix, a member of the London's Coal Smoke Abatement Society. The danger of this smog peaked in 1952 and was responsible for over 4000 deaths across the city of London (Jacobson, 2012).

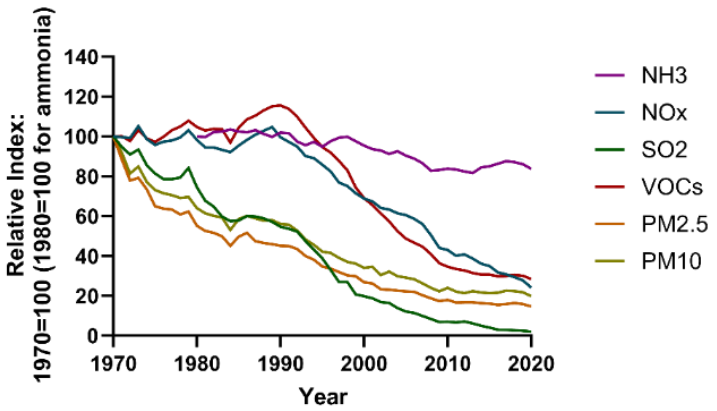

Figure 1.6 - Emission of air pollutants in the UK from 1970 to 2020 (Walters, 2021).

Since 1970 however, air pollution emissions have greatly decreased in the UK, although only a minor decrease to ammonia emissions as seen in figure 1.6, (Marshall, *et al*., 2023).

1.2.3 Air Pollution Monitoring

In the UK, the dominant rating for air pollution is the Daily Air Quality Index (DAQI), using a categorical scale of 1-10 and was initiated in January 2012. The DAQI monitors five parameters all measured in $\mu g/m^2$: Ozone (O_3) every eight hours, Nitrogen dioxide every hour, Sulphur dioxide every 15 minutes, $PM_{2.5}$ and PM_{10} every 24 hours, summarised into table 1.1 (Connolly, Fuller, Baker, & Willis, 2013).

Table 1.1 - Monitored air pollutants in the UK and the corresponding severity rating to human health – Daily Air Quality Index (DAQI). Colour-coded in correspondence to the official index.

		Ozone	**Nitrogen dioxide**	**Sulphur dioxide**	**$PM_{2.5}$**	**PM_{10}**
		8-hourly mean	1-hourly mean	15-minute mean	24-hourly mean	24-hourly mean
Band	**Index**	$\mu g/m^3$	$\mu g/m^3$	$\mu g/m^3$	$\mu g/m^3$	$\mu g/m^3$
Low	**1**	0-33	0-67	0-88	0-11	0-16
	2	34-66	68-134	89-177	12-23	17-33
	3	67-100	135-200	178-266	24-35	34-50
Moderate	**4**	101-120	201-267	267-354	36-41	51-58
	5	121-140	268-334	355-443	42-47	59-66
	6	141-160	335-400	444-532	48-53	67-75
High	**7**	161-187	401-467	533-710	54-58	76-83
	8	188-213	468-534	711-887	59-64	84-91
	9	214-240	535-600	888-1064	65-70	92-100
Very High	**10**	≥241	≥601	≥1065	≥71	≥101

Due to the long testing periods between Ozone (eight hours), $PM_{2.5}$ and PM_{10} (both 24 hours) these cannot be indicative of sudden events of high, potentially dangerous levels of pollution. Therefore, the Committee on the Medical Effects of Air Pollutants (COMEAP) devised and recommended the use of trigger concentrations for these three measurements, which are monitored every hour by public information service organisations, unlike the overarching DAQI monitoring. The trigger concentrations are highlighted in table 1.2, alongside the respective Gilbert Skill Score (GSS), which is the verification measurement of whether a categorical forecast was a true event. GSS is calculated using the number of: 'true event + false positive + no event - events due to chance' (Connolly, Fuller, Baker, & Willis, 2013).

Table 1.2 - Monitored air pollutants in the UK and their corresponding GSS.

Pollutant	Pollution Band	Trigger (µg/m^3)	GSS
PM_{10}	Moderate and above	68	0.533
	High and above	107	0.348
	Very High and above	177	0.188
$PM_{2.5}$	Moderate and above	50	0.591
	High and above	74	0.422
	Very High and above	101	0.260
O_3	Moderate and above	105	0.791
	High and above	170	0.726
	Very High and above	n/a	n/a

Micro,- nanoplastics (MNPs), in terms of monitoring, are not specifically quantified as a part of air pollution. MNPs are a constituent of particulate matter, separated based upon their size fractions, such as $PM_{2.5}$ (Kirchsteiger et al., 2023). The reason for the non-specific monitoring of MNPs is partly due to their difficulty to distinguish from within PM, and the difficulty to reliably separate it into its constituents. The use for PM as a collective identifier spanning many different materials, also describes the difficulty to pinpoint the exact components within PM, which are responsible for causing potential adverse effects (WHO, 2006). $PM_{2.5}$ is one of the most hazardous airborne materials monitored, hence the lowest concentration threshold, depicted in table 1.1. Some of the most significant constituents of $PM_{2.5}$ include ammonium, nitrates, sulphates, elemental carbon matter and organic carbon matter (Dominici, et al., 2015. Liu, et al., 2022). In the outdoor urban air of Graz, Austria, between 2nd January and 31st March 2017, 'Ultrafine' MNPs with diameter <0.1 µm, were determined to be 0.67% of the total $PM_{2.5}$ mass, and 1.7% of the organic mass. From which, three polymer types were found, polyethylene terephthalate (50%), PP (27%) and polyethylene (23%) (Kirchsteiger et al., 2023). As more time passes for existing waste plastics to degrade, and more plastic is added into the environment, these figures are likely to increase year-on-year. Furthermore, there is the potential for a future spike in PP detection, following the widespread usage of masks throughout the COVID-19 pandemic, which are predominantly constructed from PP.

1.2.4 Adverse Effects of Carbon-based $PM_{2.5}$ Constituents in Air Pollution

Air pollution both directly and indirectly affects human health. Direct effects of air pollutants arise from being inhaled and instigating a biological response. Some pollutants, usually larger particles, can be removed passively by the lungs' ciliated epithelial cells which line the trachea and bronchi, pollutants removed this way typically do not cause adverse effects. Smaller PM ($\leq PM_{2.5}$) and gaseous pollutants can pass deeper into the lungs, into the alveoli, posing the risk to pass across the endothelial barrier into the bloodstream (Li, *et al*., 2017). At present, data specifically quantifying MNPs within $PM_{2.5}$ is largely absent, however, studies have quantified organic carbon compounds within $PM_{2.5}$, which consist of both aromatic hydrocarbon compounds, such as benzene and phenanthrene, and aliphatic hydrocarbon compounds

including plastic polymers. Across Central Europe at 60 urban, rural and kerbside-monitored sites, between 20% and 47% of $PM_{2.5}$ was determined to be carbon-based matter; in the urban setting, 22% of $PM_{2.5}$ were organic carbon compounds, and 14% elemental carbon (Putaud et al., 2010). Additionally, an incineration study of municipal solid waste by Wang et al., (2018), identified organic and elemental carbon emissions to be between 46.6% and 67.2% depending on the source. With such a large percentage of $PM_{2.5}$ consisting of carbon-based materials partly of which contains MNPs it is highly important to develop more specific quantification techniques for MNPs, considering their accumulation and prevalence in the environment increasing each year, and resulting human exposure.

The terms 'Carbon Black' (CB) and 'Black Carbon' (BC) are sometimes incorrectly used interchangeably. Although they both contain carbon, they are different materials (Watson & Valberg, 2001. Long et al., 2013). CB is a purposefully engineered nanomaterial, often used as an additive for nanocomposites (Wen et al., 2012) or commonly as printer ink toner, and consists of >99% elemental carbon, whilst forming aciniform aggregates (Gray & Muranko, 2006). On the other hand, BC is soot generated from incomplete combustion. It is highly heterogeneous and can contain <50% elemental carbon, with the remainder consisting of a large percentage of organic carbon matter.

There are also many indirect pathways in which human health is put at risk by air pollution, the three significant vectors of indirect human health risk are secondary pollutants, climate change and interference of ecosystems (Orru, Ebi, & Forsberg, 2017). Further increase of anthropogenic $PM_{2.5}$ emissions over time can change the chemical and physical interactions of standard particles in the atmosphere, potentially leading to a chain reaction of altered particle reactions contributing to climate change (Fuzzi, et al., 2015). In addition to anthropogenic particles, biogenic volatile organic compounds would be altered by this pathway, due to increase of temperatures and alteration to plant metabolism, in turn, affecting secondary organic aerosols and other secondary particles (Carslaw, et al., 2010). Increases to atmospheric $PM_{2.5}$ can affect the climate and therefore indirectly affect human health, to varying degrees, depending on the PM type.

1.3 Micro,- Nanoplastics

1.3.1 Polypropylene and Additives

Polypropylene is an organic polymer, commonly used in coatings, paints, packaging and textiles. Isotactic (iPP, methyl groups arranged on the same side, figure 1.7a), syndiotactic (sPP, alternating methyl groups, figure 1.7b) and atactic, which do not follow repeating units (aPP, irregular methyl group positions, figure 1.7c). Figure 1.7 was created by myself, using Chemdraw Office software.

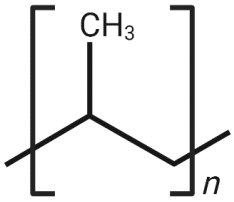

Figure 1.7a - Isotactic PP

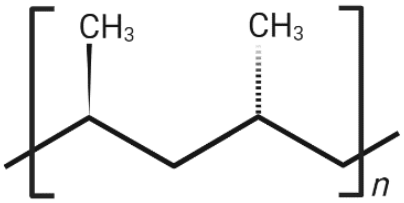

Figure 1.7b - Syndiotactic

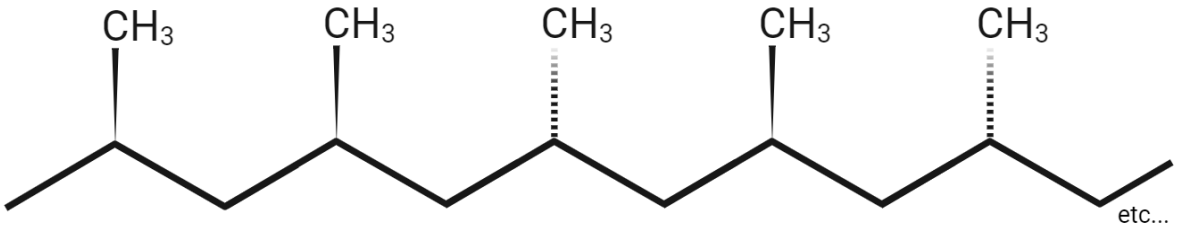

Figure 1.7c- An example of an atactic PP polymer

Atactic PP, also describes as linear low-density PP, is transparent due to lower crystallinity and low-strength in comparison to isotactic PP. Non-woven PP typically consists of isotactic PP, which is the mechanically strongest and most crystalline of the three forms, typically referred to as High-density PP. Propene can be reliably polymerised into isotactic PP *via* the use of Ziegler-Natta catalysis (Hagen et al., 2002).

PP is often produced with the inclusion of additives, to grant the material additional or improved properties, to improve its current performance or tailor it to specific purposes. Antioxidants are added to improve the longevity of the product, by reducing oxidation rate. A common antioxidant additive is pentaerythritol tetrakis(3-(3,5-di-tert-butyl-4-hydroxyphenyl)propionate), otherwise known as Irgonax 1010, at concentrations of up to 0.5% (PubChem, 2005c. Schymanski, 2019).

Both halogenated and non-halogenated flame retardants are possible to incorporate as additives, such as 2,4,6-Tris(2,4,6-tribromophenoxy)-1,3,5-triazine (PubChem, 2005d) and potassium 3-(phenylsulfonyl)benzenesulfonate (PubChem, 2005a), respectively. Halogenated flame retardants are highly effective, but non-halogenated alternatives are safer to the environment and human exposure.

There are two types of UV-stabilisers, ultraviolet light absorbers such as 2-[2-Methoxy-5-(1,1,3,3-tetramethylbutyl)phenyl]-2H-benzotriazole (PubChem, 2015) which filter away

ultraviolet light, and hindered-amine light stabilisers bis(2,2,6,6-tetramethyl-4-piperidyl) sebacate (PubChem, 2005b), which trap free-radical oxygen species from damaging the product.

CB is proficient at absorbing heat, retaining the temperature of the atmosphere (Bond, et al., 2013) and has also been used as a nanocomposite additive to plastic polymer polypropylene (PP) to increased resistance to ultraviolet-radiation, or as a black colourant (Wen et al., 2012). Degradation of the CB-PP co-polymer would lead to the release of both constituents, and therefore the potential of human exposure *via* inhalation for example.

Titanium dioxide (TiO_2) is used as a white pigment in the form of E171, and is typically found within paints, ink, cosmetics, food and commonly plastics, as a white pigment (Haider et al., 2019). E171 is the form of TiO_2, which typically contains two forms of TiO_2; anatase and rutile (Verleysen et al., 2020), depicted in figure 1.8. There is conflicting evidence for the safety of TiO_2 inhalation and has been debated amongst food safety agencies across the world for many years. The European Chemical Agency suggested TiO_2 to be a category 2 carcinogen in 2017 (CfRAR ECHA, 2017). This eventually led to a 6-month phasing-out period, banning the use of E171 *specifically* as a food additive across the EU, between 7th February 2022 until 7th August 2022 (Juelicher, 2022). The use of E171 as a food additive is still permitted in the UK and the USA however.

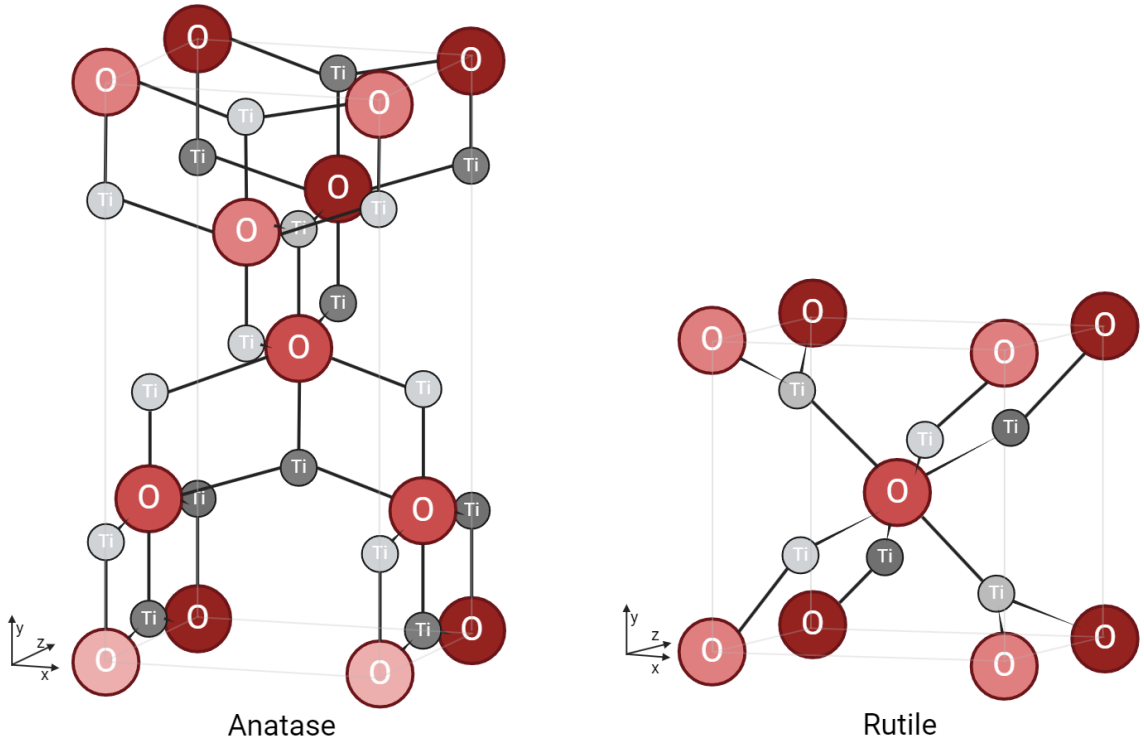

Figure 1.8 - Structural differences between anatase and rutile TiO_2 (created by myself, using Biorender.com).

1.3.2 Polypropylene-Based Face Masks

Typical level-2 surgical face masks consist of three layers of material, covering the mouth and nose, which are constructed *via* two different processes, producing two different structures. The innermost and outermost layers are constructed *via* spunbonding, which produces a coarser fibre mesh, intended for retention of structure to the overall object. Whereas, the central layer is constructed *via* melt-blowing, for a tighter meshing, and is predominantly for filtration (Henneberry and Rossettie *et al*., 2020). Despite the knowledge of potential additives in PP, the extent of what is included within surgical face masks is not completely understood, with the only clear indication being that they are predominantly PP (Fadare & Okoffo, 2020, Koester, 2022). The only way to identify the constituents of face masks is to consult the appropriate patents, as packaging does not legally have to display all of the details. However, it is difficult to determine which available patents correspond to which brand of mask specifically. With the use of TiO_2 in food being now banned in the EU, due to inhalation carcinogenicity concerns, European patents or World Intellectual Property Organisation (WIPO) (defined by patents starting with EP- or WO-, respectively) patents, interestingly still do document the use of TiO_2 in level-2 masks. WIPO patents are valid in the 193 of their member states; many are also EP- coded countries. WO2007027413A1 (mentions both PP use and potential use of anatase TiO_2 as germicidal agent), WO2017175143A1 (both PP and TiO_2 use, but no equivalent EP- patent). Both of these patents mention the potential use of TiO_2 within the masks, seemingly conflicting the EUs' rationale to ban the use of TiO_2 in foodstuffs, specifically due to inhalation concerns, considering debris from masks would also be inhaled. The European Commission guidance document regarding the regulatory requirements for medical face masks (i.e. those in medicine and placed more greatly onto the market during the COVID-19 pandemic), makes no comments towards the recognition of masks containing TiO_2 (European Commission, 2022).

1.3.3 MNP Generation from Surgical Face Masks

Poor recovery and recycling of plastics leads to the improper disposal of plastics and their infiltration into the environment, causing pollution (Geyer *et al*, 2017). Through mechanical, biological and photo- degradation, the plastics degrade over time, becoming continually smaller particles, eventually becoming microplastics and nanoplastics (PlasticsEurope, 2019. Galloway & Lewis, 2016) (figure 1.19). These particles are small enough to enter organisms through consumption (primary or secondary consumption) or inhalation (Wright & Kelly, 2017).

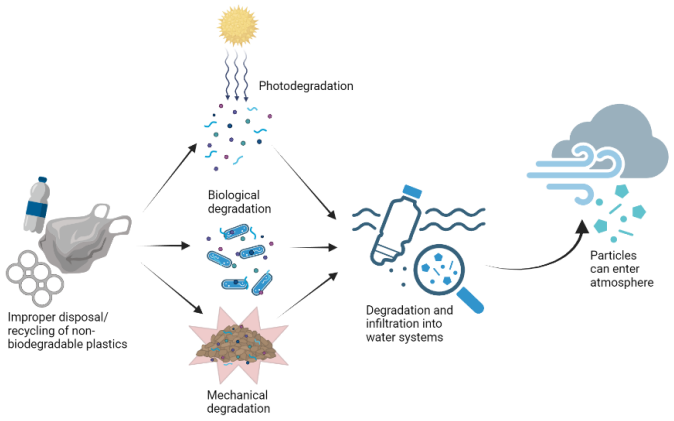

Figure 1.9 - Depiction of generation of MNPs in the environment (created by myself, using Biorender.com)

Despite much regulation in the ability for these masks to effectively filter objects and retain breathing

efficiency, current regulations do not account for the degradation of masks and inhalation of debris generated from these: International Organisation for Standardisation (ISO) Standards (ISO 22609, 16900), European Union Standards (EN 140, 143, 149, 14683), Chinese Standards (GB 19083, 2626; GB/T 32610, 38880; YY 0469; YY/T 0969), American Society for Testing and Materials (ASTM) Standards (F1862, F2100, F2101, F2299) and National Institute for Occupational Safety & Health (NIOSH) Regulation (42 CFR 84).

There is little currently known regarding mask breakdown and potential toxic effects, besides their potential for environmental pollution, and the identification of particles and chemicals which could be released from their improper disposal (Fadare & Okoffo, 2020, Hui Li *et al*., 2022).

For surgical face masks, there are two key routes *via* which human exposure could occur. The first-hand exposure of mask-derived MNPs would be due to the use of the masks. Typically, these masks are designed to be single-use, then disposed of. In institutions such as hospitals, correct practice of personal protective equipment (PPE), including masks, are usually adhered to by implementation of Standard Operating Procedures (SOPs) for management and segregation of waste. The NHS follows HTM 07-01 (NHS, 2021) for disposal of PPE. However, the general public are likely to be more lenient, reusing masks after repeated mechanical abrasion and UV-exposure (photodegradation). In turn, this increases the formation and release of MNP debris generated by the masks, those from the interior layer, being closest to the respiratory system, could be inhaled by the user (Han *et al*., 2021).

There is also the environmentally-relevant route for mask-derived MNPs to be inhaled by humans. The first stage of this process is the movement of discarded masks as 'loose waste' in landfill, entrance to bodies of water, or simply discarded as littering, all of which accelerate degradation and release of MNPs into the environment *via* processes described in figure 1.9 (Morgana *et al*., 2021, Sullivan *et al*., 2021, Shukla *et al*., 2022), similarly to other plastic objects, over time (Schnurr *et al*., 2018, Fadare *et al*., 2020). The MNPs derived from the masks by these environmental processes would be representative of the mask as a whole. There are three layers to these masks, so MNPs from all three layers would be generated over time, and are distinct from each other structurally and/or chemically.

At present it is unknown how extensively MNP mask waste is impacting the atmosphere. However, estimations of how much environmental impact they have now, can be used to predict how they may impact the atmosphere in the future. Based upon reports by Klemeš *et al* (2020) and Wang *et al* (2023) estimate that from mask production in 2020 alone, 150 million tons of PP waste, 60 million tons of other polymer waste, and 750 million tons of CO_2 were produced, originating from 120 million discarded masks. Furthermore, 1.37 quadrillion MPs were estimated to be released into bodies of water from the waste masks as a result, with the potential to further degrade to NPs (Wang et al., 2023).

In comparison, tyre-wear and road particles (TWRP) are a target for $PM_{2.5}$ and inhalable particle quantification. Studies report a range of concentrations within the air, between 1.3%-7% (Schauer et al., 2002. Blic, 2005. Kwak et al., 2013).

1.3.4 Human Exposure to Micro-, Nanoplastics

The three main routes of MNP exposure arise from consumption, inhalation, and dermal contact (Prata *et al*., 2020). Depending on the type of MNP, its source the geographical location at which the exposure occurs, some routes would be more likely to occur than others. Many studies investigate the exposure route of consumption; the drinking of contaminated water or seafood (Zhang *et al*., 2020, Gruber *et al*., 2022), whereas studies discussing their inhalation are much more limited in number. The human exposure to MNPs has received significant interest from scientific research, whilst minimal has been conducted for exposure through the air (Vianello *et al*., 2019). Therefore generally, there is limited research to determine the extent of MNPs in the air and their effects.

Few articles have been published determining the airborne prevalence of MNPs in localised areas around the large medical Centres in Sao Paolo (Amato-Lourenço *et al*., 2022), and along six sites of the Weser River in North Germany (Kernchen *et al*., 2022). Due to variations in the climate, weather systems (particulate matter movement and distribution) and urbanisation (particulate matter production), it is difficult to determine the average distribution of particulate matter and other air pollutants over large areas. Airborne microplastic particles and fibres were investigated in the air surrounding the largest medical centre in Latin America (Sao Paulo). The air at three different sites were quantified across these three sites and a total of 38 readings, and determined that the detected airborne micro-, nanoplastic were fibrous in structure (figure 1.10) (Amato-Lourenço *et al*., 2022). In the indoor home environment, Vianello *et al* (2019) determined the proportion of airborne MNPs to consist of 43% polyester, 22% nylon, 17% polystyrene, and 4% polyurethane, which was quantified by focal plane array Fourier Transform Imaging micro Spectroscopy (FPA-μFTIR). In various other indoor settings, the composition of airborne MNPs vary greatly. Zhai *et al* (2023), discovered that the greatest contributor in different settings were 18.42% polyethylene in offices, 27.96% polyvinyl butyral in laboratories, with polyamide, polyethylene and silicone resin each accounting for 14.29% in a dining hall.

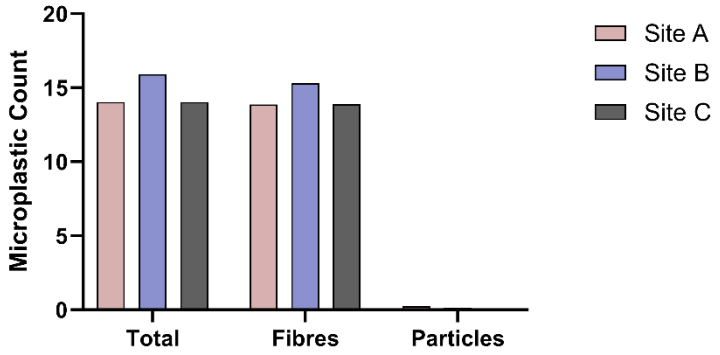

Figure 1.10 - Quantification of airborne microplastic debris around the medical centre in Latin America (Amato-Lourenço *et al*., 2022).

Lung autopsies have been studied, to detect the presence of inhaled microplastics in human lungs from the air. Parenchymal tissue samples were collected from proximal and distal regions of the left lung from 20 individuals. In 13 sets of these samples, a total of 33 particles and four fibres were found *via* Raman spectroscopy. All detected particles were less than 5.5 μm in diameter and the fibres were between 8.12 and 16.8 μm in length; polypropylene and polyethylene were the most frequent microplastic type (Amato-Lourenço *et al*, 2021). Much

research into microplastic effects to humans focuses on the digestive system, largely due to the understanding and presence of microplastics in the oceans, which fish ingest, and ultimately, humans (Galloway *et al*., 2015). However, reviews do exist which specifically discuss the inhalation of MNPs (Wright & Kelly, 2017. Prata, 2018) and human exposure as a whole. As this project intends to investigate the effects of inhaled MNPs derived from surgical face masks specifically, this limits the pool of suitable articles further. Inhaled MNPs also have the potential to pass across the alveolar barrier and enter systemic circulation, which could threaten more than just the respiratory system, namely the cardiovascular system due to proximity (Leslie *et al*., 2022. Li *et al*., 2017).

It is largely unknown at present, how MNPs could impact secondary organ systems, such as the cardiovascular, renal, or hepatic systems. As the primary organ associated with inhalation, the impact of inhaled MNPs should be predominantly assessed on lung models. Assessing the fate of the MNPs and the lung models themselves following exposure, it would assist the understanding of the full impact on the organ systems. For example, dose calculations, estimating how/what types/size/morphologies of MNPs could pass (or accumulate) in the lung, if the MNPs are changed in any way before they pass into circulation, potential to induce systemic effects prior to reaching circulation (i.e. pro-inflammatory response). Each of these factors could alter how MNPs interact with secondary organs, and understanding them would help to develop more realistic and reliable models for assessment.

Some microplastics are intentionally added to products. To qualify for intentional addition, a strict criteria must be adhered to, defined by the European Chemicals Agency *'A material consisting of solid polymer-containing particles, to which additives or other substances may have been added, and in which ≥ 1% w/w of particles have (i) all dimensions 1 nm ≤ x ≤ 5 mm, or (ii), for fibres, a length of 3 nm ≤ x ≤ 15 mm and a length to diameter ratio of > 3. Polymers that occur naturally and have not been chemically modified (other than by hydrolysis) are excluded, as are polymers that are (bio)degradable.'*. This legislation was finalised and came into effect from the 25th September 2023 (ECHA, 2019). MNPs included within this definition have to potential to also be considered engineered nanomaterials, depending on how they were created initially and their size; provided they are between 1-100 nm in any one of their dimensions. However, this definition does not accommodate unintentionally-created MNPs.

1.3.5 Size Effect on MNP Inhalation

There is a difference between the aerodynamic diameter and geometric diameter of a particle. Aerodynamic diameter defines the diameter of a particle, if it was a perfect sphere of standard, 1 g/cm^3 density, settling at its terminal velocity (DeCarlo et al., 2004).

There is a general lack of understanding on the toxicological effects of MNPs, especially via inhalation. Additionally, the vast majority of studies across any field of MNP research use polystyrene NPs, making PP-specific studies difficult to discover.

Different sizes of fluorescently-labelled PS-NPs have been tracked for their uptake within A549 alveolar epithelial cells *in vitro*. Particles of 40 nm in diameter were internalised at a significantly greater rate than particles of 20 nm or 100 nm in diameter (Varela et al., 2012).

There are many other studies investigating and proving the internalisation of commercially-available fluorescently-labelled PS-NPs, using alveolar epithelial cell lines (Salvati et al., 2011. Yacobi et al., 2008), but others have additionally proved internalisation with PS-NP particle diameters in excess of 200 nm (Lehner et al., 2019) and 535 nm (Brown et al., 2001).

Furthermore, PS-MNP particle diameters up to 1.01 μm have been observed to internalise in the HNX14C cell line (Zauner et al., 2001), L929 mouse fibroblasts and BMDM macrophages (Firdessa et al., 2014). L929 and BMBM cell lines were also observed to internalise PS-MNPs as large as 2.0 μm (Firdessa et al., 2014). The size of particle in conjunction with cell type determined the mechanism of how the particles were internalised. Typically, diffusion is the mechanism of transport as the particle size decreases, which is possible due to MNPs typically being lipophilic.

As mentioned previously, masks are known to shed MNP debris, with TEM and SEM imagery confirming that these can be as small as 0.5μm in diameter (Han *et al*., 2021), and from the atmosphere those within the $PM_{2.5}$ aerodynamic diameter range or smaller are those most likely to deposit into the alveoli.

1.3.6 Morphology Effect on MNP Inhalation

The morphology of an airborne particle affects its aerodynamic diameter. Perfectly spherical particles have a greater aerodynamic diameter in comparison to highly irregular particles and rod-shaped particles or fibres (Hassan & Lau, 2009), as factors such as surface area increase the drag factor of the particle, keeping it airborne for longer, resulting in a lower aerodynamic diameter and greater potential for alveolar deposition (Tang et al., 2004). To be defined as a fibre, the particle must be greater than a 3:1 ratio of length:diameter (Mossman et al., 2007).

The shape of particles alone is not enough to determine how the particle may interact with biological systems, and currently, there is not enough research into the morphological effects of inhaled MNPs to determine any toxicity trends. This lack of knowledge is exacerbated due to the large majority of toxicological studies investigate commercially-produced PS-NPs, which are spherical and used for their accessibility, with very little investigation into MNPs of any other morphology. As a result, it is only possible to speculate on the potential morphology effects of MNPs, based upon those discovered from other materials, namely carbon allotropes or metal. It is also important to consider that any MNP morphology studies which do exist, are often in ecotoxicological studies, using models rarely relevant to human health.

Asbestos fibres and carbon nanotubes (CNTs) are some of the most well-researched fibrous materials for their toxicological effect on the lungs. The morphology of material can greatly influence toxicity. Research into MNP morphology suggests that polyester microfibres instigate a greater adverse response than polyethylene microplastic particles in *Ceriodaphnia dubia* waterfleas (Ziajahromi *et al*, 2017), however it is difficult to definitively say this is the trend across all MNPs, because this study used two different plastics, each with different morphology and therefore cannot represent every MNP.

Many allotropes of carbon nanomaterials have been subject to toxicity studies. In terms of cytotoxicity, pristine C_{60} fullerene was the only allotrope to not exhibit cytotoxicity in alveolar macrophages, and did not induce an inflammatory response, all other allotropes tested resulted in cytotoxic effects: single-walled carbon nanotubes (SWCNT), multi-walled carbon nanotubes (MWCNT), carbon black, nanographite and single-walled carbon nanohorns (SWCNH) (Yuan *et al*., 2019). Shorter CNTs can be entirely internalised by macrophages *in vitro*, however longer CNTs can trigger frustrated phagocytosis, which is the continuous causation of an immune response alongside the production of reactive oxygen species and pro-inflammatory cytokines (Andersen, Wilbroe, & Moghimi, 2012).

Similarly, in metal nanoparticles, size and morphology have great influence on their interaction with cells and organ systems, in conjunction with the specific metal. Polyethylene glycol-modified (PEGylated) gold nanorods circulated for greater periods in the circulatory system and accumulated less in the liver than the same material with a spherical morphology of the same size in female mice (Arnida, *et al*., 2011). Furthermore, star-shaped gold nanoparticles, presented greater toxicity then spherical gold nanoparticles in both in vitro fibroblasts and RFPEC (microvascular endothelial cells) (Favi et al., 2015).

Fe_2O_3 Iron oxide NPs also display a similar toxicity trend, where rod-shaped instigated the greatest response, although iron oxide presented greater cytotoxicity, production of tumour necrosis factor-α and reactive oxygen species in mouse (RAW 264.7) macrophages (Lee, et al., 2014).

Engineered micromaterials and nanomaterials can pose threats to health, and how the material interacts with organisms is attributed to a combination of the size, shape and the material itself. Typically, the smaller the particles are in diameter and the more convoluted the geometry, the greater their surface area : volume ratio becomes, increasing likelihood of interactions occurring with cellular objects (Johnston, et al., 2010).

Encompassing fibres generally however, it is expected that following chronic exposure they induce a pro-inflammatory response in the lungs, leading to secondary genotoxicity as a result of continuous ROS production. Longer fibres typically induce greater toxicity due to their size preventing their phagocytosis (H. Greim, P. Borm, R. Schins, K. Do, 2001).

1.3.7 What is Known of the Adverse Effects of Inhaled Micro,- Nanoplastics?

There are a few studies which are demonstrating some adverse effects. An occupational report by Klimek *et al*., (2020) investigated 46 occupational-worker patients which presented with irritant rhinitis following prolonged use of filtering facepiece 2 (FFP2) respirators (not triple-layer level-2 masks) continuously for longer than two hours. Nasal lavages proved accumulation of PP fibres, with symptoms and accumulation significantly subsiding after three days of no exposure. Klimek *et al*., (2020) additionally hypothesized that due to the shortage of Personal Protective Equipment (PPE) available throughout the Covid-19 pandemic, the influx of non-CE PPE purchased to compensate may have greatly contributed to the increase of irritant rhinitis cases observed, as these occupational-workers encountered would have been

using respirators prior to the pandemic, and the poorer safety standards of cheaper masks allowed for easier degradation. This report unfortunately only identifies a correlation between the two factors from a small number of identified patients. Additionally, the study was assessing nasal lavages and not samples from the deeper lung, so the detected MNPs would be larger than those expected from the deep lung, therefore it is not sufficient to apply to the entirety of this project.

As previously stated, the vast majority of MNP inhalation studies focus on PS-NPs, due to their accessibility for assessments, however it is not representative of all MNPs. Additionally, most existing research will investigate how size differences of spherical PS-NPs impact health, with little variation to any other property. More studies need to be conducted on non-PS-MNPs.

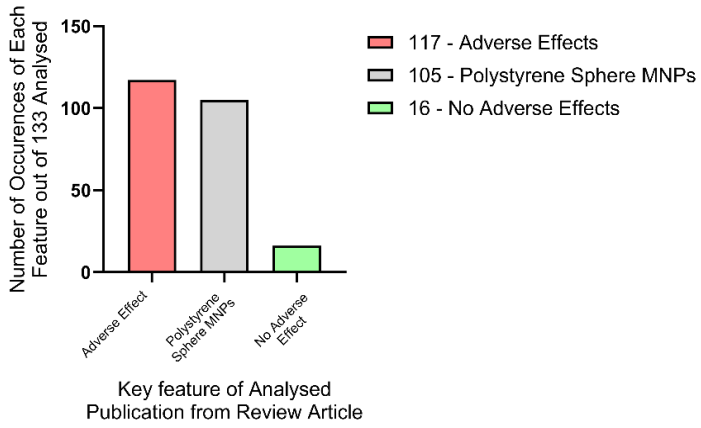

Figure 1.12 - Common features of MNP review articles concerning human health (Xu *et al*., 2022).

Some studies suggest orally-ingested PP MNPs in mice, can elicit oxidative stress, inflammation and cell death in intestinal cells 28 days post-administration (Jia *et al*., 2023). However, a vast majority utilise polystyrene MNPs, out of the 133 articles collated for the review conducted by Xu *et al*., (2022), 105 documented spherical polystyrene MNPs, but 117 recorded adverse responses occurring (figure 1.11).

When A549 cells, cultured *in vitro*, were exposed to PS-NPs approaching <25 nm in diameter, the expression of pro-inflammatory factors such as IL-6, IL-8, NF-κb and TNF-α, and pro-apoptotic proteins such as BAX, caspase-8 and caspase-9 were upregulated, in addition to significant increases to apoptosis induction after 24 hours (Xu et al., 2019). The particles around this size were readily internalised into the cells within an hour post-incubation (Debbage & Jaschke, 2008), and could potentially disrupt the cellular membranes at <20 nm (Kihara et al., 2021). Barrier disruptions can increase the cells' potential to internalise additional particles or chemicals, which may be more acutely toxic than PS-NPs.

In as little as 2 hours post-exposure to PS-NPs 64 nm in diameter, a significant increase to IL-8 was observed, which then decreased at 4 hours. This indicated a rapid internalisation, which was hypothesised to induce an oxidative stress response attributed to trigger the IL-8 expression (Brown et al., 2001). Sipos, et al., (2019), identified the increase to inflammation and oxidative stress in A549 cells following exposure to PS-NPs 200 nm in diameter. Following which, they determined that the damage to membrane integrity was attributed to the oxidative stress response. Significant cell viability loss was observed from 25 nm diameter particles at concentration of 25 µg/mL, 160 µg/mL with 70 nm diameter (Xu, et al., 2019), but the effect on viability seems to decrease as the particle size increases. Increases in particle size into the

micro-scale, to 1 µm and 10 µm in diameter, and increasing the length of exposure starting from 72 hours, a major loss of cellular tight junctions was observed, then after 96 hours of exposure, resemblance to the original cell was absent (Goodman et al., 2021).

1.4 Application into *in vitro* Laboratory Research

1.4.1 Lung Models

Using cell lines, it is also possible to formulate co-culture models, which increase the complexity of the system and increase its realism in comparison the whole lung. Due to the use of multiple cell types, it is possible to curate many combinations of cell models to represent whichever specific structure necessary. Immortalised cell lines are much more commonly used in *in vitro* assessment due to their ease of culturing and can be cultured continuously (Hiemstra *et al*., 2018). Additionally, willing client-bases must be obtained for the donation of cell samples. The acquisition of these cells requires a collection of the cells from the client, *via* methods such as biopsies, brushing or reconstructed from lung sects. Primary cultures can be successfully cultures at the air-liquid interface (ALI) (Fulcher & Randell, 2012), and once established they can replicate the gene expression and morphology of the equivalent structure *in situ* (Pezzulo *et al*., 2011).

Two of the most commonly used alveolar *in vitro* model is the monoculturing of either A549 cells or NCI-H441 cell lines (both are type-II alveolar epithelial papillary adenocarcinoma cell lines). Both of these cell lines can be additionally cultured at the ALI, improving the replication of the lung environment, and allowing for them to receive particle exposure *via* dry-powder or aerosol exposure. There are differences between these two cell lines, one of such is the average doubling time of each, with A549 taking around 22 hours, whereas NCI-H441 take up to 58 hours. However, Ren *et al*. (2016) concluded that NCI-H441 cells were more closely resembling of the alveolar epithelium than A549 cells due to their junctional protein expression and formation of a more functional barrier with greater electrical resistance, despite their slower cell cycle.

The incorporation of additional cell types into *in vitro* models increases their complexity and their relevance to the *in situ* structure they are representing. The additional cell type(s) can vary depending on the purpose of the research (Lehmann *et al*., 2011, Amann *et al*., 2014, Lawal *et al*., 2018). Costa *et al* (2019) recreated the site of gaseous exchange using a triple-cell ALI culture model, utilising NCI-H441 cells (type-II alveolar epithelial) and d-THP-1 macrophages, and HPMEC-ST1.6R (microvascular endothelium) on the apical transwell membrane surface, with an additional layer of HPMEC-ST1.6R on the basolateral transwell membrane surface. Alternatively, HPMEC-ST1.6R cells could be substituted with type-I alveolar epithelial hAELVi cells to construct a more representative model of the alveoli specifically (Kletting, 2017. Bateman *et al*., 2023). Co-cultures could also be implemented with a focus towards the immunological responses, such as the model devised by Lehmann *et al*., (2011), which utilised monocyte-derived macrophages and monocyte-derived dendritic cells in conjunction with A549 type-II alveolar epithelial cell line or 16HBE14o– bronchial epithelial cell line.

The most realistic *in vitro* lung models to represent the human system use primary cells, but due to short viability, complexity in manufacture, and cost, they are not often used in *in vitro* research. One of the most prominent producers of *in vitro* lung models is Epithelix, which use primary cells donated from clients to synthesize *in vitro* models cultured at the ALI. For example, the AlveolAir^{TM} model contains type-I pneumocytes, type-II pneumocytes and endothelial cells, all cultured at biologically-relevant ratios at the ALI (Epithelix - AlveolAir). Cell line co-cultures are commonly used to harbour a compromise between the complexity and realism of the intended biological structure, whilst remaining flexible and robust, to ensure reproducibility.

1.4.2 Exposure Methods and *in vitro* Particle Toxicology

The two key differences between particle exposure for *in vitro* assessment is based within the culturing environment of the cells. Alveolar epithelial cells can be cultured both in submerged or ALI conditions, and this affects how they can be exposed to particles, and how realistic they are in comparison to their representative model. For example, culturing alveolar epithelial cells at the ALI is more representative of the alveolar environment than submerged conditions but does require additional setup in comparison to submerged culturing (Meldrum *et al*., 2019). Furthermore, the method to expose these cells to particles differs; submerged conditions require only a concentration of particle suspension to be added into the cell culture medium, whereas culturing at the ALI opens up multiple methods of exposure. Administration of particles can still occur *via* the cell culture medium from the basal well, however the typical methods of exposure for ALI models uses dry-powder deposition systems, or aerosol exposure systems such as the Vitrocell Cloud12 (Barasova & Rothen-Rutihauser, 2019).

As previously stated, both A549 and NCI-H441 type-2 alveolar epithelial cell lines secrete pulmonary surfactant *in vitro*, when cultured at the ALI, which can reduce the uptake of positively-charged silica nanoparticles 41.2 nm in diameter (Radiom *et al*., 2020). This could also potentially reduce the uptake of other engineered nanomaterials such as MNPs.

CB is used across many *in vitro* studies and models, the toxicological effects of which are well-documented and therefore it instils confidence in the results when used in comparison to unknown samples. It is often used in studies related to occupational health hazards *via* inhalation. In addition to, but to a lesser degree, it can be argued that CB is a relevant particle control to use for PP toxicology studies, as CB and PP can be manufactured as nanocomposites together, so simultaneous exposure may occur depending on the source.

In lung epithelial cells, CB toxicity can induce hyperplasia, and due to the increased cell production, increases the likelihood of a cancerous mutation and tumour formation. The mechanism of this is determined to be due to histones modification and DNA methylation, diminishing the ability to regulate cell proliferation (Niranjan & Thakur, 2017). Furthermore, CB has been found to induce elevation of systemic levels of TNF-α, IL-1β, IL-2 and IL-6 amongst many other pro-inflammatory markers (Niwa et al., 2008. Cheng et al., 2023), and additionally IL-8 in the lungs (Zhang et al., 2014).

As there is limited research available for *in vitro* lung model exposure to PP or mask MNPs, it is logical to cover a range of toxicological assessments to develop as broad of an idea as possible behind the effects that these MNPs could have when inhaled on the lungs. Most MNP studies investigate the effects of polystyrene (PS) MNPs. Key points to investigate are cytotoxicity or cell death, genotoxicity, inflammatory response, cellular morphology, and barrier integrity, with assessment of oxidative stress and reactive oxygen species production helping to mesh the full pathway of toxic responses together, if any.

There are some standout endpoint assessments which should be conducted with a greater priority based upon effects determined by existing assessments on CB. CB has been found to induce elevated systemic levels of TNF-α, IL-1β, IL-2 and IL-6 amongst many other pro-inflammatory markers following inhalation (Niwa et al., 2008. Cheng et al., 2023), and additionally IL-8 in the lungs specifically (Zhang et al., 2014). Furthermore, multiple studies have used IL-1β, IL-6 and IL-8 to determine pro-inflammatory responses using *in vitro* models, based off of the knowledge that alveolar CB and $PM_{2.5}$ exposure can induce all of these.

IL-8 is a chemoattractant chemokine for neutrophils to the site of secretion and then proceeds to activate them (Pease & Sabroe, 2002). Due to the proximity of the alveoli to a capillary bed and being one of the main interleukins secreted by type-2 alveolar epithelial cells, IL-8 secretion is important to assess in this model (Boggaram et al., 2016. Meldrum et al., 2022). IL-6 is the other main interleukin secreted by type-2 alveolar epithelial cells but is more directly involved with cell death and apoptosis (Rincon & Irvin, 2012. Boggaram et al., 2016. Meldrum et al., 2022). IL-1β can be secreted by alveolar type-2 epithelium, and similarly to IL-6 mostly influential over apoptosis. In comparison to IL-8, it is scarcely produced in response to stimulus. All of these three interleukins, however, are main pro-inflammatory markers secreted by alveolar macrophages, in addition to TNF-α (García et al., 1999). TNF-α can be used as a positive control for pro-inflammatory assessments, due to its ability to induce strong responses in RnD Systems Sandwich ELSIA Kits, when following the SOP.

Cell viability assays determine acutely toxic responses. Exposing unprotected (without the temperature change suppression from cyrovials and insulated containers) mammalian cells to -80°C causes them to freeze too rapidly, allowing the formation of ice crystals which pierce the cellular membranes. It is an effective way to damage mammalian cells enough to achieve a very low viability (Song & Zhu, 2020).

Assessing the potential of a particle to cause genetic or chromosomal damage is relevant for determining tumourigenesis potential in a whole organism. The Micronucleus assay is an effective *in vitro* assay for genotoxic potential assessment, determined by methyl methanesulfonate (MMS), is a highly clastogenic DNA-alkylating agent, and due to this it is commonly used as a positive control for genotoxic assessments (Lundin, 2005). Cytokinesis-block (with cytochalasin-b) MN assay should be conducted in preference over non-blocked (non-cytochalasin-b) alternative, on the event that the tested material is both genotoxic and cytostatic (Fenech, 2006). Cytochalasin-b should be applied to the tested cells for 1-2 cell cycles; long enough to ensure cell division would have occurred (OECD, 2023). However, cells which proliferate at a slow rate, such as the NCI-H441 cell line (58 hours), would require

application of cytochalasin-b for 58-116 hours; the time for the cellular model to be kept at the ALI should be kept to a minimum to retain the model quality.

Adherent cells and cell lines can completely cover the base of the container in which they are growing. Using this, it is possible to conduct barrier integrity assays, such as transepithelial/endothelial electrical resistance (TEER) (Srinivasan et al., 2015), or paracellular pathways to assess integrity can be studied, by using non-digestible polysaccharides such as dextran (Frost et al., 2019). Colour or fluorescent-conjugated dextran molecules <70 kDa, can diffuse across monolayers *via* tight junctions, with damage increasing the rate of diffusion (Thomas et al., 2017. Azizi et al., 2015).

1.4.3 MNPs Synthesis and Their *in vitro* Exposure

Intentional MNP synthesis is typically conducted using two broad approaches: a top-down approach, which involves the degradation of macroplastics or standard sources of plastics into smaller particles *via* mechanical or chemical degradation; or a bottom-up approach where the particles are chemically synthesized from reagents (Ivleva, 2021). Top-down approaches (figure 1.12) include milling and centrifugation processes which mechanically break the materials down, fragmenting them into smaller particles although research into these processes is relatively young. A top-down approach such as cryogenic milling techniques such as those described by Kühn *et al*., (2018) and Parker I., (2023) utilise centrifugal grinding mills, which are intended to grind coarse particles into a smaller and more homogenous population. However, is not the most effective method by itself to acquire the smallest particles, and was subsequently followed by ball milling by Parker, *et al*., (2023), and then by size fractionation *via* sieving. These friction-based methods of synthesis produce significant heat, and due to the potential melting of plastic, constant application of liquid nitrogen must be conducted to maximise the plastics' brittleness. In comparison, the bottom-up approach (figure 1.12) typically utilises nanoprecipitation of MNPs, but at present the ability to control the size of the particles is absent, despite these observed particles being consistently <1 μm in diameter (Tanaka *et al*., 2021, 2023). This basis of this method involves the injection of a polymer solution into an antisolvent, which precipitates the polymers as nanoparticles for extraction.

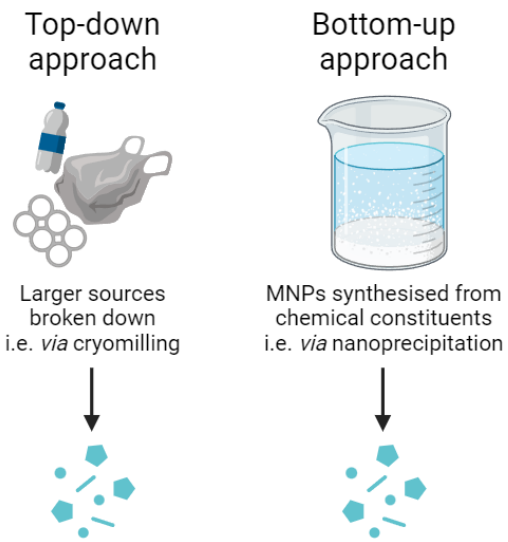

Figure 1.12 - Visualisation of top-down and bottom-up approaches (created by myself, using Biorender.com)

The determination of polydispersity index (PDI) isn't a major factor in assessing the toxic effect of particles by itself, but can be used to help understand whether the MNP synthesis method is capable of producing a homogeneous population.

It can be assessed using Dynamic Light Scattering (DLS), and is calculated from the relationship between two factors, both of which are additionally determined by DLS: the Z-

average (mean particle diameter, d) and the standard deviation (SD) of particle diameter (σ). $PDI = (\sigma/d)^2$ (Raval et al., 2019). For example, if a sample has an SD of 100 nm and a Z-average of 500 nm, then PDI = 0.08, which is at the low-end of a 'narrow monodisperse' population, whereas if SD = 900 nm and Z-average = 1000 nm, then PDI = 0.81, which is a 'broad polydisperse' population (Nobbmann, 2021).

An understanding of the particles themselves is necessary in order to develop idea as to why certain events are happening, even before implementing them into exposure systems. The key points to cover here are: Average size (or aerodynamic diameter), realism to purpose and lung model, their ability to co-operate with exposure system (i.e. are they too large to pass through exposure system? would these particles realistically interact with these cells?); Zeta potential (i.e. handing - material loss, cellular interactions (Shao *et al*., 2015)); morphology (as discussed previously, i.e. fibrous/rod-shaped/spherical etc); elemental analysis (determination of what constitutes the material, are there any contaminants from the production process).

In an ideal particle inhalation toxicology assessment, the aerodynamic diameter of the particles would be calculated. The aerodynamic diameter of a particle is defined as its diameter, at equal terminal velocity as if that particle was a perfect sphere of standard, 1 g/cm^3, density (DeCarlo et al., 2004). It is possible to calculate the aerodynamic diameter from the geometric diameter provided you know/can assess the particle density (ρ_P), density of gaseous medium (such as atmospheric pressure, ρ_0), and the dynamic shape factor (χ) (de Boer et al., 2002. Moebs et al.). $Aero.diameter = Geo.Diameter \times \sqrt{\frac{\rho P}{\rho 0\, \chi}}$ (Miyamoto et al., 2020).

Zeta potential is the measure of electrical charge of a particle at the 'slipping plane', which is an imaginary boundary of a field of ionic charge. Figure 1.13 depicts a particle, the ionic field, separated into the strongly-bound stern layer and the looser diffuse layer, and the slipping plane where zeta potential is measured (Lowry et al., 2016). More positive zeta potential values of nanoparticles of the same material have been shown to elicit increased cell death due to much greater interaction force to cells, a feature that Shao *et al* (2015) demonstrated using biopolymer nanoparticles.

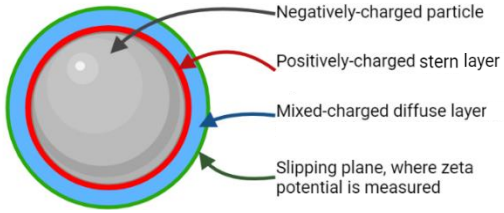

Figure 1.13 - Zeta potential diagram (created by myself, using Biorender.com)

Physicochemical assessment of the materials following their production is imperative to determine whether the material is correct following production, and it also enables to form predictions of how the material could interact with the cell models and why (Tantra, *et al*., 2016).

Using the cellular models mentioned above it is possible to expose these cells to chemicals and particles in a variety of ways. Most commonly, the exposure *via* submerged conditions, where cells are cultured in a flask and a concentration of particle or chemical is added to the cell culture medium. However, in the interest of inhalation models, it is possible to conduct exposures at the air-liquid interface, using either aerosol exposure systems or dry-powder systems. Due to the exposure conditions this project intends to replicate, an aerosol system would be more suitable than a dry-powder system for exposure. Throughout this thesis, the use of 'Vitrocell' refers to the Vitrocell Cloud 12 Aerosol Exposure system.

1.5 Aims, Objectives, Hypothesis

1.5.1 Aims

The aim of this project is to determine the constituent materials/elements of level-2 face masks, and to determine the impact that PP MNPs and MNPs derived from surgical level-2 face masks could potentially have on human lungs when inhaled.

1.5.2 Objectives

- Synthesis of PP MNPs, and two distinct batches of MNPs derived from surgical face masks, representative of (A) the debris inhaled from mask misuse, and (B) the MNPs generated from whole-mask waste in the environment.
    - Conduct characterisation on the created MNPs: size distribution, zeta potential, morphology, elemental analysis
- Cultivate a monoculture of NCI-H441 type-2 alveolar epithelial cells, at the air-liquid interface, and deposit a concentration range of the created MNPs.
- After 24 hours, process the cell models to undergo a range of endpoint assessments to scope the particle exposure effect
    - pro-inflammatory response, cell viability, genotoxicity, barrier integrity and cellular morphology

1.5.3 Hypothesis

The surgical mask MNPs will instigate the greatest adverse effects in comparison to PP MNPs due to the potential presence of additive chemicals, which are unknown. The whole-mask MNPs will produce a greater response than the innermost layer only, due to the additional two layers of material, which are structurally different, and the blue layer of which, is coloured so by an unknown additive which could cause an adverse response. At the current state of research, an increase to IL-8 production is expected across the MNP samples.

Chapter 2 - Materials and Methods

I would like to give additional acknowledgement to the Environmental Research Group at Imperial College London for this section, without whom, the acquisition of the MNPs used in this project may not have been possible.

Dr Stephanie Wright: External supervisor

Eric Auyang: Milling processes of plastics

Joseph M. Levermore: Pyrolysis-GC-MS

2.1 Outline of Data Collection Methods

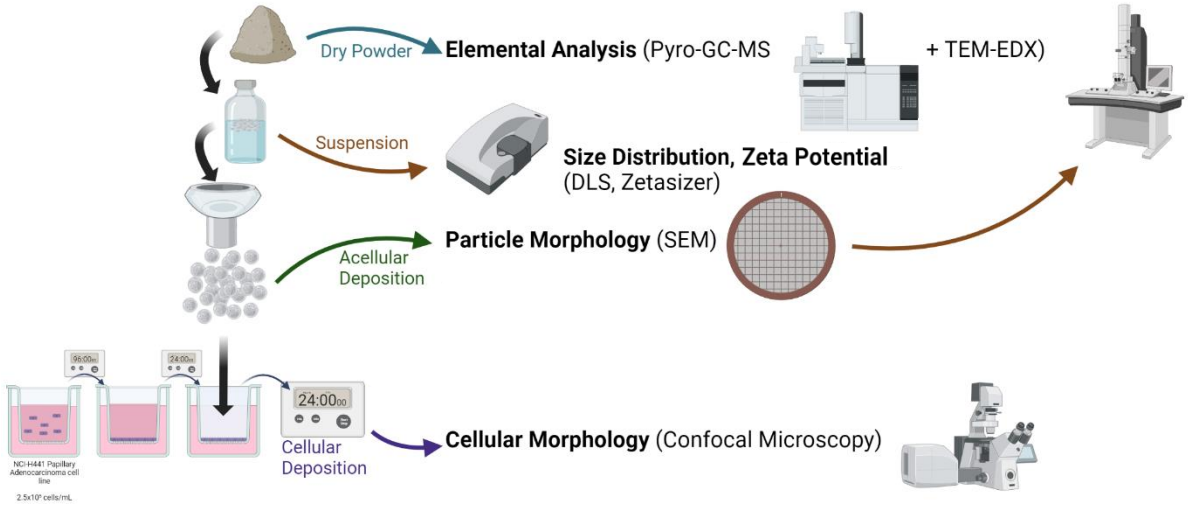

Figure 2.1 - Graphical outline of exposure approach and data acquisition (created by myself, using Biorender.com)

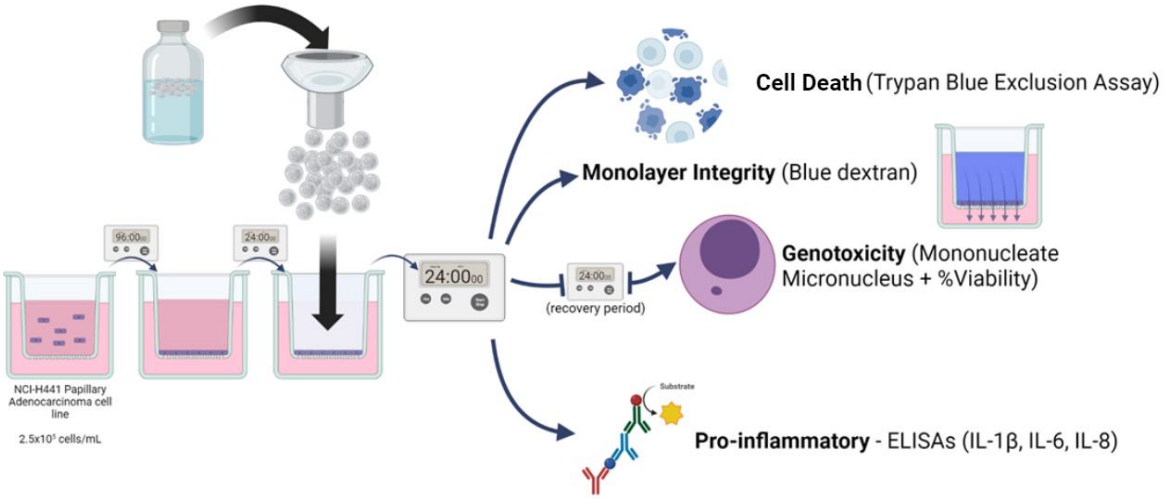

Figure 2.2 - Graphical outline of exposure approach and cellular endpoint analysis (created by myself, using Biorender.com)

2.2 Chemicals and Reagents

Table 2.1 - List of materials and chemicals, and their source companies

Roswell Park Memorial Institute (RPMI) 1640 Cell Culture Medium	Gibco, UK (31870-025)
Phosphate Buffered Saline (PBS)	Gibco, UK (10010-015)
Penicillin/Streptomycin (P/S)	Gibco, UK (15140-122)
Trypsin-Ethylenediaminetetraacetic acid (EDTA) 0.05%	Gibco, UK (25300-062)
L-Glutamine 200mM	Gibco, UK (25030-024)
Foetal Bovine Serum (FBS)	Gibco, UK (A5256701)
Giemsa MN Staining Buffer Gurr	Gibco, UK (10582-013)
Sodium Chloride (NaCl)	Sigma Aldrich, UK (S3014-5KG)
Bovine Serum Albumin (BSA)	Sigma Aldrich, UK (A7906-100G)
Triton-X100	Sigma Aldrich, UK (23,472-9)
Paraformaldehyde (PFA)	Sigma Aldrich, UK (158127)
Glycine	Sigma Aldrich, UK (1003262288)
Trypan Blue (0.4%)	Sigma Aldrich, UK (T8154-100ML)
Dimethyl Sulfoxide (DMSO)	Fisher Scientific, UK (J66650.AK)
Ethanol (EtOH) Absolute	Fisher Scientific, UK (E/0650DF/17)
Tween20	Fisher Scientific, UK (BP337-100)
Xylene	Fisher Scientific, UK (383940050)
Dibutylphthalate Polystyrene Xylene (DPX)	Fisher Scientific, UK (D5330/05)
Pluronic F-127	Fisher Scientific, UK (P6866)
Phalloidin (Alexaflour 633)	Fisher Scientific, UK (A22284)
DuoSet Human IL-1β/IL-1F2	R&D Systems, USA (DY201-05)
DuoSet Human IL-6	R&D Systems, USA (DY206)
DuoSet Human IL-8/CXCL8	R&D Systems, USA (DY208)
Substrate Solution	R&D Systems, USA (DY999)
Blue Dextran	GE Healthcare (17-0360-01)
Tris(hydroxymethyl)aminomethane (Tris)	Melford Biolaboratories Ltd. (T6040)
DAPI with Vectashield	Vector Laboratories, USA (H-1200)
Giemsa Stain Gurr	VWR Chemicals, UK (MFCD00081642)
Immersol 518F	Zeiss, UK (10539438)

2.2 Material Preparation

Prior to their cellular deposition, material characterisation or endpoint assessment, the formation of the MNPs was conducted at Imperial College London using novel techniques. Commercial, non-respirable PP MNPs (C-PP) and commercial respirable PP MNPs (R-PP) preparation will be discussed in section 3.2.1, whereas the preparation for mask MNPs will be detailed in section 4.2.1.

2.3 MNP Characterisation

2.3.1 Pyrolysis - Gas Chromatography - Mass Spectrometry

Pyrolysis-Gas-Chromatography Mass-Spectrometry (pyro-GC-MS) (LECO Pegasus® BT 4D GCxGC TOF MS + OPTIC 4. LECO, UK) was conducted using some of the dry mass of MNPs created. Each type of MNP individually underwent thermal desorption (350°C), and pyrolysis (800°C), both of which elicit different classes of degradation.

The ChromaTOF® software (LECO, UK) was used to identify the eluted compounds represented by the spectral peaks generated, by cross-referencing the retention indices of each peak (or collection of peaks) with the known compound retention indices of the National Institute of Standards and Technology (NIST) Library (NIST MS Search 2.3), using a plastic-focused data processing protocol derived from compounds eluted from tyre-wear. The presence of PP was confirmed using targeted analysis within each sample, which is typically eluted as 2,4-dimethyl-1-heptene or other C_9H_{18} compounds (Ballice & Reimert, 2002).

Untargeted analysis was used determined the presence of other eluted compounds, by the application of filtering criteria; peaks without a NIST Library retention index were removed from the list, and any peaks or peak groups which had a similarity score of less than 800 to a NIST Library compound were also removed. From the detected compounds, -siloxanes were also omitted, as they are indicative of glass contaminants from the sample vial.

The lists of eluted compounds for each material were merged together respectively for thermal desorption and pyrolysis. For each degradation level, all of the eluted compounds across all materials were cross-referenced, removing all duplicate peaks, to produce a list of all unique compounds for each material. The product datasheet states that the size of C-PP particles were <90 μm diameter (Withers, 2019), so to confirm this, a high-resolution inverted microscope to determine the average diameter of the particles, and to observe the agglomeration of the particles.

2.3.2 Size Distribution, Dynamic Light Scattering and Zeta Potential

Dynamic Light Scattering (DLS) was conducted using a Zetasizer Nano ZS (Malvern Panalytical, UK) with ZEN0040 low-volume disposable cuvettes. Each MNP was suspended in ddH_2O at 100 μg/mL and run ten times each at 25°C and 37°C (room temperature and average internal human temperature, respectively), refreshing the tested volume between each run, following washing with Ethanol Absolute and air-drying, to determine the Polydispersity Index (PDI), the homogeneity of the suspended particles.

Zeta potential was measured using an MNP suspension concentration of 1 mg/mL drawn into DTS1070 disposable folded capillary cells. Ten individual runs each at 25°C and 37°C, were conducted for each material, and the capillary cells were washed with Ethanol Absolute and air-dried in between each run, whilst a new, clean capillary cell was used per material.

2.3.3 Suspension

Due to PP being an organic compound without any polar regions, it does not suspend effectively in water, without agitation, it returns to the surface of the water within a couple of minutes. Using a variety of different dispersants, the ability to suspend C-PP was investigated. These dispersants were double-distilled water (ddH_2O) (figure 2.3A), PBS (figure 2.3B), 1% DMSO (figure 2.3C), 1% BSA (figure 2.3D), 0.1% Tween20 (figure 2.3E), and 0.1% Pluronic-F127 (figure 2.3F). However, exposing lung models to these materials questions the realism of their use in this system, as all suspensions other than water, are not materials which are typically inhaled. Both Tween20 and Pluronic-f127 are detergents, and Tween20 can be used for mammalian cell lysis at concentrations as low as 0.05% (Neugebauer, 1990), exposing cell models to this would interfere with the assessment of PP toxicity.

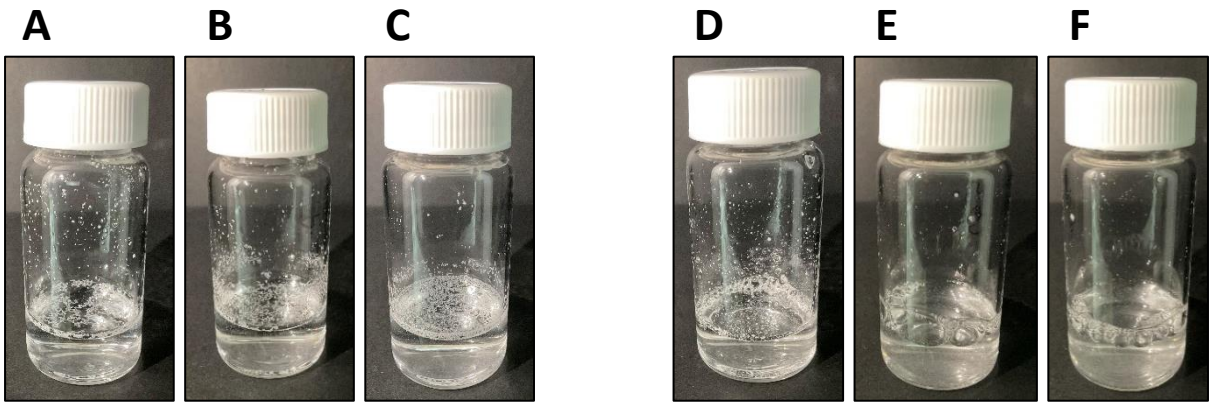

Figure 2.3 - The behaviour of commercial polypropylene in various solutions. ddH_2O (A), PBS (B), 1% DMSO (C), 1% BSA (D), 0.1% Tween20 (E), 0.1% Pluronic F-127 (F). Images photographed by myself.

2.4 Cell Culture

2.4.1 Type-II alveolar epithelial Cell Line (NCI-H441)

All tissue culture was conducted inside a standard Class II Laminar Flow Hood (Scanlaf Mars, Denmark). When working with toxic materials a designated Class II Laminar Flow Hood fitted with additional particle filtration was used. NCI-H441 (type-II alveolar epithelial cell line. American Type Culture Collection (ATCC) number: CRM-HTB-174^{TM}) (ATCC, 2023) cells were acquired from liquid nitrogen, stored in cryovials containing 95% CCM and 5% DMSO, to a total volume of 2 mL. To thaw, the vials were placed into a buoyancy aid inside a water bath (set to 37°C) for two minutes. Whilst thawing, 15 mL of RPMI 1640 Cell Culture Medium (CCM) (Gibco®, UK), featuring 10% FBS, 1% P/S, and 1% L-Glutamine was pipetted into a T-75 vented cell culture flask and placed into the incubator to equilibrate. The thawed cells were pipetted into a 15 mL falcon tube and topped with 10 mL CCM. The tube was centrifuged at 125g for five minutes to form the cell pellet. The supernatant was removed, and the pellet was resuspended in 1 mL CCM before being transferred into the T-75 flask.

2.4.2 Passaging of NCI-H441

Every three or four days, when cells became highly confluent, they were passaged by removing the media and washed once with 7 mL of sterile PBS (Gibco®, UK). The PBS was poured off and replaced by 4 mL trypsin-EDTA (0.02%), then the flask was returned to the incubator for 10 minutes to detach the adherent cells. Every second day in-between passaging, the running flask would undergo a media change, where the current CCM would be removed from the flask and replaced with fresh CCM. After most cells had detached, the flask was returned to the culture hood, 6 mL CCM was added to the flask to neutralise the trypsin, and all 10 mL of suspension was transferred into a 15 mL falcon tube and centrifuged at 125g for five minutes. The supernatant was poured away, and the formed pellet was resuspended in 1 mL CCM. From the resuspended cells, 100 µL was transferred into a fresh flask containing 15 mL CCM and were distributed evenly throughout the flask.

2.4.3 Cell Seeding

Following centrifugation during the passaging process, the resuspended cell pellets for each harvested flask were compiled into a single 15 mL tube. The cell suspension was assessed using a Luna II^{TM} automated cell counter (Logos Biosystems, France). Into an Eppendorf tube, 10:10 µL volume ratio of cell suspension:(0.4%) Trypan Blue mixture was prepared and transferred onto a Luna II slide to determine live cell count, and the necessary CCM dilution for cell seeding ($2.5x10^5$ cells/mL). The seeding concentration of was chosen due to consistency in forming 1-2 layers of confluent cells at the ALI 72-hours post seeding (Ren *et al*., 2016), in 12-well inserts (Corning, USA). A volume of 1.5 mL CCM was pipetted into each basal well of the 12-well Companion Plate and 1mL into each apical well (Corning, USA) as depicted in figure 2.4A.

The seeded inserts were incubated at 37°C for 96 hours, after which the basal wells received a media change, and the apical wells were taken to the ALI by removing the apical well media (figure 2.4B). The plates were returned to the incubator for 24 hours. Cells were seeded for three consecutive weeks for each material sample to achieve a triplicate of distinct biological replicates for each endpoint to be conducted.

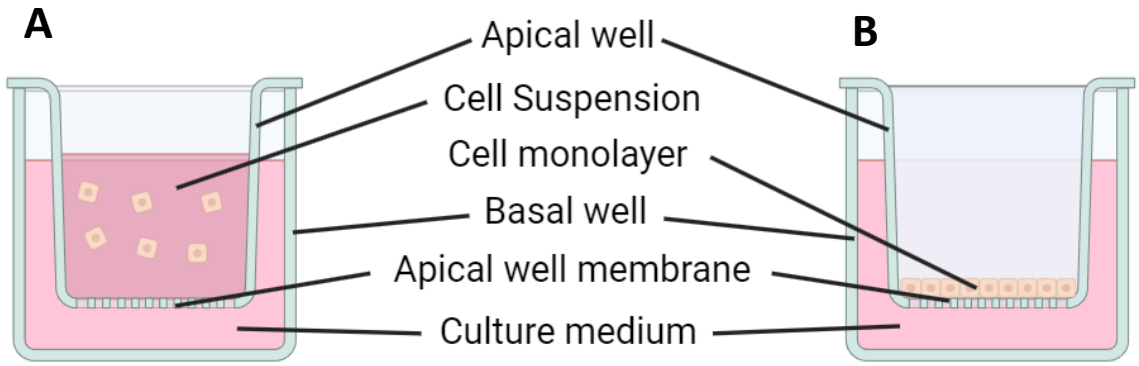

Figure 2.4 - Depiction of well layout following cell seeding (A). Depiction of well layout following transfer to ALI (B). (created by myself, using Biorender.com)

2.5 Aerosol Exposure and Deposition Measurement

To deposit material onto the ALI cell cultures, the Vitrocell® Cloud12 (Vitrocell Systems, Germany) (referred to as 'Vitrocell', from here on in) was utilised, alongside Aeroneb® Lab Nebulizer Unit, and 4.0-6.0 μm Median Mass Aerodynamic Diameter, (MMAD) pore mesh nebulisers (Aerogen, Ireland). An established SOP was followed throughout the deposition process. The Vitrocell was used inside a designated toxic material handling hood, and at least 30 minutes prior to use, it is switched on and the baseplate is left to heat up to 37°C (± 1°C fluctuation). Once heated, 3 mL of CCM was added into each well of the Vitrocell, except for the quartz crystal microbalance (QCM) well. The cultured apical wells were placed into the base wells containing CCM. Data acquisition was activated, to determine the stability of the signal prior to exposure, and was acceptable if fluctuation was within ± 25 ng/cm^2 in 30 seconds. Once acceptable, 200 μL of material suspension was added into the nebuliser, data acquisition restarted and the nebuliser was activated until the suspension had fully passed through, at which point, the nebuliser was deactivated and timed for six minutes. After six minutes had passed, the exposure chamber was removed for 1 minute to allow the QCM to dry, and then replaced onto the base module for two minutes. Mass deposition was determined by the mean average of the last 30 values recorded during the two-minute period when the exposure chamber had been replaced onto the system (Bannuscher *et al*., 2022). Appropriate quality control measures were also conducted throughout, by the SOPs' recommendations.

Figure 2.5 - Vitrocell Cloud12 Aerosol Exposure System. Image photographed by myself.

2.6 Microscopy

2.6.1 Scanning Electron Microscopy (SEM)

Transmission Electron Microscopy (TEM) grids placed into the Vitrocell TEM grid holder and into a dry base module well and inserted alongside cellular depositions. The target deposition on these grids was 1.0 μg/cm^2.

One TEM grid was mounted onto the SEM stage and inserted into the SEM, immediately followed by image calibration. The castle method was used to collect representative images of each material, with images being collected at x3000, x15,000 and x40,000 magnification. Brightness and focus were adjusted throughout image collection to maximise the quality of the images collected. The most effective image collected for each material at each magnification was selected as the representative.

2.6.2 Scanning-Transmission Electron Microscopy – Energy-Dispersive X-Ray (STEM-EDX)

The TEM-FEI TALOS was used to acquire additional information from the deposited samples which the SEM could not provide. TEM images were acquired following the same process as the SEM, as described in 2.6.1, but using different magnifications in relation to the viewed artefacts. Images acquired from TEM were collected as a representative.

In addition to TEM, STEM-EDX was conducted to collect High-Angle Annular Dark-Field (HAADF) images which mapped the elements detected in the viewed sample at 14,000x magnification. All elements were open to detection, however, only maps for the detected elements were plotted and used as a representative for the sample. Each elemental map was overlayed onto the dark-field image to depict the density and distribution of each element in the image. Sodium and chlorine were grouped together in their presentation, as they are both present within the nebulised suspension.

2.6.3 Confocal Laser Scanning Microscopy (LSM)

To fix the samples for confocal Laser Scanning Microscopy (LSM) imaging, the media was removed and the transwell membranes were washed three times with PBS. Both the apical and basal wells were filled with Paraformaldehyde (PFA), for 15 minutes, before being replaced with glycine and the plate being sealed and kept at 4°C until use. The glycine was removed, and the wells washed with ice-cold PBS three times, before adding Triton X-100 for 15 minutes to permeabilise the cells and being washed again with ice-cold PBS three times The membranes were cut from the wells and placed cells-down into PBS to hold, whilst a drop of 1:100 4′,6-diamidino-2-phenylindole (DAPI) and 1:1000 Phalloidin was placed onto parafilm. The membrane (still cells-down) was transferred onto the DAPI/phalloidin drop, and another drop was added to the topside, and incubated at room temperature, in darkness for 45 minutes. Three wells of a 6-well plate were filled with PBS, and the membranes were transferred across all three wells to wash them, then placed cells-up onto a microscope slide, and a drop of Dibutylphthalate Polystyrene Xylene (DPX) was added to the topside, before affixing a cover slip. The cover slips were secured using clear nail varnish and stored at 4°C in darkness until they were imaged the following day.

Representative images were taken at 200x magnification and 630x magnification (10x eyepiece + 20x / 63x objective), across the top concentration exposure for each material sample. The smart setup function was used to provide the best signal outcome multi-channel image between phalloidin and DAPI, of the LSM setting. Master gain was adjusted accordingly to balance the fluorescence of each fluorophore prior to taking the image and by using the ‘range indicator’ function.

The two fluorophores used were DAPI, which binds to dense regions of adenine-thymine in DNA, and Alexafluor^{TM} 633 Phalloidin, which binds to the membrane protein, F-actin.

2.7 Trypan Blue Exclusion (TBE) Assay

The basal well media was collected for use in the Enzyme-Linked Immunosorbent Assays (ELISAs). The Trypan Blue Exclusion Assay was conducted 24 hours following exposure. Each corresponding apical well was washed with 1mL sterile PBS, which was then replaced by 500 µL 0.4% trypsin-EDTA and returned to the incubator for 10 minutes, after which, an additional 500 µL trypsin-EDTA was added for a further 10 minutes. Once cells had mostly detached, they were lightly agitated by a pipette tip, and transferred into a 10 mL falcon tube. 1 mL of CCM was re-added into each apical well and agitated to maximise the collection of cells, and also transferred into the same falcon tube, before another 1 mL CCM was added to the top of the falcon tube. The falcon tubes were balanced and centrifuged at 125g for five minutes to form a pellet. The supernatant was poured away, and the pellet was resuspended in 1 mL CCM. A mixture of 10:10 µL volume ratio of Trypan Blue:cell suspension was made as in section 2.4.3, and using the haemocytometer, the % cell viability and live cell count were calculated in cells/mL. This was conducted in biological triplicate.

2.8 Blue Dextran

Firstly, the media was collected for use in the ELISAs, and the apical wells were washed three times with sterile PBS. This endpoint assessment had two different positive controls; one did not contain an epithelial cell monolayer, and the other did contain a monolayer, but was exposed to trypsin following the method in section 2.7 (these cells were only exposed to trypsin, not removed from the well).

In the basal well, 1mL of fresh media was added, and 250 µL of (2.5 mg/mL) Blue Dextran solution (in sterile PBS) was added to the apical well and returned to the incubator for two hours. After two hours had passed, the plate was removed from the incubator and 3x200 µL of media from the basal well of each exposure condition was pipetted into different wells of a 96-well plate as technical triplicate. The plate was then read by a spectrophotometer (Tecan – Sunrise^{TM}, Switzerland) to determine the absorbance of each media sample. Each technical triplicate was additionally conducted as biological triplicate.

2.9 Mononucleated Micronucleus Assay

This assay followed the mononucleated form of the protocol from the Organisation for Economic Cooperation and Development (OECD)-approved Micronucleus assay - Test number 487: *In vitro* Mammalian Cell Micronucleus Test (OECD, 2023). The most common version of this method would use cytochalasin-b, followed by the scoring of binucleated cells containing a micronucleus, followed by the calculation of the Cytokinesis-Block Proliferation Index (CBPI). In this approach, cytochalasin-b was not used, mononucleated cells containing a micronucleus were scored, and corresponding cell death (% viability) by using the TBE assay. Data was collected as a technical quadruplet in biological triplicate.

The purpose for the assessment of mononucleated cells is to determine the genetic damage prior to cellular division, whereas the binucleated approach identified both genetic damage which has occurred both prior to, and during cellular division. Therefore, if conducting the exact same experiments, but both the mononucleated and binucleated approaches were conducted on the same appropriate cell line, then the prevalence of micronuclei in binucleated

cells could be greater than in mononucleated, due to their formation by multiple mechanisms (Kirsch-Volders, 2001. Fenech et al., 2003).

A positive control of Methyl methanesulphonate (MMS), a known and potent clastogen, was used at a concentration of 1.5 μg/mL.

2.9.1 Harvesting

After 24 hours post-exposure, each apical well was washed with 1 mL PBS three times, the basal well media was changed, and the plate was returned to the incubator for a 24-hour recovery period.

The plates were removed from the incubator after 24 hours, and the apical wells were washed once more with PBS. The TBE method as previously written was conducted, with one adjustment; the cell pellet was resuspended in PBS instead of CCM. The remaining cell suspension proceeded with the Mononucleated micronucleus (mono/MN) assay.

2.9.2 Slide Preparation

Four glass slides per condition/concentration were mounted onto Cytospin clips and placed inside the Cytospin. Into mount, 100 μL of the corresponding cell suspension was added, before being spun 10 minutes. The slides were removed and immediately fixed in 90% Methanol at -20°C for 10 minutes. The slides were air-dried overnight. Once dry, the cytodots were stained with a 1:4 volume ratio mixture of Gurr Giemsa stain:Gurr staining buffer and let to permeate for 12 minutes, before being washed three times in vats of staining buffer. The slides were again air-dried overnight. The slides were submerged in xylene for five seconds, then laid flat to air-dry and a drop of DPX mounting medium was placed onto the cytodot and a cover slip was laid on top and pressed to release air bubbles.

2.9.3 Scoring

The castle-method was used to count unique cells on each slide. Each condition for each material had four slides, and 1000 mononucleated cells were counted on each slide, whilst also noting how many of which also contained a micronucleus, which was identified by the following characteristics: the same colour as the main nucleus, the same shape as the main nucleus, and if it is <1/3 of the size of the main nucleus.

2.10 Interleukin-1β, Interleukin-6, Interleukin-8 Sandwich Enzyme-Linked Immunosorbent Assays (ELISAs)

Reagent diluents were made for each ELISA type. Both IL-1β and IL-6 reagent diluents were a solution of 1% BSA in PBS, whereas IL-8 required a solution of 0.1% BSA, 0.05% Tween 20 in Tris-buffered saline (20 mM Tris base + 150 mM NaCl). Each ELISA required the specific standard concentration, capture antibodies, detection antibodies, and Streptavidin-HRP from the corresponding lot number. Wash buffer consisted of 0.05% Tween20 in PBS, block buffer consisted of 1% BSA in PBS, and stop solution consisted of 2N H_2SO_4.

All ELISAs were conducted accordingly to the SOP produced by R+D Systems. The IL-1β ELISA required undiluted supernatant, whereas the IL-6 and IL-8 both required 1:10 dilutions, in respective reagent diluent, for suitable interleukin detection. Tumour Necrosis Factor-α (TNF-α) was used as a positive control across all ELISAs at the concentration of 1 μg/mL. Three biological replicates were conducted for each interleukin, in technical triplicate.

The working concentration (specific to lot number used) of the respective capture antibodies were diluted in PBS (without BSA), 50 μL of which was added into each well of a 96-well half-plate. The plate was covered in foil and incubated at room temperature overnight.

In a container was filled with 500 mL wash buffer, the plates were washed three times, then aspirated and blotted onto paper towels. Each well was filled with 50 μL block buffer and incubated at room temperature for one hour. The plates were again washed and aspirated as before, and 50 μL of the appropriate supernatant samples were added to the wells in technical and biological triplicate. The first three columns of wells were reserved for a standard curve, by using a dilution series of a known concentration of interleukin, acquired by dilution factor of two, six times, in reagent diluent. The starting IL-1β concentration was 250 pg/mL, IL-6 was 600 pg/mL and IL-8 was 2000 pg/mL. The plates were covered and left to incubate for two hours at room temperature. This incubation step was followed by the addition of 50 μL of detection antibodies at their working concentration; the plate was covered and left to incubate at room temperature for a further two hours.

Aspiration and washing was repeated again, and the wells were filled with 50 μL Streptavidin-HRP at a dilution specific to the lot number, in reagent diluent. The plates were re-covered and incubated for 20 minutes at room temperature. The plates were washed again, and 50 μL of substrate solution was added to each well, the plates were covered and incubated at room temperature for 20 minutes. The substrate solution was a 1:1 ratio of Reagent A (H_2O_2) and Reagent B (Tetramethylbenzidine), and these should only be mixed immediately before application. After incubation, 50 μL of stop solution was added to each well, to prevent further colour change, and the plates were immediately read on the spectrophotometer (Tecan – Sunrise™, Switzerland).

2.11 Data and Statistical Analysis

All graphical data presents the mean average as a horizontal line, and each biological replicate as a point, in relation to the negative control as a fold-increase. Exceptions for this are the mononucleated micronucleus prevalence (presented as mean average ± Standard Error of the Mean), and blue dextran graphs which are presented as the raw mean average and raw biological replicate. These differences are both detailed in their respective figure legends. The labelled statistical analysis significance (*/$^{\#}$) corresponds to the one-way Analysis of Variance (ANOVA) and Tukey's Multiple Comparisons Post-hoc analysis on the raw data. Statistical analysis was conducted using Prism GraphPad 9 software (updated to Prism GraphPad 10 as of 27/06/2023). Significance across the results is labelled as one icon (*/$^{\#}$) if $p<0.05$, or two icons (**/$^{\#\#}$) if $p<0.001$.

Chapter 3 - Investigating the Synthesis of Commercial PP MNPs, Their Physicochemical Characterisation and Their Impact on Human Alveolar Monocultures *in vitro*

3.1 Introduction

Studies amalgamating the novel degradation techniques of PP MNPs, and their *in vitro* inhalation exposure are absent, which highlight a significant knowledge gap. The majority of MNP research primarily investigates the effects of PS MNPs and cannot be used as a representative covering the vast range of different plastics. As each different plastic possesses different phys-chem properties, conjugates, and structure, each of which play a part in the potential adverse effects to the human lungs upon inhalation. milling, degradation and handling required to effectively acquire the desired size range consistently. Additionally, there are no routine or standardised method for the milling of any plastic into MNPs for toxicological research, as MNPs are a relatively young concept in the toxicological field.

There is currently no documentation for the use of MNPs through a Vitrocell Cloud12 system or their cellular exposure at the ALI, so there was no guidance on biologically relevant mass depositions to use with *in vitro* ALI alveolar monocultures. Therefore, deposition masses derived from occupational CB exposures (Søs Poulsen *et al*., 2013) were utilised. Additionally, as much *in vitro* research on carbon black has been conducted, it was adopted as a positive particle control for use in comparison to PP, and to determine whether the exposure system, and endpoint assessments worked correctly.

Polypropylene powder is often used as an adulterant in industrial coatings and paints, but is also the main (and only) listed material used in the construction of surgical face masks. Inhalation exposure to pure PP is primarily a material which would be a more relevant safety concern in an industrial setting but is present within ambient air and water systems (Li *et al*., 2018). In 2023, PP dominated 20.0% of global market share for plastic polymers, second to polyethylene at 24.0%. However, Plastics Europe (2022) discerned from the Conversio Market & Strategy GmbH and nova-Institute, that 19.3% of polymers produced for the market in 2021 by any means globally, were PP, which was the greatest share by 4.9%. This large proportion of production highlights the necessity to research the impact that inhaling PP MNPs could have to humans. Despite this, there is a high variation of identified atmospheric MNP proportion between quantification studies. For example, some studies have identified PP to be the most prevalent or a highly-prevalent MNP, in contrast to many others who did not detect PP at all (Luo et al., 2024).

Both PP MNPs directly from purchase and cryomilled PP will be investigated in this chapter. The purchased PP powder is advertised to be <90 μm diameter particles, with no defined lower limit, >50% of which are between 55-75 μm in diameter. This size range does not represent the size of particles which would interact with the alveoli, typically requiring particles to possess an aerodynamic diameter <5 μm. Therefore, a cryomilling technique following an approach similarly conducted by Parker, *et al*., (2023), would be necessary to represent this.

The aim of this chapter is to determine how PP MNPs could potentially impact the human lung upon inhalation, by using various toxicological endpoint assessments, on an *in vitro* alveolar model exposed to aerosolised PP MNPs.

This will be conducted by the following objectives:

- Synthesise R-PP MNPs using novel degradation techniques and characterise their average diameter, polydispersity index, zeta potential, morphology, and elemental composition.
- Expose NCI-H441 monocultures, cultured at the air-liquid interface, to these PP MNPs for 24 hours.
- After 24 hours, harvest the necessary components of the models to determine a range of endpoint assessments: pro-inflammatory response, cell death, genotoxicity, monolayer barrier integrity and cellular morphology.

It is hypothesized that PP MNPs will not instigate an overall toxicological response as CB would but based upon their exposure to models representative of other organs, an increase to IL-8 production is expected.

3.2 Methods

3.2.1 Outline of Milling Process

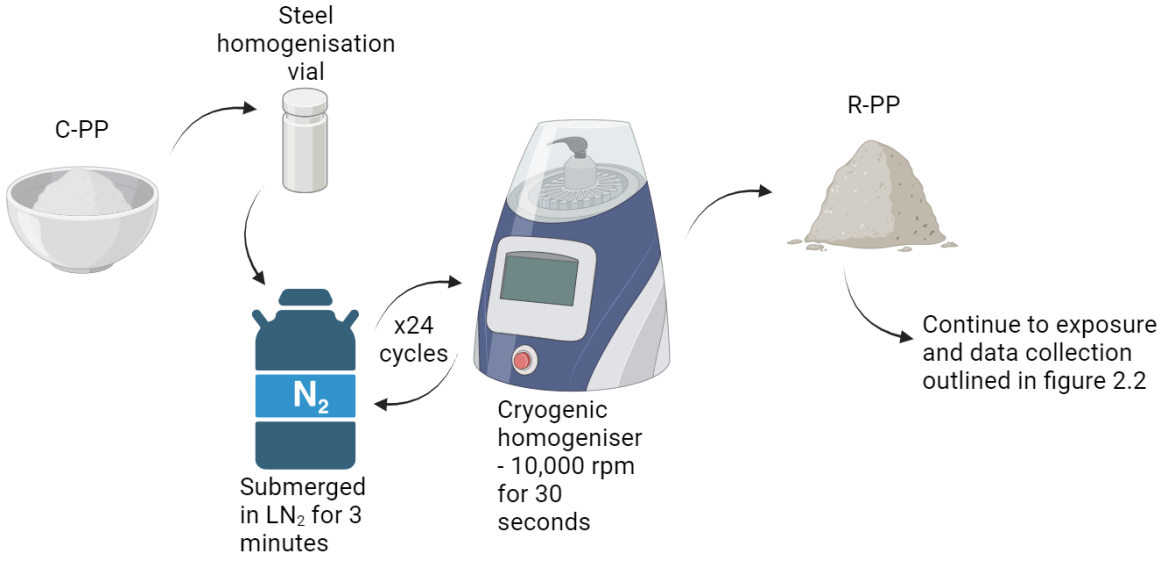

Figure 3.5 - Outline of C-PP to R-PP milling process (created by myself, using Biorender.com)

3.2.2 Particle Milling and Preparation

The preparation of R-PP MNPs will be described in sections 3.2.1.1. CB, and C-PP required no prior manipulation. Manipulation of C-PP was necessary to acquire R-PP.

3.2.1.1 Milling and Extraction

The C-PP powder (Goonvean Fibres Ltd., UK) was added to a steel homogenisation vial at a ratio of 1:1 g dry volume:steel mill balls. For 24 cycles, these vials were submerged in liquid nitrogen for three minutes, followed by 30 seconds at 10,000x rpm in a Cryolysis Evolution cryogenic tissue homogeniser, (Bertin Industries, France).

Ethanol Absolute was pipetted along the walls of each vial and to the inside of the lid, to allow transfer into a 50 mL Falcon tube. The contents of each falcon tube were poured onto the top of a stack of Endecott's Sieves, with descending pore sizes of 20 µm, 10 µm, 5 µm, then the receiver which collects particles <5µm in diameter. The contents contained in the receiver were collected and dried in the drying oven.

3.2.2 Material Characterisation

3.2.2.1 Pyrolysis-GC-MS

A dry mass of R-PP was used for pyro-GC-MS following the method in section 2.3.1.

3.2.2.2 Size Distribution, DLS, Zeta Potential

Size distribution, DLS and zeta potential were conducted as described in section 2.3.2, utilising PP and R-PP.

3.2.3 Cell Handling
Cell passaging was conducted as in section 2.4.2 and seeding was conducted as noted in section 2.4.3.

3.2.4 Aerosol Exposure
Prior to aerosolisation, all suspensions underwent sonication to break apart agglomerated and improve the efficiency of deposition, following the laboratory SOP. The probe was activated at 10% power, alternating 10 seconds on:off, for a total of four minutes uptime. Aerosol exposure was conducted as described in section 2.5 using CB, C-PP and R-PP. However, C-PP was ineffective with the exposure system, so the only target deposition of 0.5 $\mu g/cm^2$ was achievable.

3.2.5 Microscopy
SEM was conducted as described in section 2.6.1, STEM-EDX as in section 2.6.2, and Confocal LSM as in section 2.6.3, using CB, C-PP and R-PP.

3.2.6 Trypan Blue Exclusion Assay
The TBE assay was carried out in accordance with the method outlined in section 2.7, using CB, C-PP and R-PP.

3.2.7 Blue Dextran Assay
The process for the Blue Dextran monolayer permeability assay followed the description in section 2.8, using CB, C-PP and R-PP.

3.2.8 Mononucleated Micronucleus Assay
This assay was conducted as described in section 2.9, using CB, C-PP and R-PP.

3.2.9 Pro-inflammatory Cytokine Sandwich ELISAs
All interleukin ELISAs were conducted, with the necessary adjustments to reagents and samples based upon whichever interleukin was being quantified, as described in section 2.10, using CB, C-PP and R-PP.

3.3 Results

3.3.1 Characterisation

3.3.1.1 Dynamic Light Scattering (DLS)

Both the DLS and Zeta potential assessment demonstrated the heterogeneity of the commercial PP samples, both before and after milling. Both temperatures of C-PP PDI analysis returned the same values, 0.73±0.27, which peak at the maximum value and suggest the sample is greatly heterogenous. Additionally, the variance of R-PP also peaked at the maximum value of 1, but had midpoints of 0.75 and 0.96 at 25°C and 37°C, respectively (table 3.1). The R-PP MNPs possessed a more negative zeta potential than the C-PP MNPs as demonstrated in table 3.1. Temperature also affected the zeta potential, decreasing at the higher temperature. Variance within the PP was relatively low (6.83 mV at 25°C, and 9.13 mV at 37°C) in comparison to R-PP (33.71 mV at 25°C and 29.97 mV at 37°C) (table 3.1).

Table 3.1 - Polydispersity Index midpoint and midpoint-range, and Zeta Potential midpoint and midpoint-range of C-PP and R-PP at 25°C and 37°C.

Sample and Temperature (°C)	PDI Midpoint & Variance	PDI Mean Average	Midpoint & Variance (mV)	Zeta Potential Mean Average
C-PP 25	0.73 ± 0.27	0.726	-30.65 ± 3.42	-29.96
C-PP 37	0.73 ± 0.27	0.916	-35.06 ± 4.57	-34.64
R-PP 25	0.75 ± 0.26	0.668	-45.06 ± 16.86	-45.12
R-PP 37	0.96 ± 0.04	0.991	-55.06 ± 14.99	-51.96

3.3.1.2 Pyrolysis Gas-Chromatography Mass-Spectrometry

During Thermal Desorption (350°C), PP eluted into 14 unique compounds detected through pyrolysis-GS-MS, but 18 total peaks, with duplicate peaks of 'Ethanol, 2-(2-butoxyethoxy)-, acetate', '2-Propanol, 1-chloro-, phosphate (3:1)', '1,2-Benzenedicarboxylic acid, bis(2-methylpropyl) ester', and 'Hexanedioic acid, bis(2-ethylhexyl) ester' (figure 3.2).

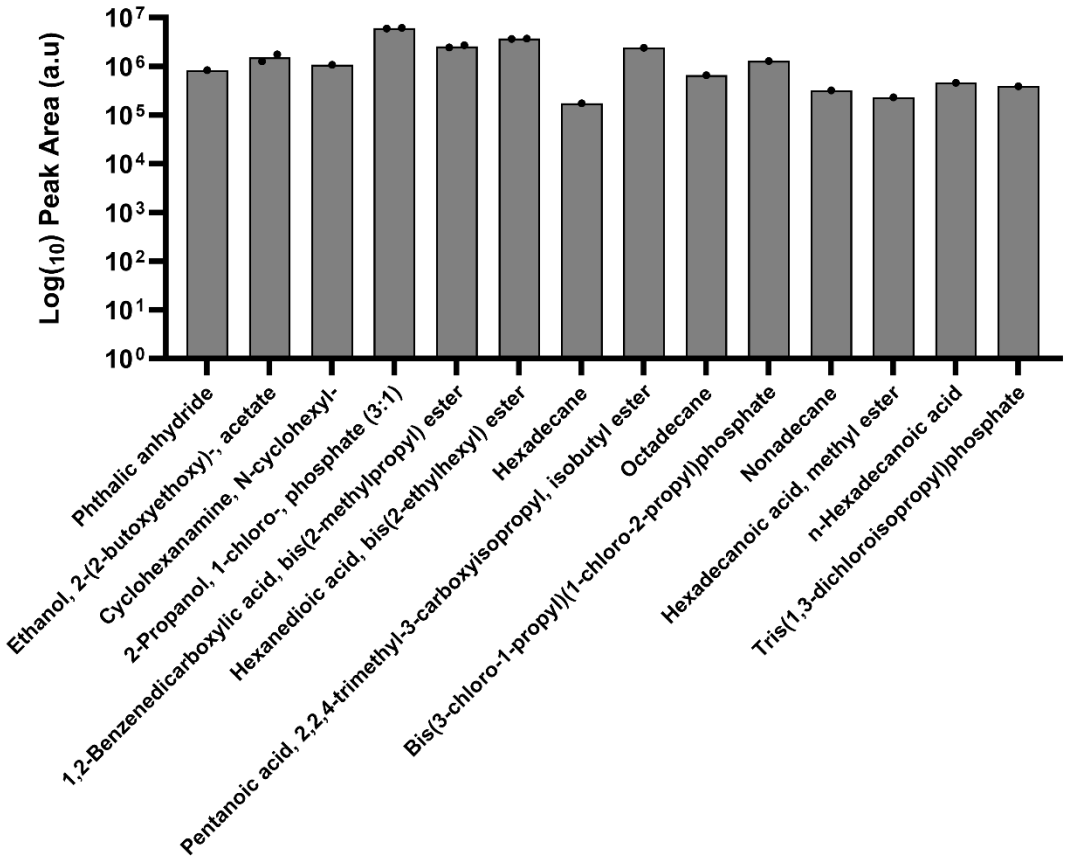

Figure 3.6 - Bar Chart displaying all unique compounds eluted from C-PP powder during Thermal Desorption (350°C), their number of recorded peaks, and the area under each peak.

When the temperature was increased to 800°C, targeted analysis of the sample allowed for the identification of polypropylene within the elute. Polypropylene typically eluted to 2,4-dimethyl-1-heptene, but also sometimes eluted to other C_9H_{18} compounds, but for simplicity, were all compiled to 2,4-dimethyl-1-heptene. After targeted analysis of PP, untargeted analysis was used to determine the other remaining compounds listed in figure 3.3, and their respective areas under the peak.

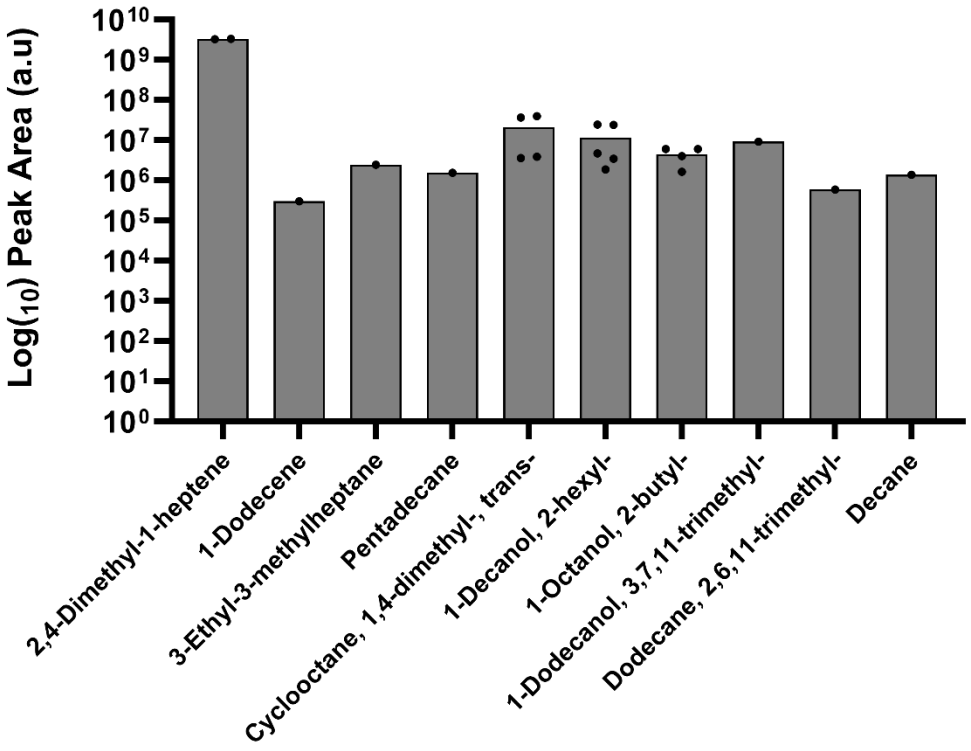

Figure 3.7 - Bar Chart displaying all unique compounds eluted from C-PP powder during Pyrolysis (800°C), their number of recorded peaks, and the area under each peak.

3.3.2 Aerosolisation

3.3.2.1 Mass Deposition

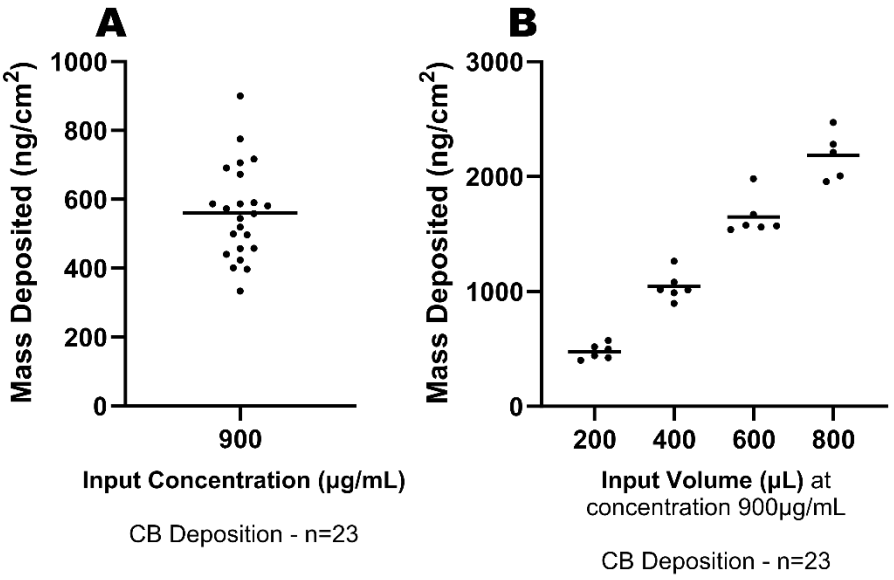

C

Target (µg/cm²)	Accuracy ± Precision (µg/cm²)		
0.5	**0.460**	±	**0.059**
1.0	**0.989**	±	**0.092**
2.0	**2.215**	±	**0.257**

Figure 3.8 - Deposition Data for CB. (A) Deposition scatter chart displaying the added mass of each individual deposition. (B) Deposition scatter chart showing the accumulative addition of mass throughout each cellular exposure. (C) Table showing the three chosen deposition targets, the actual achieved deposition medians, and variation within each target. Each point represents one deposition reading.

Target depositions of 0.5, 1.0 and 2.0 µg/cm^2, required one, two and four depositions of CB respectively, each of 200 µL at 900 µg/mL concentration, except for the third replicate of LSM samples, which only required one, two and three depositions to acquire each, for a total of 23 readings as seen in figures 3.4A and 3.4B. The mean average deposition was 0.561 µg/cm^2, as shown in figure 3.4A, and from this, the midpoint of the mass depositions were calculated for each target, and their variance. Figure 3.4C shows how the target concentrations were successfully met within these ranges.

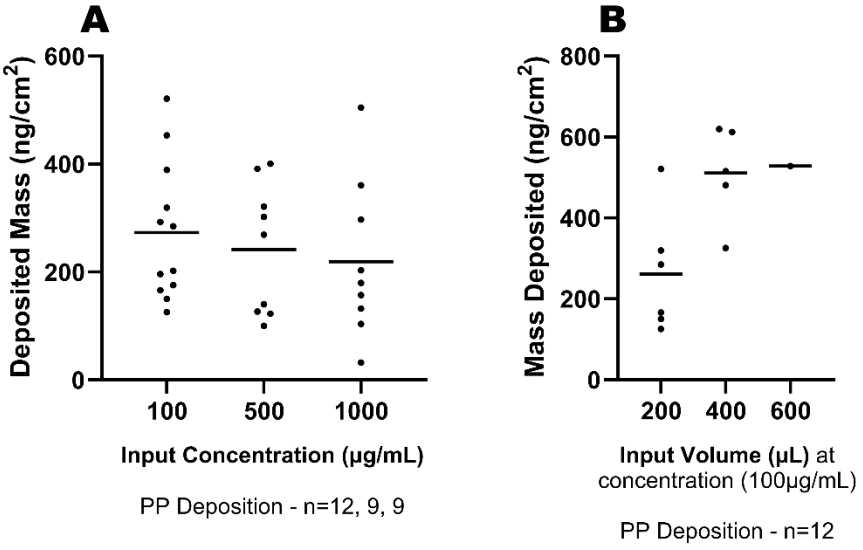

C

Target (µg/cm²)	Accuracy ± Precision (µg/cm²)		
0.5	**0.550**	±	**0.069**

Figure 3.9 - Deposition Data for C-PP. (A) Deposition scatter chart displaying the added mass of each individual deposition. (B) Deposition scatter chart showing the accumulative addition of mass throughout each cellular exposure. (C) Table showing the three chosen deposition targets, the actual achieved deposition medians, and variation within each target. Each point represents one deposition reading.

Only the lowest deposition target of 0.5 µg/cm^2 was achievable. Based upon these depositions in figures 3.5A and 3.5B it could have taken between 8-12 runs to achieve 2.0 µg/cm^2, at which point the cells would have been out of incubation in excess of two hours, which opposes the SOP for this approach (Barasova and Rothen-Rutihauser, 2019). C-PP presented a negative correlation of input concentration vs deposited mass in figure 3.5A, where there was also a large variation between nebulisation of the same concentration.

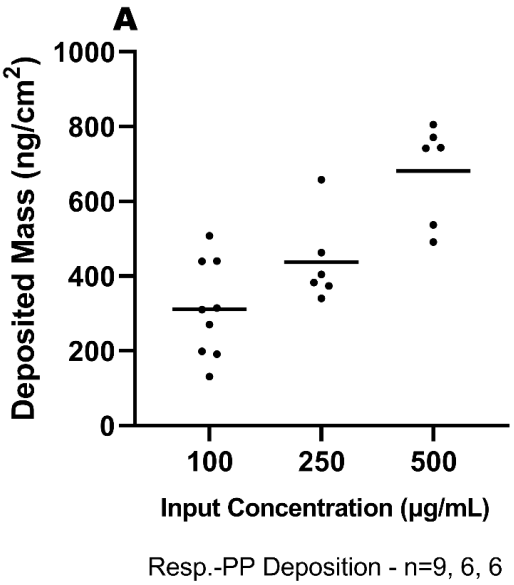

B

Target (µg/cm²)	Accuracy ± Precision (µg/cm²)		
0.5	**0.549**	±	**0.108**
1.0	**1.024**	±	**0.070**
2.0	**2.068**	±	**0.171**

Figure 3.10 - Deposition Data for R-PP. (A) Deposition scatter chart displaying the added mass of each individual deposition. (B) Table showing the three chosen deposition targets, the actual achieved deposition medians, and variation within each target. Each point represents one deposition reading.

Figure 3.6 does not have a cumulative deposition graph like every other sample material as shown in figures 3.4B and 3.5B, and that is due to the use of multiple input concentrations throughout cellular exposures, hence it cannot be drawn.

R-PP followed a positive correlation between input concentration and mass deposition shown in figure 3.6A. All target masses were achieved successfully within the range of the accuracy and precision of the system as demonstrated in figure 3.6B. Achieving top concentration took either four or five depositions depending on the variation.

3.3.3 Microscopy

3.3.3.1 SEM and TEM

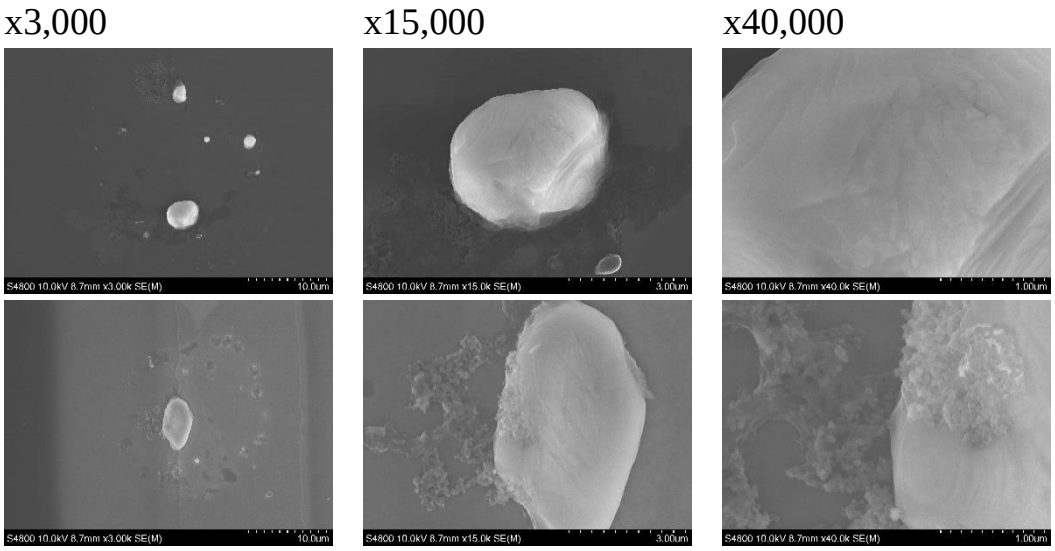

Figure 3.11 - SEM imagery for C-PP following deposition at magnifications of x3,000, x15,000, and x40,000

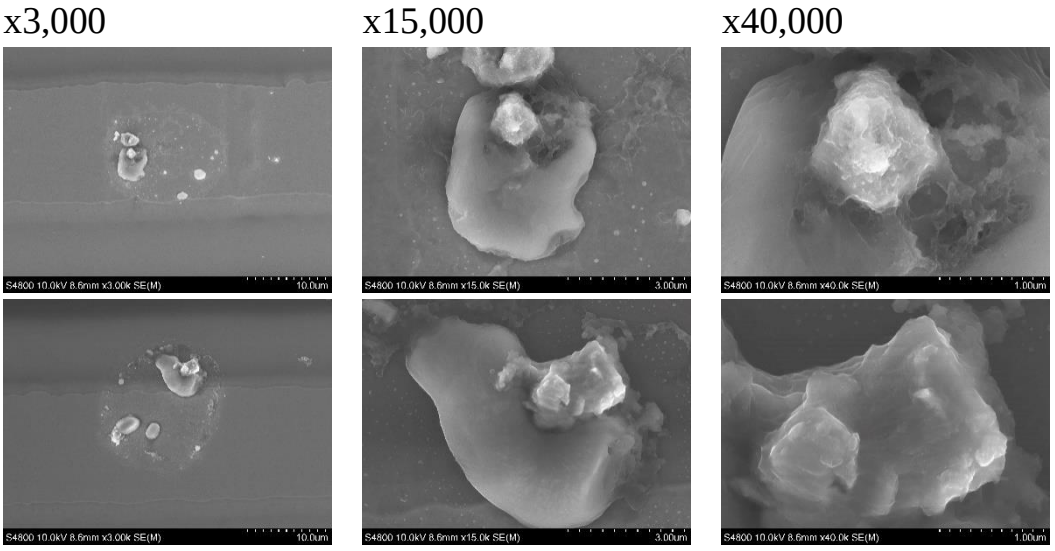

Figure 3.12 - SEM imagery for R-PP following deposition at magnifications of x3,000, x15,000, and x40,000

The deposition of C-PP onto TEM grids presented the formations in figure 3.7. Each dried droplet of aerosol formed a ring of material, containing at least one larger artefact confirmed to be PP, and patches of smaller artefacts which were presumably NaCl. The general appearance of the PP artefacts are a smooth, yet irregular shape, however their surface structure appear to have consistent angular grooves, which could be present due to manufacturing processes. Due to the average particle size of C-PP, all of the input sample could not be represented following aerosolisation and deposition, as larger particles were unable to pass. Deposition of R-PP formed several larger PP artefacts, surrounded by smaller artefacts. Respirable PP underwent cryomilling prior to deposition, so a more irregular, fractured appearance is observed (figure 3.8).

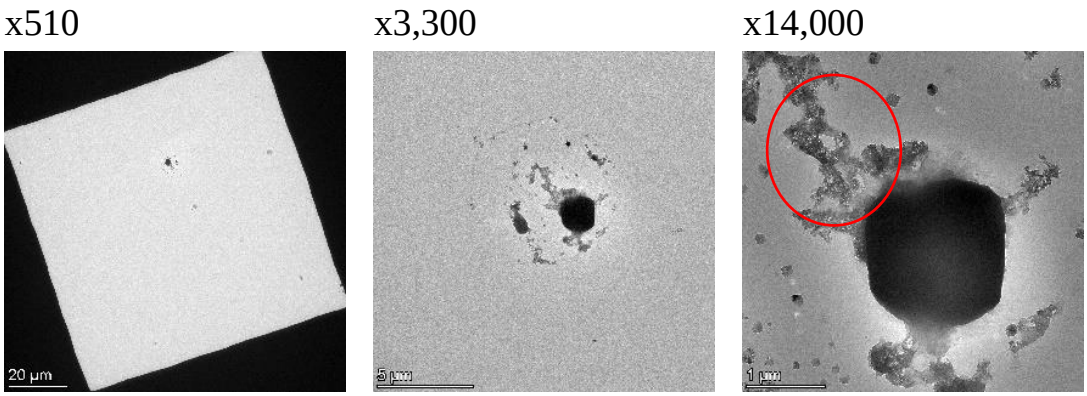

Figure 3.13 - TEM imagery for R-PP following deposition at magnifications of x510, x3,300 and x14,000

TEM imagery also presents the larger artefact surrounded by smaller surrounding artefacts, however, due to the contrast, it is easier to observe the hazy-region highlighted by the circle, than the SEM imagery (figure 3.9).

3.3.3.2 STEM-EDX

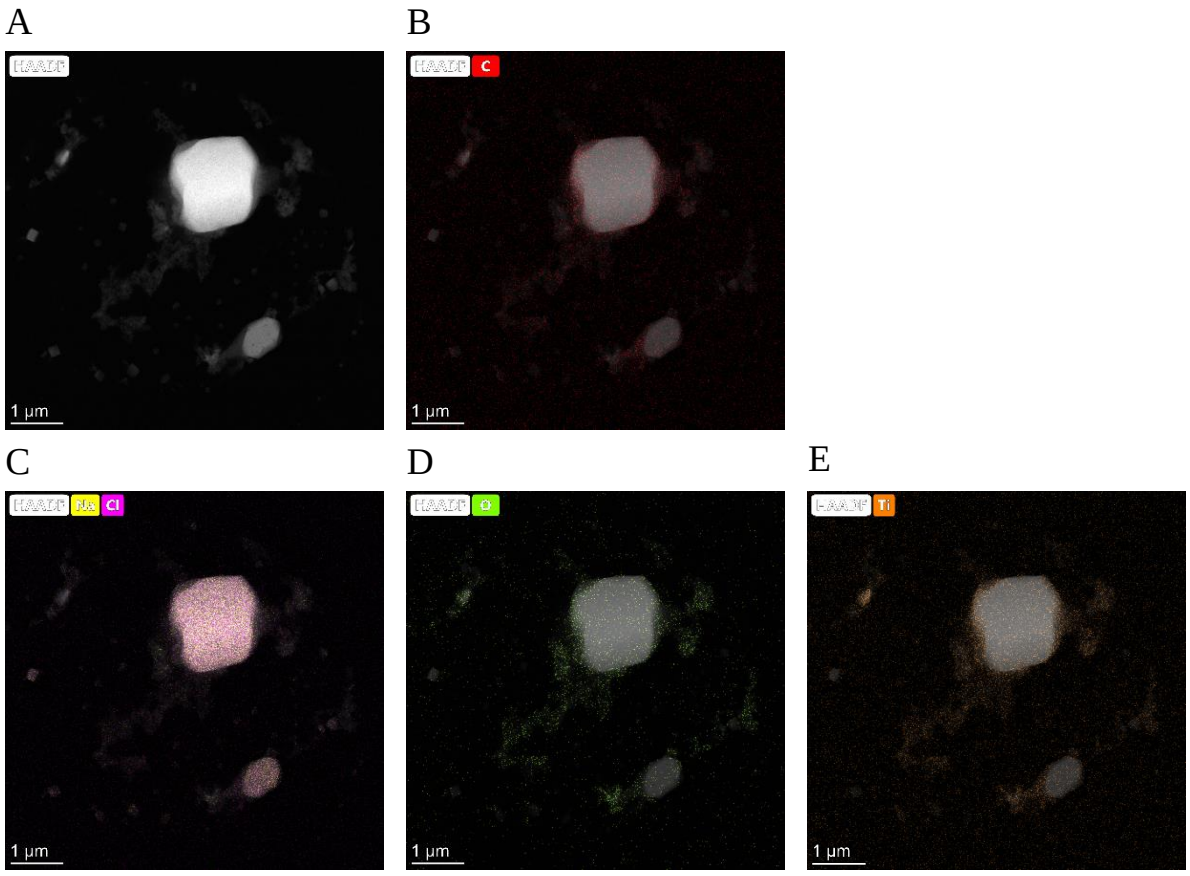

Figure 3.14 - R-PP STEM-EDX imagery following aerosolisation. Full HAADF elemental image (A), Carbon (B), Sodium + Chlorine (C), Oxygen (D) and Titanium (E) at x14,000 magnification

The main detected elements in PP STEM-EDX were carbon, sodium, chlorine oxygen and titanium. Despite PP being a hydrocarbon polymer, the most dense and abundant elements detected from the sample was sodium and chlorine. Oxygen and titanium are most dense in the hazy region observed connected to the large artefact, as highlighted in figure 3.10, whereas carbon was most dense in the outer edge of the large artefact.

3.3.2.3 Confocal LSM Microscopy

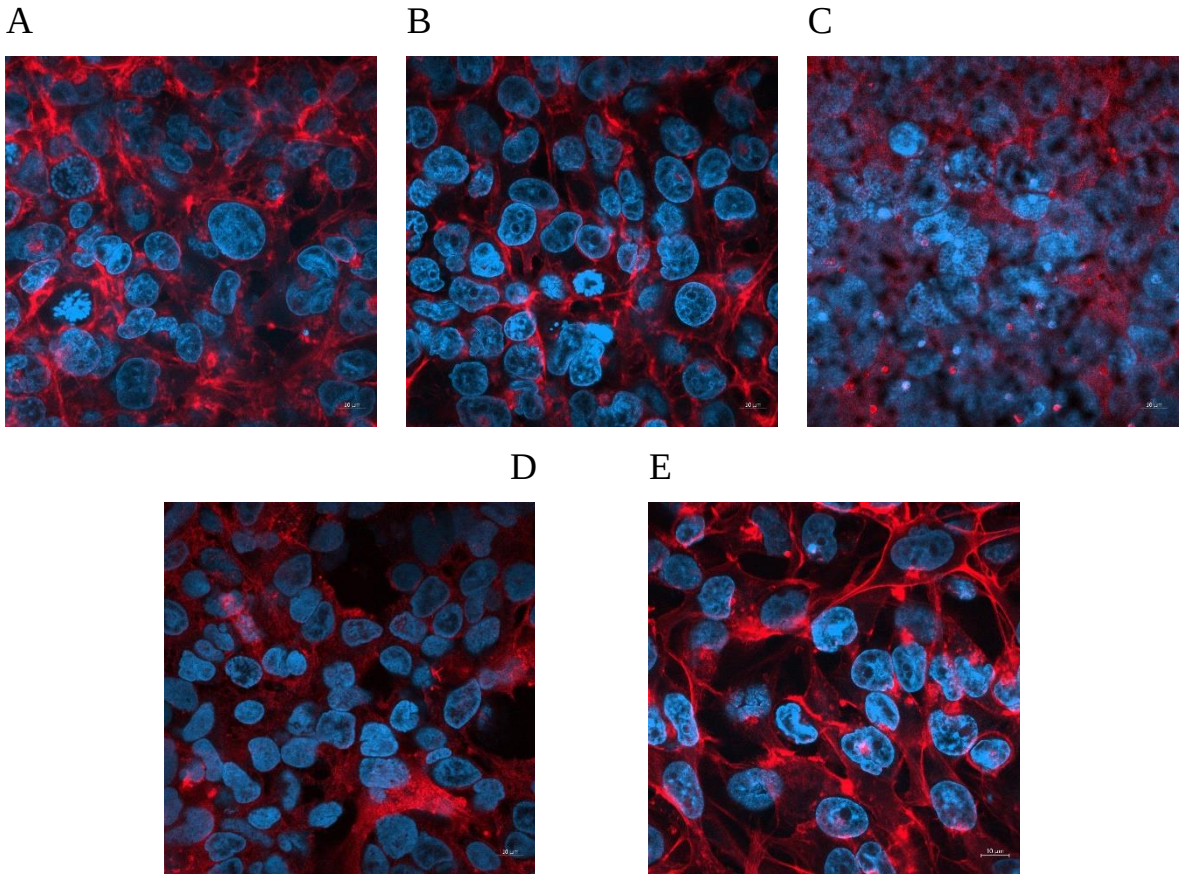

Figure 3.15 - Confocal LSM Microscopy for negative control (A), NaCl vehicle control (B), carbon black (C), C-PP (D), and R-PP (E) following deposition, displaying a multi-channel image of Alexafluor 633 Phalloidin and DAPI

Cell density is consistent across negative control, NaCl vehicle control and C-PP, although the cytoskeleton appears less defined in regions of the C-PP sample. Cytoskeleton of R-PP appears defined, although the population of nuclei is less dense. CB is difficult to interpret due to the obfuscation of the image by the particles, however, it is possible to determine that the nuclei are more granular following exposure to CB than the other samples (figure 3.11).

3.3.3 Cellular Endpoints

3.3.3.1 Cell Death – Trypan Blue Exclusion Assay

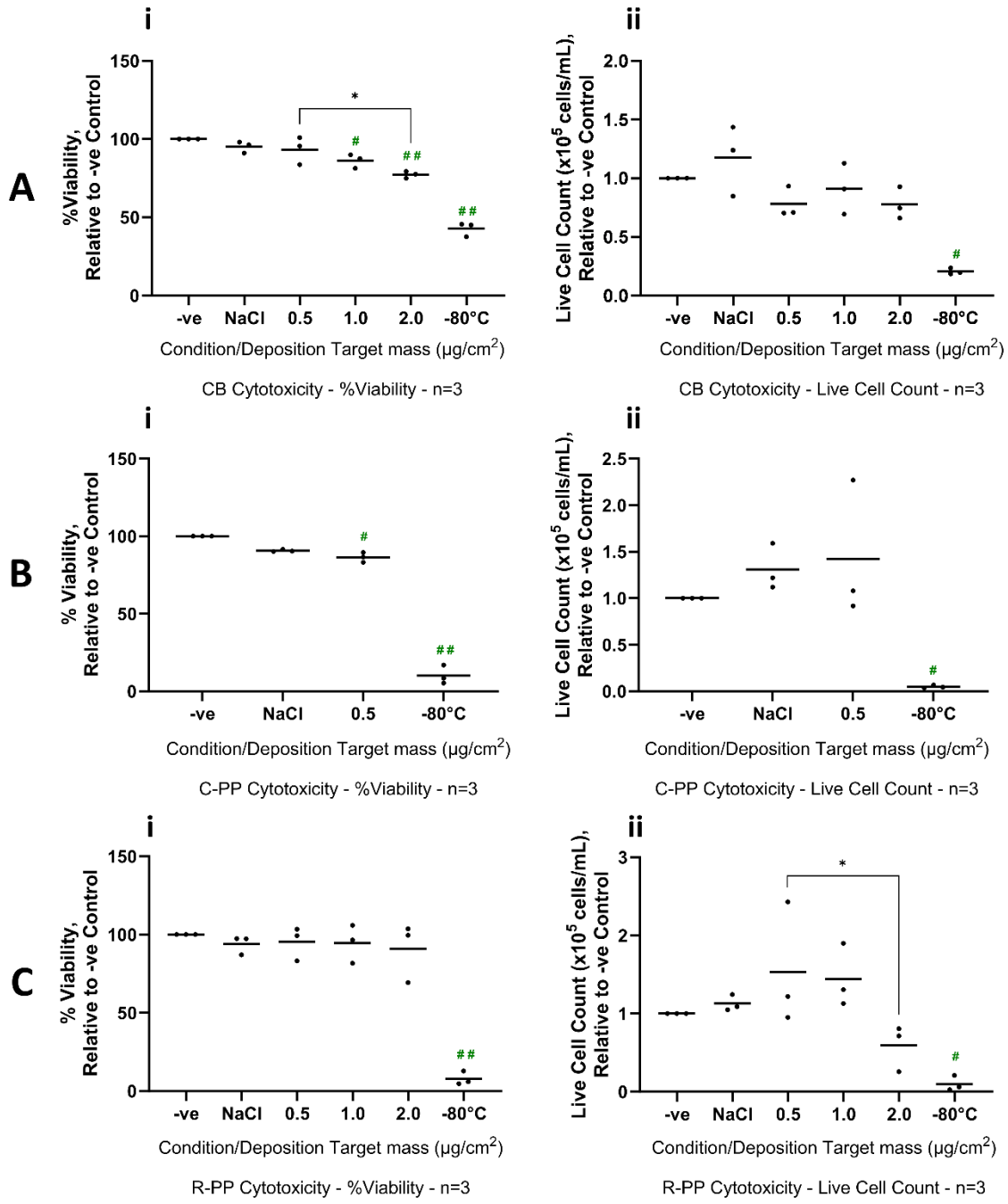

Figure 3.16 - % Viability (i) and live cell count (ii) of NCI-H441 cells following 24-hours exposure to Carbon Black (A), C-PP (B), and R-PP (C). Data presented as each replicate (points) and mean average between replicates (bar) within each concentration.

- significance to -ve control, * - significance between concentrations.

Number of symbols determines level of significance: 1x symbol = $p \leq 0.05$, 2x symbols = $p \leq 0.001$

Carbon black elicited a dose-dependent decrease for cell viability following 24-hours exposure, becoming a significant decrease compared to the -ve control at a concentration of 1.0 μg/cm^2 ($p \leq 0.05$) seen in figure 3.12A(i). Live cell count also demonstrates a dose-dependent decrease, but does not follow the trend as tightly as %viability does, and is not considered statistically significant except for the relation between the +ve and -ve controls ($p \leq 0.05$) shown in figure 3.12A(ii). These data are also biologically significant, as there is large and clear decrease in cell viability and are derived from realistic exposure levels.

Despite only one tested concentration of C-PP (0.5 μg/cm^2) did demonstrate a significant decrease in cell viability ($p \leq 0.05$), although determining whether this is a dose-dependent decrease is impossible due to only one concentration as seen in figure 3.12B(i). Live cell count for non-respirable PP does not follow an observed trend, demonstrated in figure 3.12B(ii), but again the +ve control is a significant decrease in live cell count compared to the -ve control ($p \leq 0.05$). The statistical significance of C-PP cell viability percentage is unlikely to be biologically significant, as there is only one tested concentration and therefore not possible to determine whether a trend of data could occur at additional concentrations.

R-PP does not exhibit a statistically significant dose-dependent decrease to cell % viability, although the mean average does decrease with an increase to concentration (figure 3.12C(i)). However, live cell count is significantly decreased at 2.0 μg/cm^2 ($p \leq 0.05$) when compared to 0.5 μg/cm^2, as shown in figure 3.12C(ii), but not statistically significant when compared to the negative control. As there is no statistical significance amongst the data, there is also no biological significance.

3.3.3.2 Membrane Integrity – Dextran Blue Assay

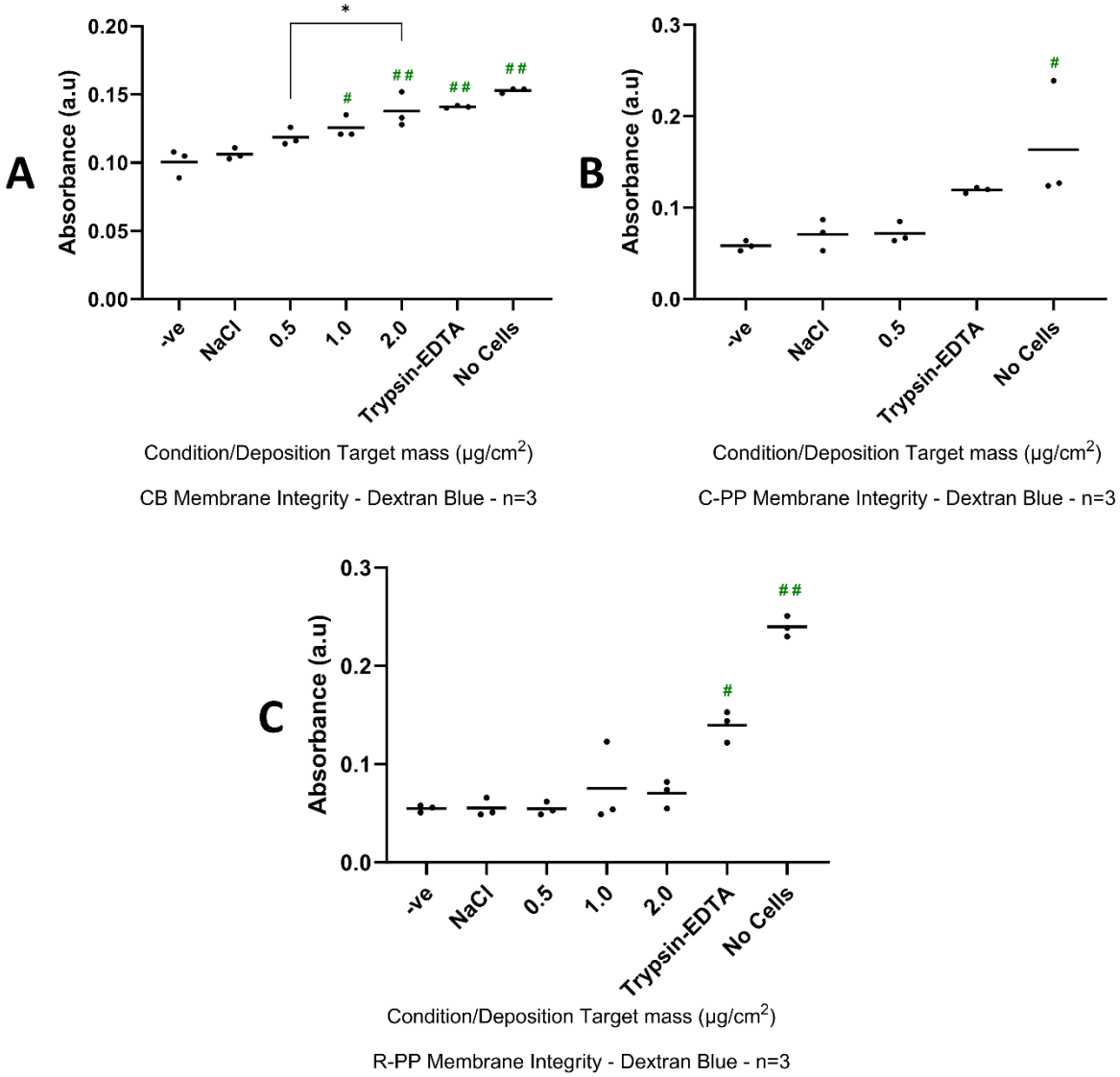

Figure 3.17 - Absorbance of basal well media of NCI-H441 cells following 24-hours exposure to Carbon Black (A), C-PP (B) and R-PP (C), after two hours of Dextran Blue solution diffusion. Data presented as each replicate (points) and mean average between replicates (bar) within each concentration.

- significance to -ve control, * - significance between concentrations.

Number of symbols determines level of significance: 1x symbol = $p \leq 0.05$, 2x symbols = $p \leq 0.001$

Carbon black was the only material which exhibited a significant response, or any observed response at all. At the lowest concentration of 0.5 μg/cm^2, the permeability of the monolayer culture had been significantly compromised ($p \leq 0.05$), and by the top concentration of 2.0 μg/cm^2, significance was great ($p \leq 0.001$), as seen in figure 3.13A. Similarly to the cell viability data, CB also presents biological significance, but due to great permeability increase again at realistic exposure levels.

At the only tested non-respirable C-PP deposition, both +ve controls from the carbon black set (trypsin-EDTA and no cells) displaying a significant increase to absorbance ($p \leq 0.001$), during the R-PP testing, only the no cells control exhibited any significance ($p \leq 0.05$) as shown in figure 3.13B.

No significant response to membrane integrity was observed across any of the tested R-PP depositions (figure 3.13C). Both of the +ve controls, Trypsin-EDTA and no cells ($p \leq 0.001$) are significantly different to the -ve control.

Neither C-PP or R-PP are biologically significant for this endpoint, as there was no observed statistically significant increase to permeability anyway.

3.3.3.3 Genotoxicity – Mononucleated Micronucleus

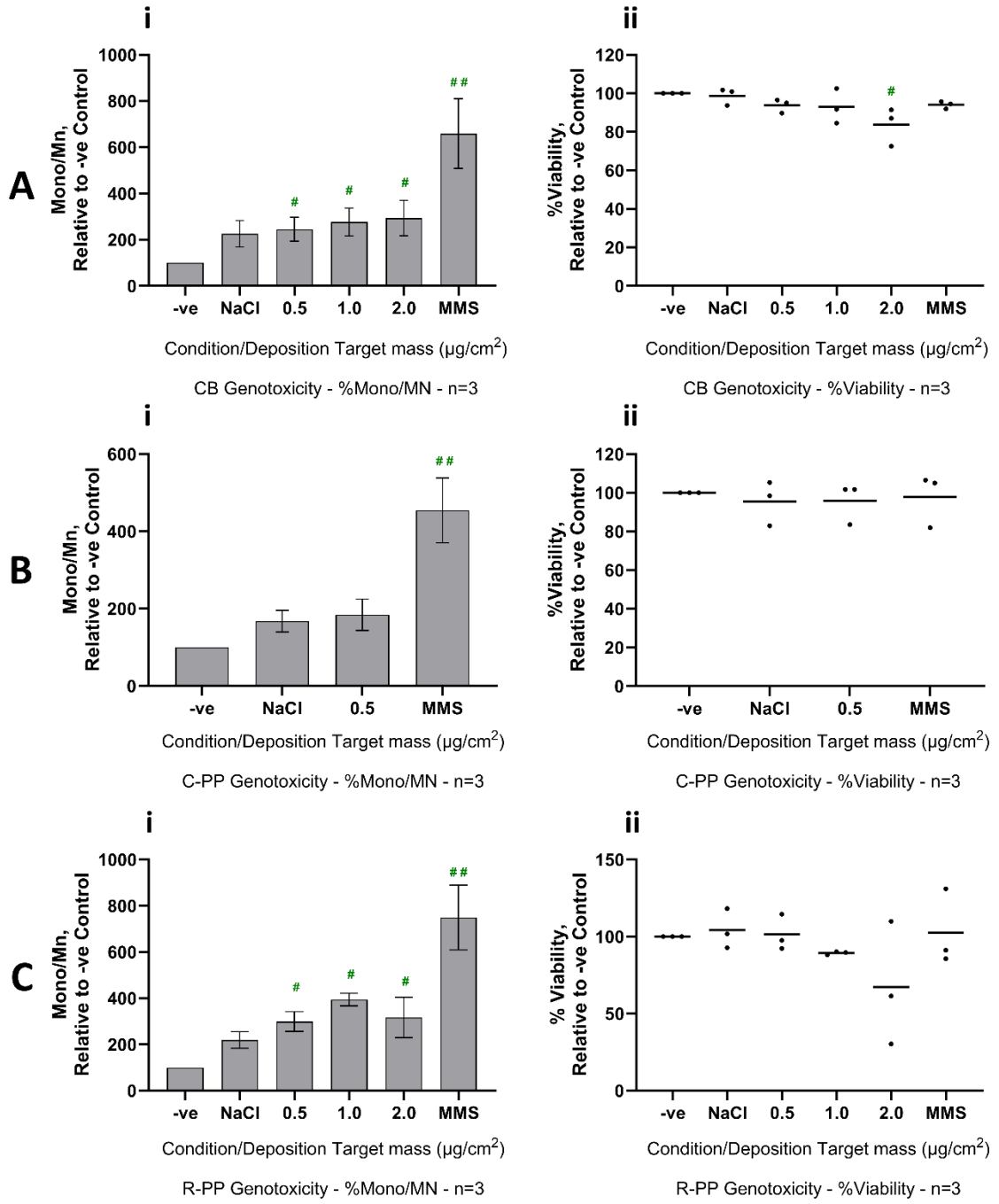

Figure 3.18 - % Mononucleated micronucleus formation (i) and % viability (ii) of NCI-H441 cells following 24-hours exposure to Carbon Black (A), C-PP (B), and R-PP (C). Data presented as mean average MN formation ± standard error of the mean (i), and as each replicate (points) and mean average between replicates (bar) (ii).

- significance to -ve control, * - significance between concentrations.

Number of symbols determines level of significance: 1x symbol = $p \leq 0.05$, 2x symbols = $p \leq 0.001$

All conditions and concentrations of CB tested, including NaCl vehicle control, were statistically significant ($p \leq 0.05$, but $p \leq 0.001$ for MMS +ve control) increases to mononucleated-micronucleus formation compared to the -ve control, which can be seen in figure 3.14A(i). The accompanying cell % viability for genotoxic assessment did not exhibit any statistical significance, despite the visual dose-dependent decrease, except for the MMS +ve control as seen in figure 3.14A(ii), which for this assessment is not intended to be cytotoxic, but as a clastogenic genotoxic agent. As the positive particle control, CB is biologically significant in this assessment, due to the dose dependent increases. However, the vehicle control also induced a MN% increase not too dissimilar to the CB particle tests, despite not being statistically significant.

C-PP presented a significant increase to MN formation at the only tested concentration (figure 3.14B(i)); the mean average increased to 8.48% from 5.12% in the negative control. No significant effects were observed in cell viability (figure 3.14B(ii)). C-PP was not biologically significant in this assessment, as the only tested dose was not a statistically significant increase, and is a similar value to the vehicle control.

MN formation following R-PP exposure presented a dose-dependent increase up to 1.0 $\mu g/cm^2$, then decreased at 2.0 $\mu g/cm^2$. The increases were not significant compared to the negative control, except for the positive control (figure 3.14C(i)). The accompanying cell viability was also not statistically significant, despite displaying a dose dependent decrease (figure 3.14C(ii)). R-PP presents a biologically significant effect, being statistically significant at all three concentrations, with a visibly greater MN% prevalence even compared to the NaCl vehicle control. Additionally, the MN% prevalence rivals that of the CB positive particle control, especially at 1.0 $\mu g/cm^2$, which is greater than CB at any concentration.

3.3.3.4 Pro-inflammatory Response – ELISAs – IL-1β, IL-6, IL-8

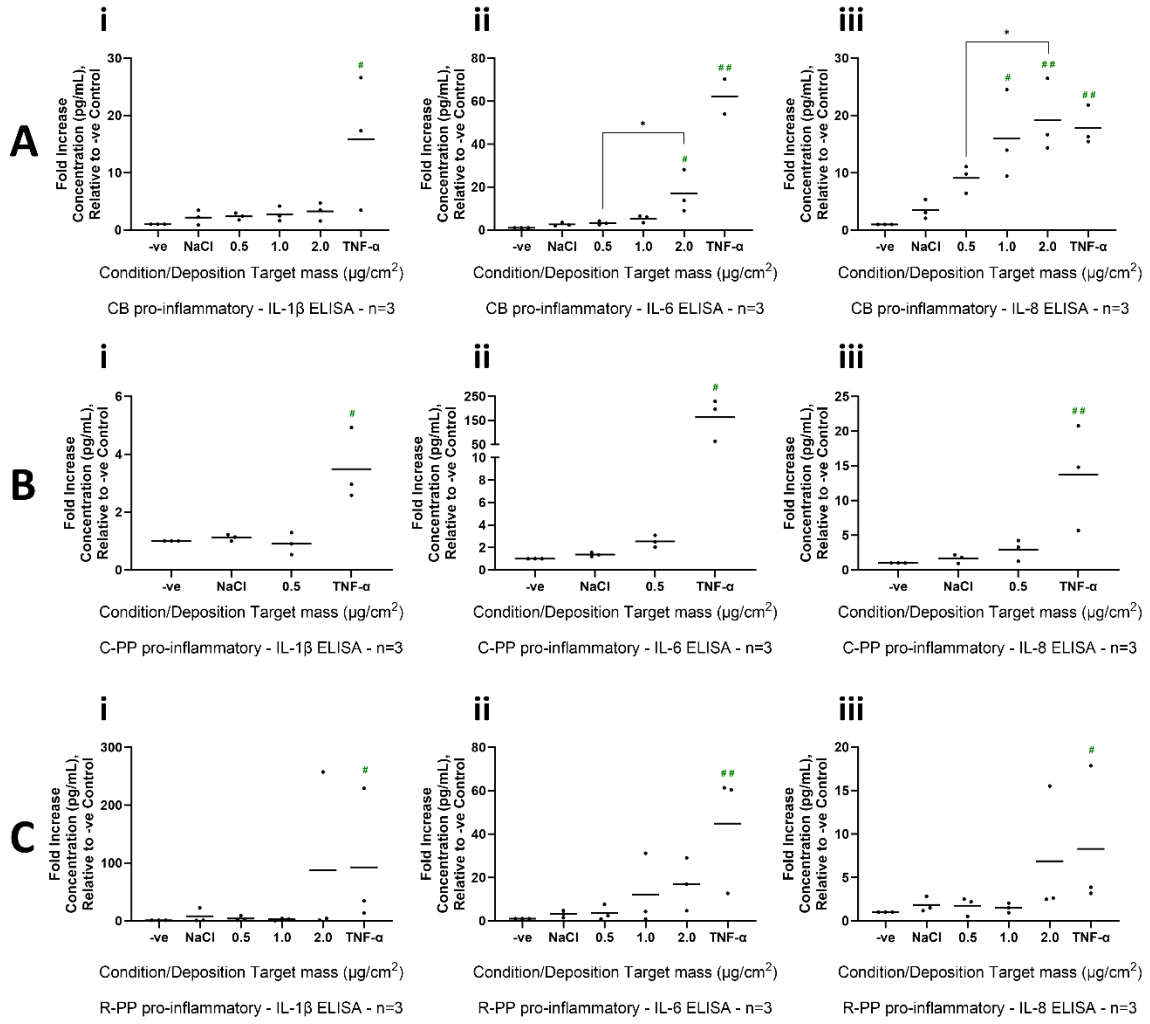

Figure 3.19 - Pro-inflammatory IL-1β (i) and IL-6 (ii) cytokine and IL-8 (iii) chemokine production from NCI-H441 cells, following 24-hours exposure to Carbon Black (A), C-PP (B) and R-PP (C). Data presented as each replicate (points) and mean average between replicates (bar) within each concentration.

- significance to -ve control, * - significance between concentrations.

Number of symbols determines level of significance: 1x symbol = $p \leq 0.05$, 2x symbols = $p \leq 0.001$

Carbon black did not show any significant increases to IL-1β production at any concentration in figure 3.15A(i), or IL-6 production, except at top concentration of 2.0 μg/cm^2 ($p \leq 0.05$), which was also a significant increase from the NaCl vehicle control and 0.5 μg/cm^2 ($p \leq 0.05$) as seen in figure 3.3.15A(ii). IL-8 on the other hand, in figure 3.14A(iii) had presented a strong dose-dependent production increase, being significant at every concentration ($p \leq 0.05$ at 0.5 μg/cm^2, then $p \leq 0.001$ at 1.0 μg/cm^2 and 2.0 μg/cm^2). The top concentration demonstrates a greater IL-8 increase than the TNF-α +ve control did ($p \leq 0.05$), although statistical significance was determined to be the same level in both.

Both IL-1β and IL-6 for C-PP did not demonstrate any significant or observable changes at the only tested concentration as seen in figures 3.15B(i and ii). However, 0.5 μg/cm^2 did instigate a significant increase ($p \leq 0.05$) to IL-8 production, as figure 3.15B(iii) shows.

None of the tested ELISAs for R-PP demonstrate significant changes across any tested concentration, as seen in figure 3.15C. At 2.0 μg/cm^2 and TNF-α +ve control there are anomalous readings for IL-1β production, which are vastly greater than the other two readings for the condition. Despite these readings, only the +ve control is significantly different to the -ve ($p \leq 0.05$). The readings for IL-6 production at 1.0 μg/cm^2, 2.0 μg/cm^2 and the +ve control also have a large variance, which can be observed in figure 3.15C(ii), however only the +ve control is statistically significant ($p \leq 0.001$). Similarly, again for IL-8, there is a large outlying reading for both 2.0 μg/cm^2 and +ve control seen in figure 3.15C(iii).

3.4 Discussion

3.4.1 Introductory

Many quantification studies have determined the ubiquitous presence of MNPs within the atmosphere and environment, but the investigation of how these MNPs impact human health is a relatively young target for research. In 2018, 96% of MNP studies focused on the marine systems (Li *et al*., 2018), with toxicological research stemming from this primarily investigating the consumption of MNPs *via* water or seafoods. Polypropylene is one of the most common types of plastic used for product manufacture, and when observed in pollution quantification studies (Di & Wang, 2018. Ferrario, 2021. Hernández-Fernández *et al*., 2023).

As previously stated, the typical mechanism for CB toxicity is initiated by uptake into eosinophils and mast cells, leading to fibroblast activation, and in relation to lung models, epithelial cell hyperplasia, which is one of the proposed routes leading to cancer. The other cancerous route associated with CB is DNA methylation and histones modification, which can supress the regulation of cellular growth and replication (Niranjan & Thakur, 2017). As there are so many MNPs in existence, and being relatively young field, there is limited understanding as to the mechanisms of induced toxicity. Toxicity and mechanistic assessment is dominated by exposure to polystyrene MNPs *via* various routes. However, PP and PS are not the same material, so current research cannot be directly associated with PP exposure, but could act as a guide (Stapleton, 2021). PS exposures have indicated reductions to neurotransmitter activity (Lei *et al*., 2018), accumulation in reproductive organs (Fournier *et al*., 2020. Xu *et al*., 2021. An *et al*., 2021), decreased cell proliferation rate (Ding *et al*., 2021), and increases to pro-inflammatory cytokine production (Hwang *et al*., 2019) and oxidative stress (Sun *et al*., 2021).

3.4.2 Characterisation analysis

STEM-EDX analysis presented that the larger artefacts present were not identified to be primarily carbon; the main expected element for these particles. With additional collaboration from Dr Stephanie Wright, she confirmed that these artefacts are PP, based upon their morphology. However, the elemental analysis suggests this is incorrect, as the larger artefacts are detected to be electron dense regions of Sodium and Chlorine, which are indicative of the NaCl vehicle control during aerosolisation. However, there is an explanation which can explain this phenomenon. PP as an MNP, is a known electrostatic hydrophobe, and when in a colloidal system, the surfaces of hydrophobes are negatively charged when in contact with water, the formation of an electrical double-layer occurs (Nauruzbayeva *et al*., 2020). The central particle is negatively charged at its surface, and when in contact with an ion-containing

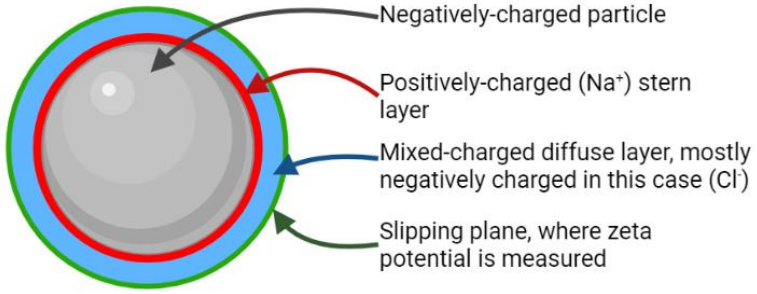

Figure 3.20 - Visualisation of The Electrical Double-Layer theory (created by myself, using Biorender.com)

liquid (in this particular model, water containing Na^+ and Cl^- ions) the positively-charged Na^+ ions form a layer surrounding the particle, called the stern layer. The stern layer is loosely surrounded by a mixed-charged ion layer, called the diffuse layer (but regarding PP specifically, this layer is a negatively-charge CL^- ion layer). The outer edge of the diffuse layer is called the slipping plane, at which the measurement of zeta potential is conducted and due to the accruement of mostly negatively-charged ions throughout the diffuse layer, the zeta potential is a negative value (Analytik, 2020). This theory is visualised in figure 3.16. As a result of this phenomenon, elemental analysis using this approach may initially present a false-negative response for carbon, so further investigation could be necessary to explain this. Additionally, the incorporation of the NaCl vehicle control has the potential to interfere with the cellular endpoint analysis as well as the PP particles, therefore cellular exposures to only the NaCl vehicle control were conducted also.

The negativity of the zeta potentials and its effect on agglomeration indicate a biologically relevant assessment. The objects which humans may be exposed to may be larger than just the individual particles, but could be agglomerates of particles (Demerjian & Mohnen, 2008). Therefore, deposition into different compartments of the lung may vary.

3.4.3 Cellular endpoint analysis

Literature suggests that MNPs can be internalised by mammalian cells up to diameters as great as 10μm in some cell types *via* endocytosis, and this is how the resultant toxic effects could potentially arise, in conjunction with the particular surface characteristics of the specific MNP exposure (Matthews *et al*., 2021). However, studies also report lung type-II epithelial cell internalisation of PS-MNPs up to 0.2 μm in diameter (dos Santos *et al*., 2011. Kuhn *et al*., 2014. Ji *et al*., 2021).

The most significant responses from R-PP exposure observed in this project were increased pro-inflammatory cytokines production (IL-6 and IL-8) and genotoxicity, with increased mononucleated micronucleus formation. Although the results were not statistically significant for IL-6 and IL-8 production there is a dose dependent increase. At even greater concentrations than those tested here, these effects could become both statistically and biologically significant, so this indicates potential support for the initiation of an acute immune response found across literature and would initiate the chemoattraction of neutrophils in mammals to aid MNP clearance. The dose-dependent increase of IL-6 production suggests the onset of an acute phase response initiated by alveolar epithelial cells, but IL-6 is predominantly produced by macrophages to a greater degree. IL-1β, however is not expected to elicit an increase, as there are no antigen presenting cells present within the model. The introduction of macrophages as a co-culture model therefore should present a greater IL-6 response and would increase realism to a whole human system.

Both CB and R-PP demonstrated dose-dependent significant increases to MN formation. R-PP exposures presented a dose-dependent increase up to 1.0 $\mu g/cm^2$, whilst decreasing at 2.0 $\mu g/cm^2$. Alongside this decrease in MN formation to 2.0 $\mu g/cm^2$, cell viability also decreased

at top concentration, although not a statistically significant result, which could account for decrease to MN prevalence, with the initiation of cell death instead. The additional 24-hour period necessary to wait before the harvesting of the cells for this assay allow the cells more time to replicate, as NCI-H441 cells are relatively slow, replicating every 58 hours, and the combination of this assay, in conjunction with the original cell death assay, suggest that these death effects take longer than the acute inflammatory response to arise. It support of Woo (*et al*., 2023) could therefore be suggested that generation of reactive oxygen species (ROS) generated *via* mitochondrial damage may be responsible for many of these effects, through activation of the NF-κB signalling pathway, which is known to elicit the production of inflammatory cytokines and eventually cell death or DNA damage, which could lead to cancer.

3.4.4 Limitations

A practical limitation is the electrostatic interactions of the PP samples with the many surfaces throughout the handling and exposure process, the concentration of the MNP suspension and input concentration into the exposure system is lower than it theoretically was. Based upon the lack of solubility, great agglomeration, and difficulty in handling MNPs, these materials are electrostatically attracted to many of the surfaces used throughout handling, resulting in loss at every stage, including the aerosolisation itself, as the nebuliser heads, exposure chamber, and the transwell inserts are all made from various plastics, electrostatically attracting the MNPs. In addition, sonication had no lasting effect on the suspensions, reverting to a surface layer within a couple of minutes, and further impacting the concentration of the suspension to be lower than calculated.

C-PP was not expected to present any significant responses from a practical standpoint, as only the lowest mass deposition was achievable due to the size of the particles. Less than 50% of which were identified as 55-75 μm diameter (Withers, 2019), in comparison to the pores in the Vitrocell Cloud12 nebuliser pores only being 4-6 μm MMAD. Therefore, due to the size of the C-PP particles, they are not expected to trigger any significant responses in the alveoli, as the particles are too large to pass into the deep lung or internalise into epithelial cells. In humans, the cilia lining the trachea and bronchi would aid the removal of particles this large (Bustamante-Marin & Ostrowski, 2016), before reaching the alveoli, represented by the use of NCI-H441 type II epithelial cells. Whereas R-PP successfully demonstrated an input concentration-dependent increase to deposition mass, and due to the size of the particles these would have the potential to deposit into the deep lung structures (Thakur *et al*., 2020).

A methodological limitation encountered involves the mononucleated micronucleus assay, which was adapted from a cytokinesis-block binucleated micronucleus assay approved by OECD (OECD, 2023). NCI-H441 cells replicated too slowly (54 hours) for the cytochalasin-b to take effect, which was left to expose for only 24 hours, so the time for the cytochalasin-b to take effect was too short. Due to initially acquiring poor results, a simple trial was run to determine whether the poor results were caused by lack of cytochalasin-b traversing the transwell membrane, so a series of +ve (MMS) and -ve controls (incubator) were run on cells cultured in transwell inserts in ALI, or quasi-ALI conditions, where a small volume of 200 μL

of cytochalasin-b dilution was added to the upper surface in the apical well. There were minor increases to micronucleus formation in the quasi-ALI cells, however these still returned insufficient responses, so the mononucleated approach was adopted instead, in which cyto-b was absent.

At the current state of research, there are no other publications investigating the culturing of NCI-H441 cells and their suitability for the micronucleus assay, l*et al*one the incorporation of ALI culturing, with my own published abstract for the Inhaled Particles 13 Conference (2023), being the only returned document with mention of this (Hodgetts *et al*., 2023). As this is the only investigation of this cell line with the mononucleated micronucleus assay, it is not yet possible to definitively conclude whether NCI-H441 cells are suitable for the assay. The OECD suggest that at least 20 experiments with comparable conditions are necessary to determine accurate negative control values (OECD, 2023). Typically, negative controls should present 1.5-2.0% micronucleus formation here. Although most of the values for these are no greater than 2.5% for these three material test batches, there were some outlying values of 5.82% for the CB set, and 7.39% for C-PP, with the other two values for C-PP being 3.32% and 4.66%. This breadth of values may suggest that the NCI-H441 cell line is genetically unstable and may be unsuitable for the mononucleated micronucleus assay.

Another limitation, which was unavoidable, was simply the light interaction of the transwell membranes with the fluorescent microscope and confocal LSM microscope. Initially, cellular morphology was attempted on a fluorescent microscope, but due to the illumination of the entire sample, the membrane flooded the image with light, and prevented the ability to focus effectively on the nuclei and cytoskeleton, therefore, cellular morphology was moved onto the confocal LSM, which has a much more direct area of illumination. The light could pass through the insert more effectively, developing a greater contrast between the background and the cellular foreground. Despite the enhanced illumination and image capability, the insert membranes were still not completely transparent nor level, so the contrast was not ideal and caused interference to the cells, especially at lower magnification.

3.4.5 Knowledge gaps + future direction

Determination of an oxidative stress response should still be collected from future research, as it was absent form this study. Oxidative stress and production of ROS are a key to the toxic responses and adverse outcome pathways. Understanding their occurrence will further develop the full breath of impact which MNPs could potentially cause to alveoli.

As this study investigated a single 24-hour exposure, analysed responses are considered acute, but does not represent chronic or repeated exposures. Therefore, longer exposure periods or repeated particle depositions, for continuous and repeated exposures respectively.

There are more realistic *in vitro* lung models available to use, such as the additional co-culturing of type-I epithelial cells and/or macrophages, to simulate more cell types of the alveoli and the realism of their interactions. However, the development of this would increase the need to optimise the micronucleus assay even further and would increase the complexity of every endpoint assay involved. Alternatively, models of primary cells could be purchased, such as the Epithelix MucilAir (Epithelix, since 2006), which are cultured from live donors, and can be tailored to originate from 'healthy' donors, or those with pre-existing respiratory conditions such as asthma, or cells from cigarette smokers. Despite the greater realism of commercial primary models such as these, they are very expensive, so a cost-benefit analysis should be conducted. So generally, novel studies would be better suited to less expensive, more reproducible models initially. On the other hand, *in vivo* models, such as embryonic zebrafish could be utilised to investigate whole-organism effects. However, with such models as embryonic zebrafish, specific respiratory investigations are not effective, and other *in vivo* models should be more appropriate. Ethical approval and laboratory licensing could limit this opportunity, especially considering the implementation of the NC3Rs for animal studies.

In addition to further cellular experimentation, further investigation into the phys-chem of the MNPs should be done to fully understand all of the potential interaction derived from in the environment. For example, the use of Raman-IR spectroscopy should provide additional elemental and compound analysis on top of that collected from pyro-GC-MS and STEM-EDX, as it would bypass the melding issue encountered during pyro-GC-MS, and would assist with predicting potential adverse effects. This also leads into the development and optimisation of the synthesis and exposure processes, maximising yield, minimising contamination, and improving the transferral of sample materials onto the cellular models, with minimal sample loss.

3.4.6 Realism

MNPs are already ubiquitous across the environment and atmosphere, however the extent that these have on human health is largely unknown, and polypropylene is one of the most commonly found MNPs and is used primarily as an additive to coatings or as a structural plastic, such as in surgical face masks. As most of the toxicological research investigates the consumption of MNPs, the approach simulating the inhalation of MNPs was used. A dry powder Vitrocell was also available to use as an alternative to the aerosol system, however this

system requires multiple grams of material for an exposure, which was not possible due to the mass yields from MNP acquisition. Polyethylene terephthalate (PET) MNPs can act as nuclei for water vapour attraction (Wlasits *et al*., 2023), so PP could also act in this same way due to their electrostatic interactions, and therefore using the aerosol exposure system for MNPs is still suitable and representative of a realistic state at which humans would be exposed to MNPs.

Initial findings demonstrate that there are potential impacts to human *in vitro* lung models when exposed to R-PP MNPs over 24 hours. IL-6 and IL-8 production, and micronucleus formation presented statistically significant effects. Further research must be conducted to reinforce these findings however, utilising the same methods and with a variety of MNPs. The collaboration between the material preparation techniques, exposure system (with MNP use) and the cellular model interaction with MNPs, have not been previously researched, so repetition of these methods will support the reliability of the processes and responses, and their translation into *in vivo* laboratory studies, and human exposures.

3.4.7 Conclusion

Table 3.2 - Summary of CB, C-PP and R-PP endpoint statistical significance. Darker shades of yellow-orange arbitrarily depict greater mean average difference, in comparison to the negative control, following exposure response. Statistical significance depicted by '#', and absence of '#' depicts no statistical significance. (#) depicts statistical significance for accompanying dataset – [live cell count] in Cell Death, and [% viability] in Mono/MN. Data not applicable for 1.0 and 2.0 μg/cm^2 for C-PP due to methodological limitations.

= p<0.05, ## = p<0.001

Material / Assessment	CB			C-PP			R-PP		
Mass Target (μg/cm^2)	0.5	1.0	2.0	0.5	1.0	2.0	0.5	1.0	2.0
Cell Death		#	##	#	N/A	N/A			
Barrier Int.		#	##		N/A	N/A			
Mono/MN	#	##	## (#)		N/A	N/A		#	#
IL-1β					N/A	N/A			
IL-6					N/A	N/A			
IL-8	#	##	##		N/A	N/A			

To conclude, the deposition of R-PP MNPs elicit some adverse responses in type-II alveolar cells when cultured at the ALI, summarised in table 3.2. R-PP provided a guide as to how the mask samples could interact with the cell model in Chapter 4. Being predominantly PP-based, the masks could instigate similar responses (increases to IL-6 production, IL-8 production and micronucleus formation). However, as masks contain additives rather than PP alone, these effects demonstrated from the pure respirable-PP sample should be exacerbated in the mask samples, or display additional effects, depending on what the additives are within the masks.

Although at present, it is not exactly known how relative these deposition masses are to current exposure to inhaled PP MNPs, but this project does provide insight into how the human lungs could be affected if MNP prevalence in the atmosphere continues to increase and their fate when inhaled by humans.

Chapter 4 - Investigating the Impact of Inhaled MNPs derived from Surgical Face Masks, Their Physicochemical Characterisation and Their Impact on Human Alveolar Monocultures *in vitro*

4.1 Introduction

Surgical masks have been routinely used across medical practice and occupational settings, however throughout the Covid-19 pandemic, the use of these masks was extended to the majority of the general public. As a result, the demand for these masks soared during 2020 and 2021 outlined in figure 4.1 (Richter, 2023), inevitable resulting in an influx of disposed material.

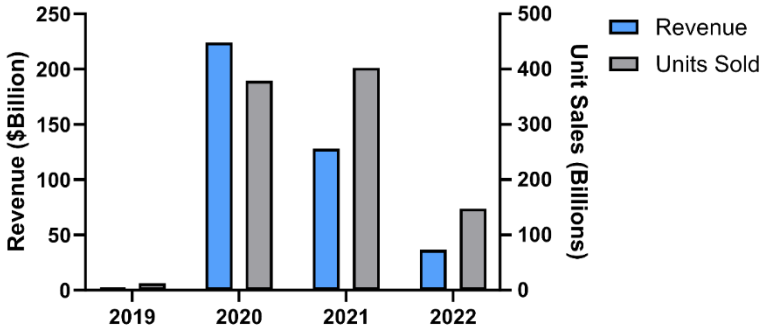

Figure 4.6 - Estimated mask revenue and unit sales per year between 2019 and 2022.

Improper use and disposal of these masks leads to their degradation and their potential to form MNPs, *via* two main routes. Firstly, the direct route is dominated by improper use, as these are deemed single-use masks, they are intended to be correctly disposed of after a single use. Retaining and reusing FFP2 respirators for continuous and repeated periods of time, may induce symptoms of irritant rhinitis, attributed to significant presence and accumulation of PP fibres within nasal lavage fluid (Klimek et. al., 2020). Nasal mast cells were determined to stimulate tryptase secretion, with no elevation of eosinophil activation or IgE production. PP presence in the lavages significantly decreased after a period of mask absence. FFP2 respirators are less accessible than surgical masks due to their enhanced filtration ability and fit for purpose regulations. Therefore, surgical masks are generally less robust and may shed an increased number of particles. These PP fibres are indicative of the innermost layer of the mask, being closest to the respiratory system, breaking down, therefore, one of the mask samples curated for this project consist of a milled powder of the innermost layer, dubbed 'White' due to its colour.

Alternatively, the indirect scenario pertains to the improper disposal of masks into landfill and bodies of water (Morgana *et al.*, 2021). Over time these masks degrade, usually mechanically, biologically, or chemically, although theories and research into photodegradation is gaining momentum, causing the breakaway of particles and fibres from the mask. These continue to degrade further into MNPs and have the potential to become airborne if small enough, typically <5 μm aerodynamic diameter, and then inhaled. This route can involve the entire mask forming MNPs, therefore, a batch of mask powder particles formed from all three mask layers was created, dubbed 'Blue', also due to its colour.

The aim of this chapter is to determine how respirable surgical mask-derived MNPs could potentially impact the human lung upon inhalation, arisen by their improper use, or by their degradation in the environment, represented by two distinct batched of MNPs. This will be conducted by using various toxicological endpoint assessments, on an *in vitro* alveolar model exposed to aerosolised PP MNPs.

This will be conducted by the following objectives:

- Synthesise two batched of mask-derived MNPs using novel degradation techniques and characterise their average diameter, polydispersity index, zeta potential, morphology, and elemental composition.
- Expose NCI-H441 monocultures, cultured at the air-liquid interface, to these MNP batches individually for 24 hours.
- After 24 hours, harvest the necessary components of the models to determine a range of endpoint assessments: pro-inflammatory response, cell death, genotoxicity, monolayer barrier integrity and cellular morphology.

It is hypothesized that whole mask (blue)-MNPs will instigate a greater adverse response due to the potential presence of additive chemicals/dyes, which are currently unknown, but the innermost (white)-MNPs will instigate a response similar to R-PP MNPs. Primarily an increase to IL-8 production is expected.

4.2 Methods

4.2.1 Outline of Milling Process

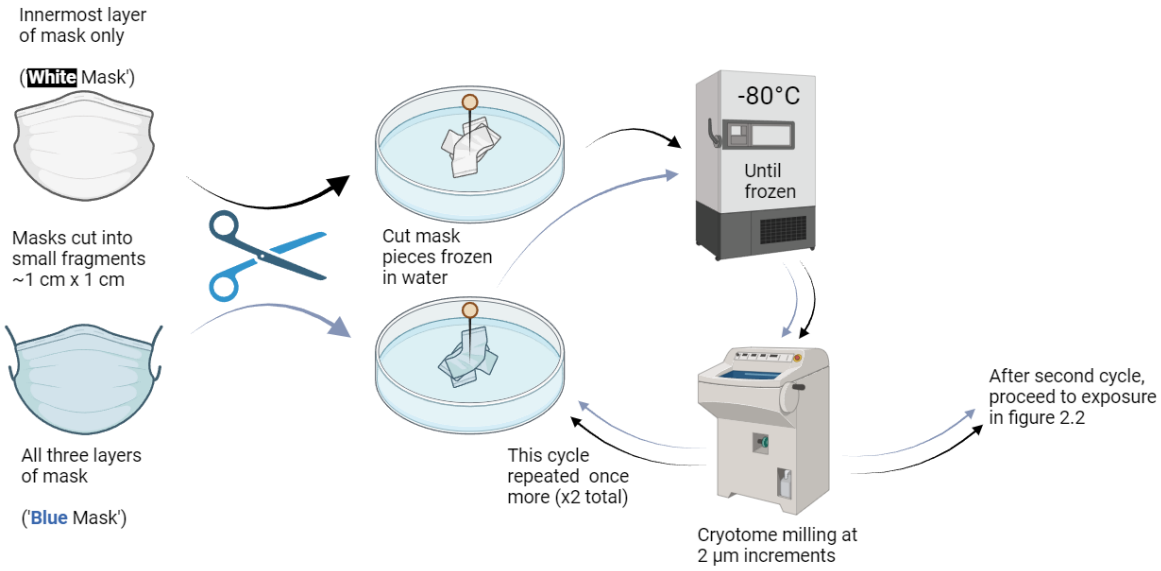

Figure 4.10 - Outline of both mask milling processes (created by myself, using Biorender.com)

4.2.2 Mask Milling and Preparation

4.2.1.1 Acquisition of masks

Three brands of mask were purchased from two popular high-street pharmacists Boots and Superdrug: Boots – 'Boots Protective Face Masks' (£4.50 for five masks), Boots – 'LyncMed Face Mask' (£10.00 for 50 masks), and Superdrug – 'Termin8 Disposable Medical Face Mask' (£9.99 for 50 masks).

4.2.1.2 Cryomilling of Masks – Cryo-homogenisation

The masks were cut into small pieces, ~1cm^2 and equal volume of each mask was inserted into the vial. Two batches of mask pieces were prepared, the innermost layer of the mask (white mask), and all three layers of the mask ('blue mask'). To each vial, 1:1 g mass ratio of mask : mill balls were added. These underwent the same protocol as described in section 3.2.1.1. It was very ineffective however, by the end, the samples were contaminated with steel contaminant fragments from the milling balls and the yield was abysmal. So, an alternative method was attempted, shown in figure 4.2 and described in the following section 4.1.2.3.

4.2.1.3 Cryomilling of masks - Cryostat

Multiple layers of mask were folded together, submerged, and frozen into a petri dish containing Millipore ddH_2O, at -80°C. Once frozen, the sample was carved out and mounted into the Cryostat using mounting media. The Cryostat stage was set to move in 2 µm increments every wheel rotation. The shavings were collected, reconstituted and refrozen, in preparation to run through the Cryostat again.

4.2.2 Material Characterisation

4.2.2.1 Pyrolysis-GC-MS

A dry mass of White mask and Blue mask MNPs were used for pyro-GC-MS following the method in section 2.3.1.

4.2.2.2 Size Distribution, DLS, Zeta Potential

Size distribution, DLS and zeta potential were conducted as described in section 2.3.2, using White mask and Blue mask MNPs.

4.2.3 Cell Seeding

Cell passaging was conducted as in section 2.4.2 and seeding was conducted as noted in section 2.4.3, using White mask and Blue mask MNPs.

4.2.4 Aerosol Exposure

Prior to aerosolisation, all suspensions underwent sonication to break apart agglomerated and improve the efficiency of deposition, following the laboratory SOP. The probe was activated at 10% power, alternating 10 seconds on:off, for a total of four minutes uptime. Aerosol exposure was conducted as described in section 2.5, using White mask and Blue mask MNPs.

4.2.5 Microscopy

SEM was conducted as described in section 2.6.1, STEM-EDX as in section 2.6.2, and Confocal LSM as in section 2.6.3, using White mask and Blue mask MNPs.

4.2.6 Trypan Blue Exclusion Assay

The TBE assay was carried out in accordance with the method outlined in section 2.7, using White mask and Blue mask MNPs.

4.2.7 Blue Dextran Assay

This assay was conducted as described in section 2.8, using White mask and Blue mask MNPs.

4.2.8 Mononucleated Micronucleus Assay

All interleukin ELISAs were conducted, with the necessary adjustments to reagents and samples based upon whichever interleukin was being quantified, as described in section 2.9, using White mask and Blue mask MNPs.

4.2.9 Pro-inflammatory Cytokine Sandwich ELISAs

The process for the Blue Dextran monolayer permeability assay followed the description in section 2.10, using White mask and Blue mask MNPs.

4.3 Results

4.3.1 Characterisation

4.3.1.1 DLS

Table 4.1 - Polydispersity Index midpoint and midpoint-range, and Zeta Potential midpoint and midpoint-range of PP and respirable-PP at 25°C and 37°C.

Sample and Temperature (°C)	PDI Midpoint & Variance	PDI Mean Average	Zeta Potential (mV)	Zeta Potential Mean Average (mV)
White 25	0.56 ± 0.10	0.545	-19.89 ± 11.55	-19.57
White 37	0.86 ± 0.14	0.880	-27.74 ± 7.07	-28.92
Blue 25	0.68 ± 0.17	0.656	-29.63 ± 2.92	-29.44
Blue 37	0.75 ± 0.24	0.884	-25.79 ± 3.41	-25.99

The polydispersity indices of both mask samples are greater at 37°C than 25°C, with blue mask PDI is greater on average than white mask. The zeta potential across all four tests are negative, similarly to pure PP, and white mask became more negative at 37°C in comparison to 25°C, whereas blue mask the inverse was observed (table 4.1).

4.3.1.2 Pyrolysis Gas-Chromatography Mass-Spectrometry

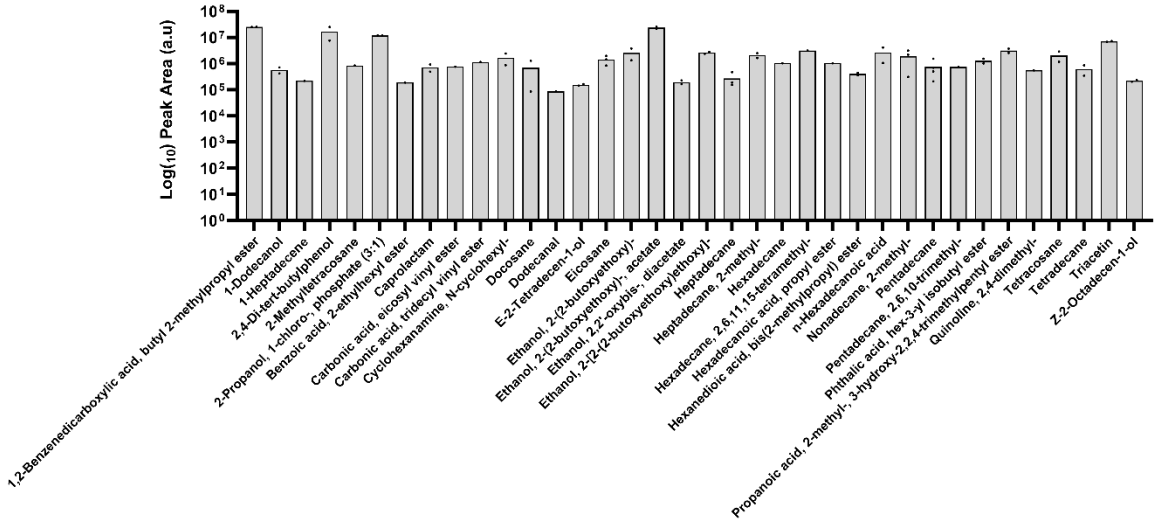

Figure 4.11 - Bar Chart displaying all unique compounds eluted from White Mask powder during Thermal Desorption (350°C), their number of recorded peaks, and the area under each peak.

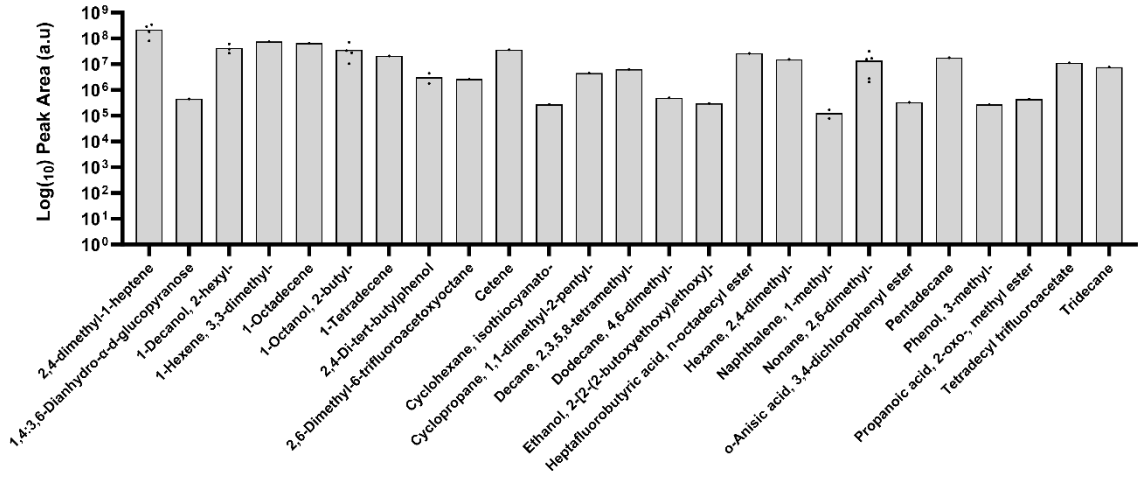

Figure 4.12 - Bar Chart displaying all unique compounds eluted from White Mask powder during Pyrolysis (800°C), their number of recorded peaks, and the area under each peak.

The white mask sample eluted into a vast array of compounds, from Thermal Desorption in figure 4.3, it eluted into 36 unique compounds, with a total of 66 hits across two runs. Thermal desorption analysis was untargeted, so PP was not actively searched for, as it can only be detected at pyrolytic temperatures. 2,4-dimethyl-1-heptene, amongst other C_9H_{18} compounds are typical eluents for PP, so for pyrolysis, targeted analysis was conducted to confirm its presence, and based on the linear values from the peak area, was at 2.95x more abundant than the most abundant compound found by untargeted analysis (1-hexene,3,3,dimethyl-), and 1789.72x more abundant than the least abundant compound detected (Naphthalene, 1-methyl-), as seen in figure 4.4. during pyrolysis, white mask eluted into 25 unique compounds, including 2,4-dimethyl-1-heptene, with a total of 39 hits across two sample runs.

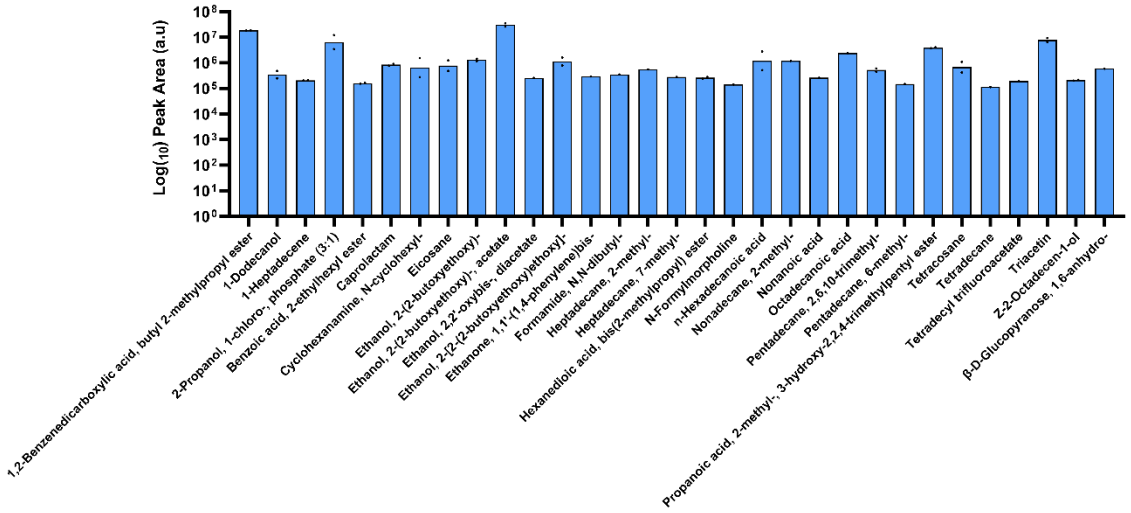

Figure 4.13 - Bar Chart displaying all unique compounds eluted from Blue Mask powder during Thermal Desorption (350°C), their number of recorded peaks, and the area under each peak.

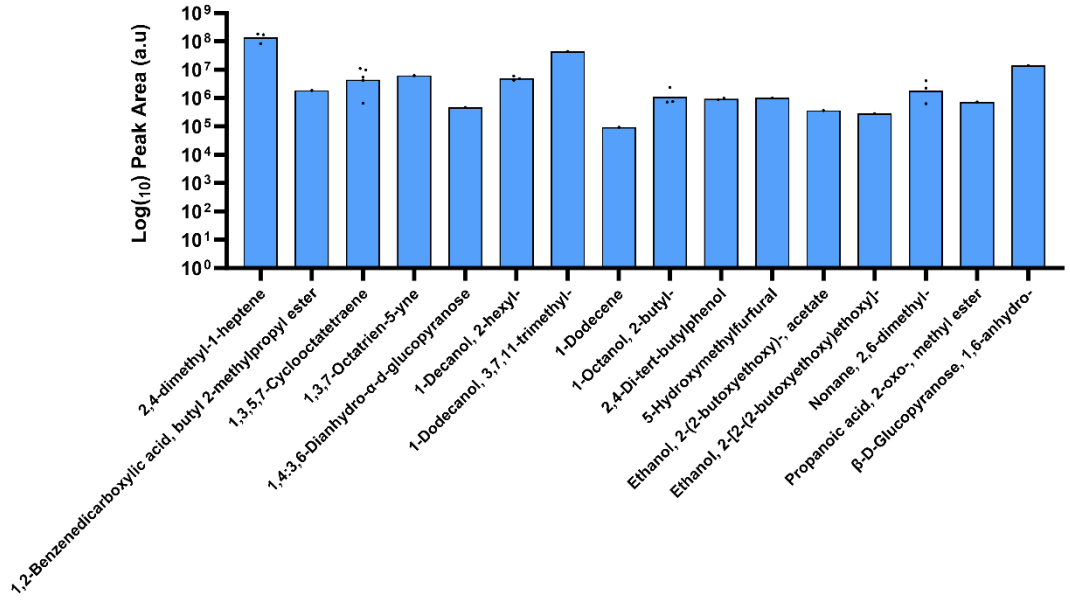

Figure 4.14 - Bar Chart displaying all unique compounds eluted from Blue Mask powder during Pyrolysis (800°C), their number of recorded peaks, and the area under each peak.

During thermal desorption, Blue mask eluted into 31 unique compounds, listed in figure 4.5, with 49 hits across two sample runs. Ethanol, 2-(2-butoxyethoxy)-, acetate was the most abundant compound eluted from the blue mask sample during thermal desorption, 273.23x more abundant than Tetradecane, the least abundant eluent. Following pyrolysis, blue mask also underwent targeted analysis to determine the presence of 2,4-dimethyl-1-heptene, eluent of PP. Similarly to white mask, 2,4-dimethyl-1-heptene was greatly more abundant than every other eluent, 3.28x more abundant than 1-dodecanol, 3,7,11-trimethyl-, and 1555.89x more abundant than 1-dodecene, the least abundant eluent. Figure 4.6 also shows that blue mask eluted into 16 unique compounds, with 29 total hits across two sample runs.

4.3.2 Aerosolisation

4.2.1 Mass Deposition

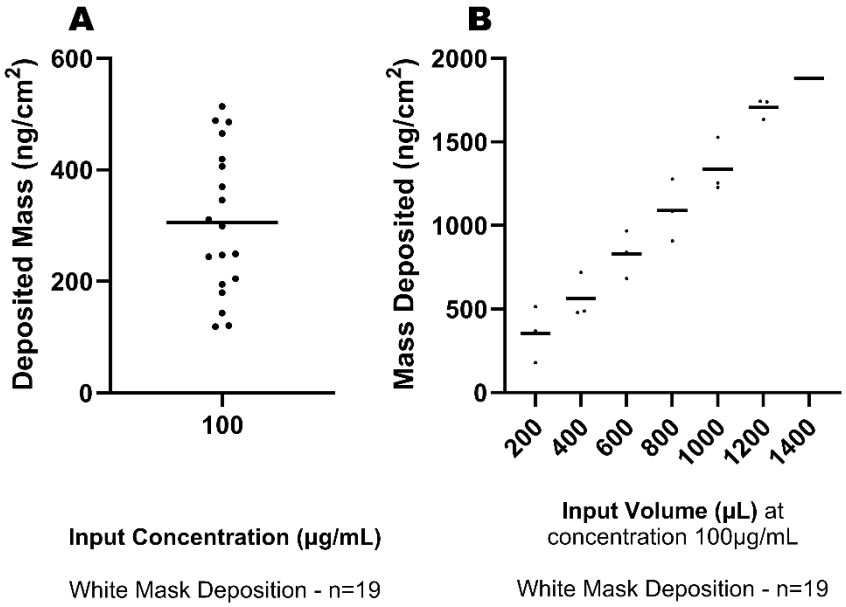

C

Target (µg/cm²)	Accuracy ± Precision (µg/cm²)
0.5	**0.496 ± 0.017**
1.0	**0.996 ± 0.088**
2.0	**1.810 ± 0.071**

Figure 4.15 - Deposition Data for White Mask. (A) Deposition scatter chart displaying the added mass of each individual deposition. (B) Deposition scatter chart showing the accumulative addition of mass throughout each cellular exposure. (C) Table showing the three chosen deposition targets, the actual achieved deposition medians, and variation within each target. Each point represents one deposition reading.

There was a large range of white mask deposition; 394.904 ng/cm^2 between the highest (513.615 ng/cm^2) and smallest deposition (118.711 ng/cm^2). The 0.5 and 1.0 µg/cm^2 targets were successfully acquired within precision range, but 2.0 µg/cm^2 was under range by 119 ng/cm^2 as described in figure 4.7C. This was attributed to adherence to the SOP, and keeping samples out of incubation for less than two hours (Barasova and Rothen-Rutihauser, 2019) demonstrated in figure 4.7B.

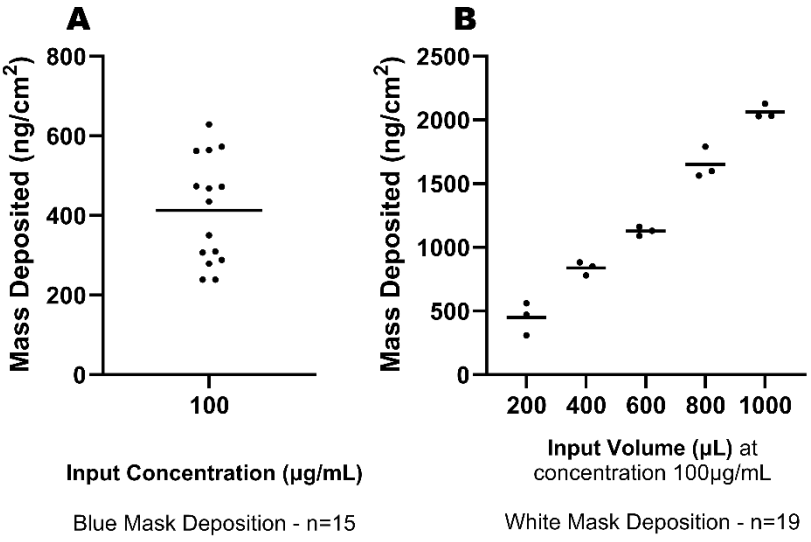

C

Target (µg/cm2)	Accuracy ± Precision (µg/cm2)		
0.5	**0.436**	±	**0.126**
1	**1.126**	±	**0.036**
2	**2.079**	±	**0.049**

Figure 4.16 - Deposition Data for Blue Mask. (A) Deposition scatter chart displaying the added mass of each individual deposition. (B) Deposition scatter chart showing the accumulative addition of mass throughout each cellular exposure. (C) Table showing the three chosen deposition targets, the actual achieved deposition medians, and variation within each target. Each point represents one deposition reading.

Blue mask average deposition was 305.601 ng/cm^2 per 200 µL at 100 µg/mL concentration, blue mask depositions were on average 107.211 ng/cm^2 greater with 412.812 ng/cm^2 and only recorded a 4.892 ng/cm^2 smaller range than white mask (figures 4.8A). The target of 0.5 µg/cm^2 was successfully achieved, however, 1.0 µg/cm^2 and 2.0 µg/cm^2 were both above target precision as calculated in figure 4.8C.

4.3.2.2 SEM and TEM

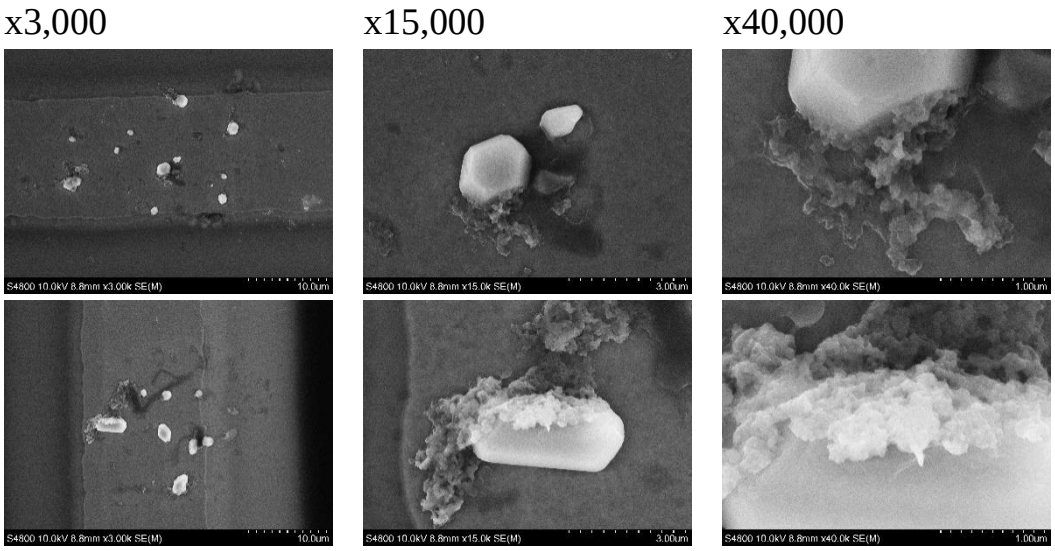

Figure 4.17 - SEM imagery for White Mask at magnifications of x3,000, x15,000, and x40,000

The aerosolised white mask SEM images in figure 4.9 also follow the same group structure as PP does, as seen in figures 3.7 and 3.8, due to the process of the aerosolisation, deposition and then drying of the sample. Typically, the white mask particles possess many flat edges in comparison to C-PP or R-PP. It can be observed that there are more MNP particles per cluster compared to PP and appear more consistently 5µm in diameter or smaller.

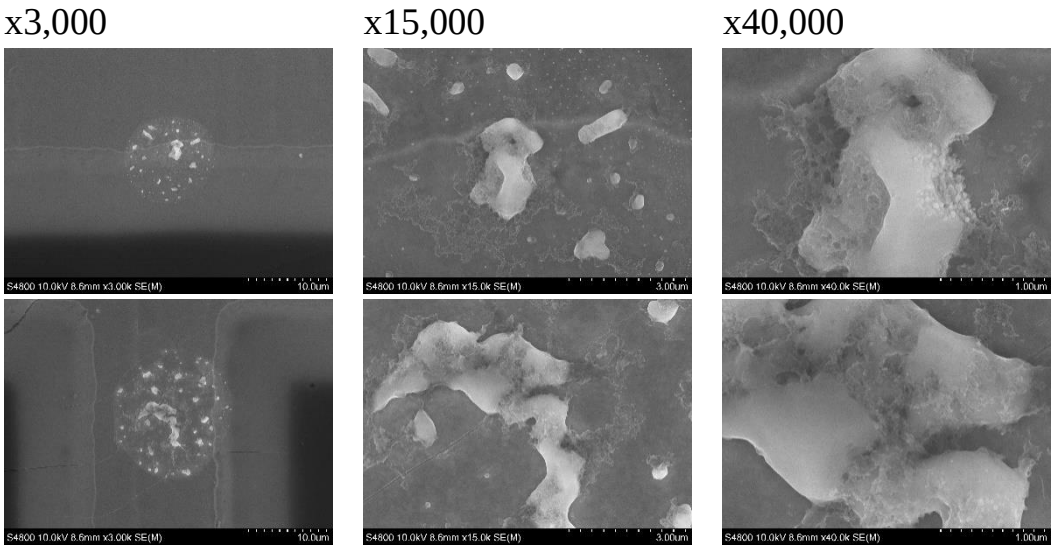

Figure 4.18 - SEM imagery for Blue Mask at magnifications of x500, x3,000, x15,000, and x40,000

The blue mask clusters observed in figure 4.10 also follow the same deposition clustering as all MNP SEM images collected, larger MNP particles surrounded by patches of NaCl crystals. However, the blue mask MNPs possess a ‘molten’ appearance unlike every other observed MNP in this project.

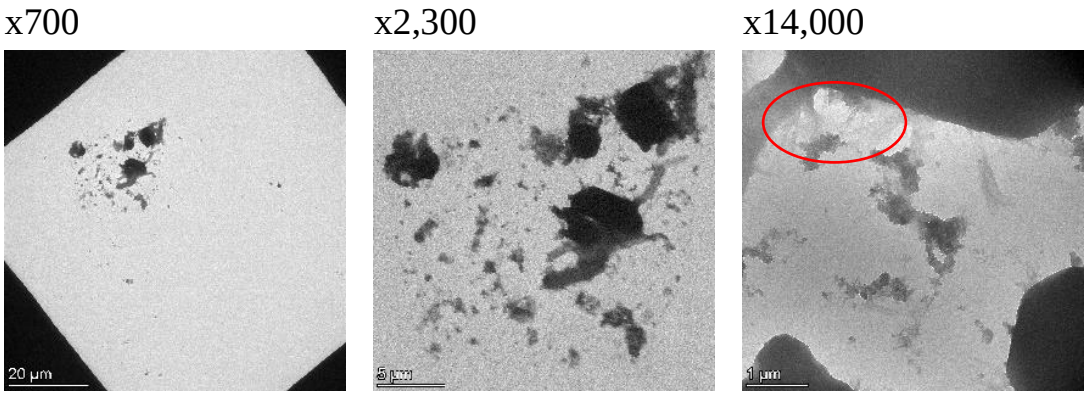

Figure 4.19 - TEM imagery for White Mask following deposition at magnifications of x700, x2,300 and x14,000

Figure 4.11 changes the contrast of the samples, to allow the observation of the hazy areas, emanating from the larger artefacts, as also observed in figure 3.9. Furthermore, less contrasting 'leaching'-effects are highlighted by the red ring, also stemming from the larger artefacts.

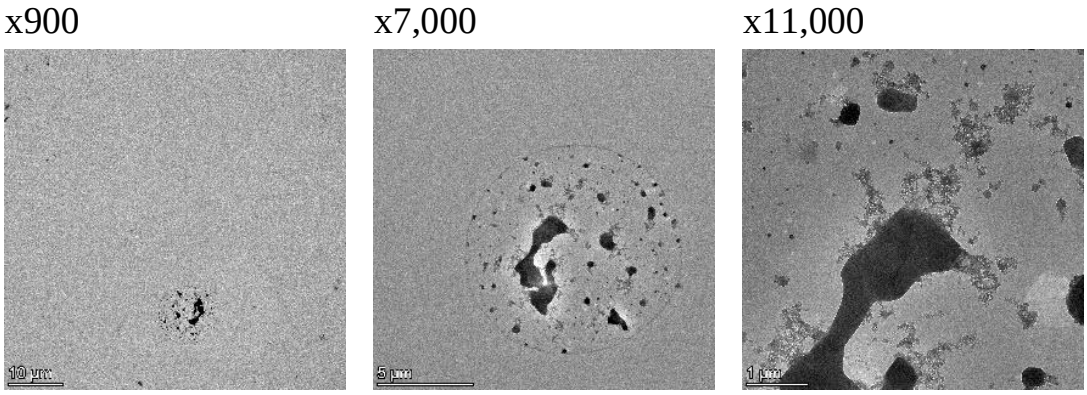

Figure 4.20 - TEM imagery for Blue Mask following deposition at magnifications of x900, x7,000 and x11,000

As previously also observed, the hazy regions surrounding the larger artefacts are also present, however the blue mask MNP images (figure 4.12), they appear more crystalline when compared to the other equivalent imaged from the other MNPs. These regions also appear flecked, with scattered light dots throughout these hazy regions. The large artefacts observed here from blue mask MNPs, still appear less angular than the other observed MNP samples.

4.3.2.3 STEM-EDX

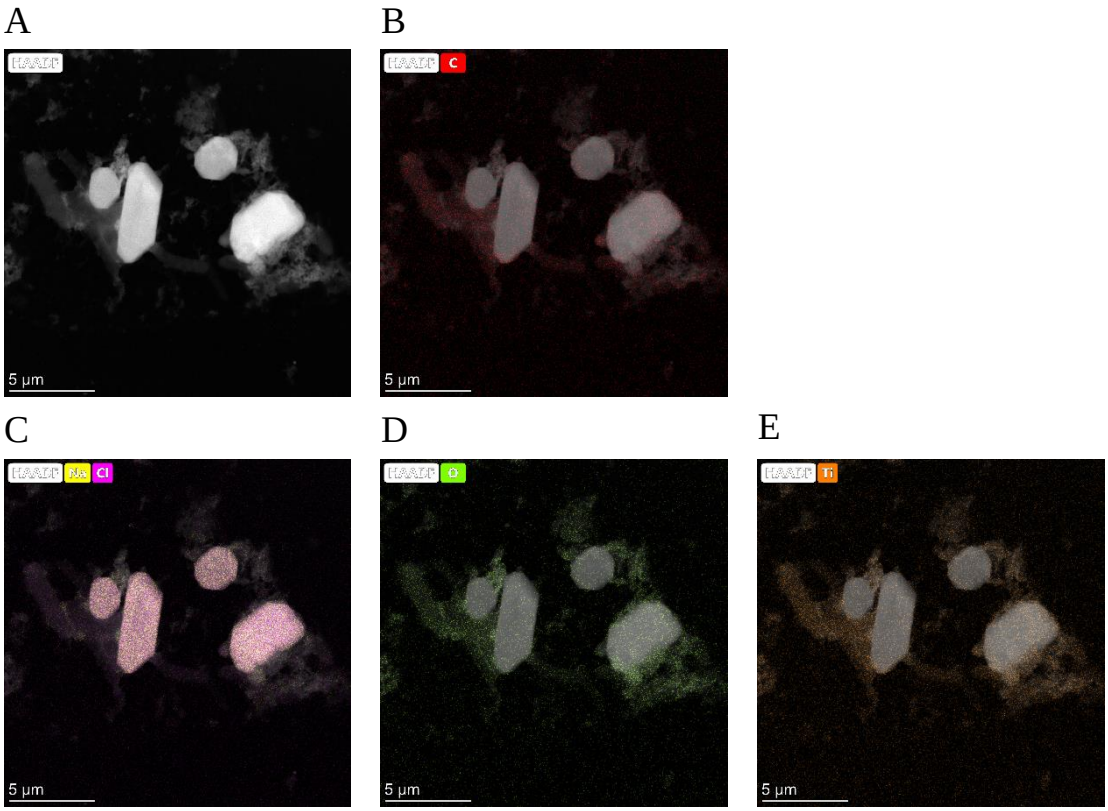

Figure 4.21 - STEM-EDX imagery (A) for White mask following deposition, displaying Carbon (B), Sodium + Chlorine (Chloride) (C), Oxygen (D) and Titanium (E) at x14,000 magnification

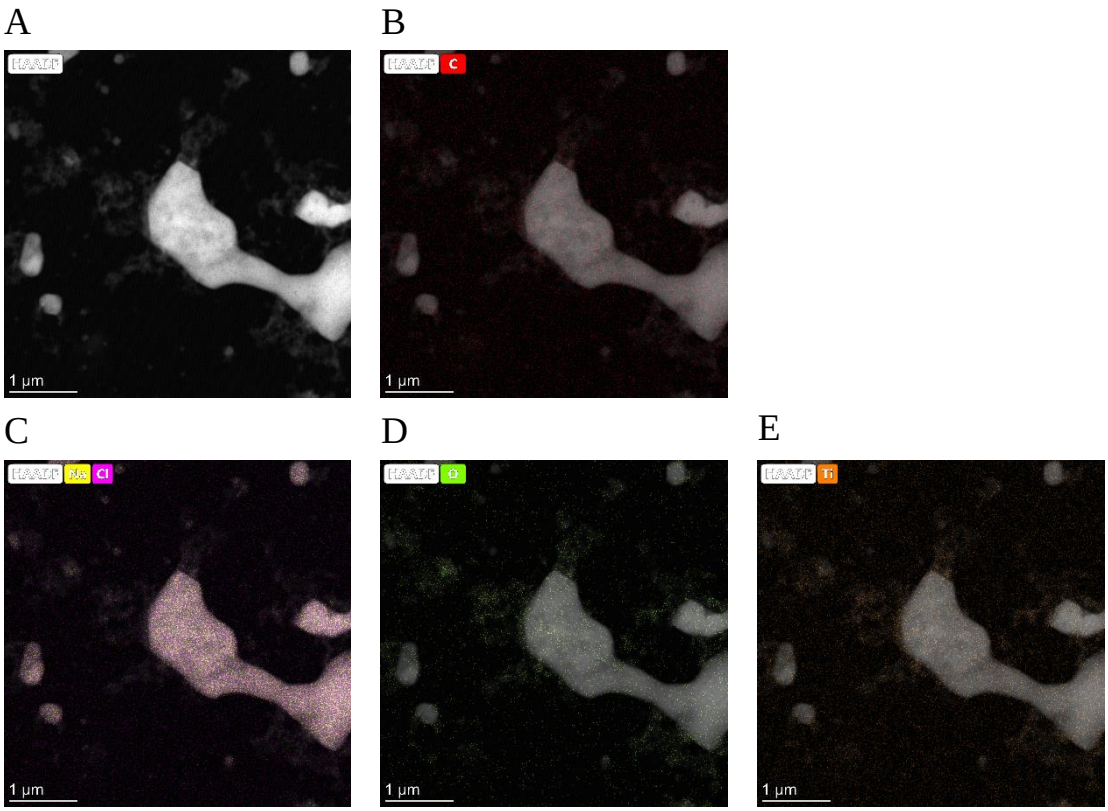

Figure 4.22 - STEM-EDX imagery (A) for Blue mask following deposition, displaying Carbon (B), Sodium + Chlorine (Chloride) (C), Oxygen (D) and Titanium (E) at x14,000 magnification

The main detected elements in white mask STEM-EDX were carbon, sodium, chlorine oxygen and titanium. The most dense and abundant elements detected from the sample was sodium and chlorine, which are concentrated on the shapes of the large artefacts. Carbon, oxygen and titanium are most dense in the hazy regions observed connected to the large artefact (figure 4.13).

The main detected elements in blue mask STEM-EDX were carbon, sodium, chlorine oxygen and titanium. The most abundant elements detected from the sample was sodium and chlorine, which were most densely concentrated in the regions of the large artefacts. Oxygen and titanium are most dense in the hazy regions observed connected to the large artefact (figure 4.14). However, the density of detected carbon, oxygen and titanium is lower than observed in the white mask sample.

4.3.2.4 Confocal LSM Microscopy

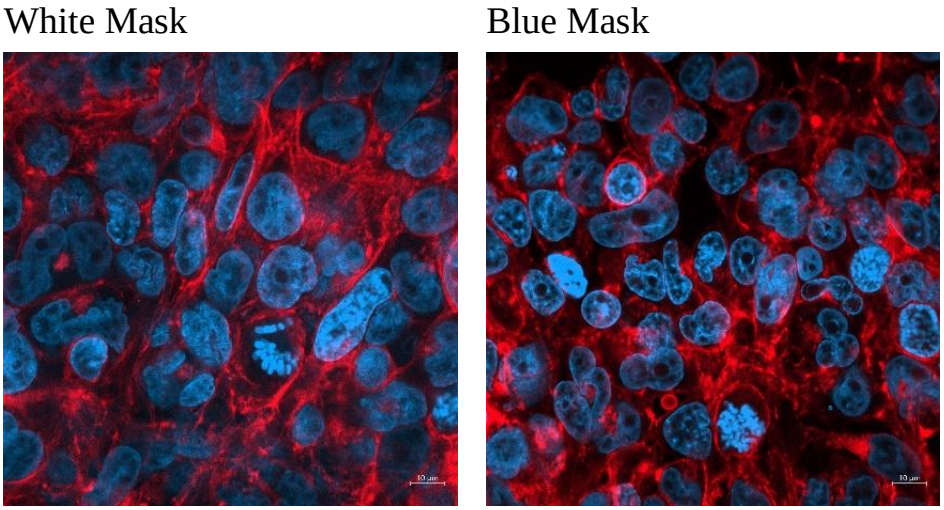

Figure 4.23 - Confocal LSM Microscopy for White Mask and Blue Mask following deposition, displaying a multi-channel image of Alexafluor 633 Phalloidin and DAPI

Cell density is consistent across both mask MNP samples. Cytoskeleton of both samples is visible, but definition is inconsistent throughout. The nuclei are more defined in the blue mask image, however the nuclei present greater proportion of granularity than white mask (figure 4.15).

4.3.3 Cellular Endpoints

4.3.3.1 Cell Death – Trypan Blue Exclusion Assay

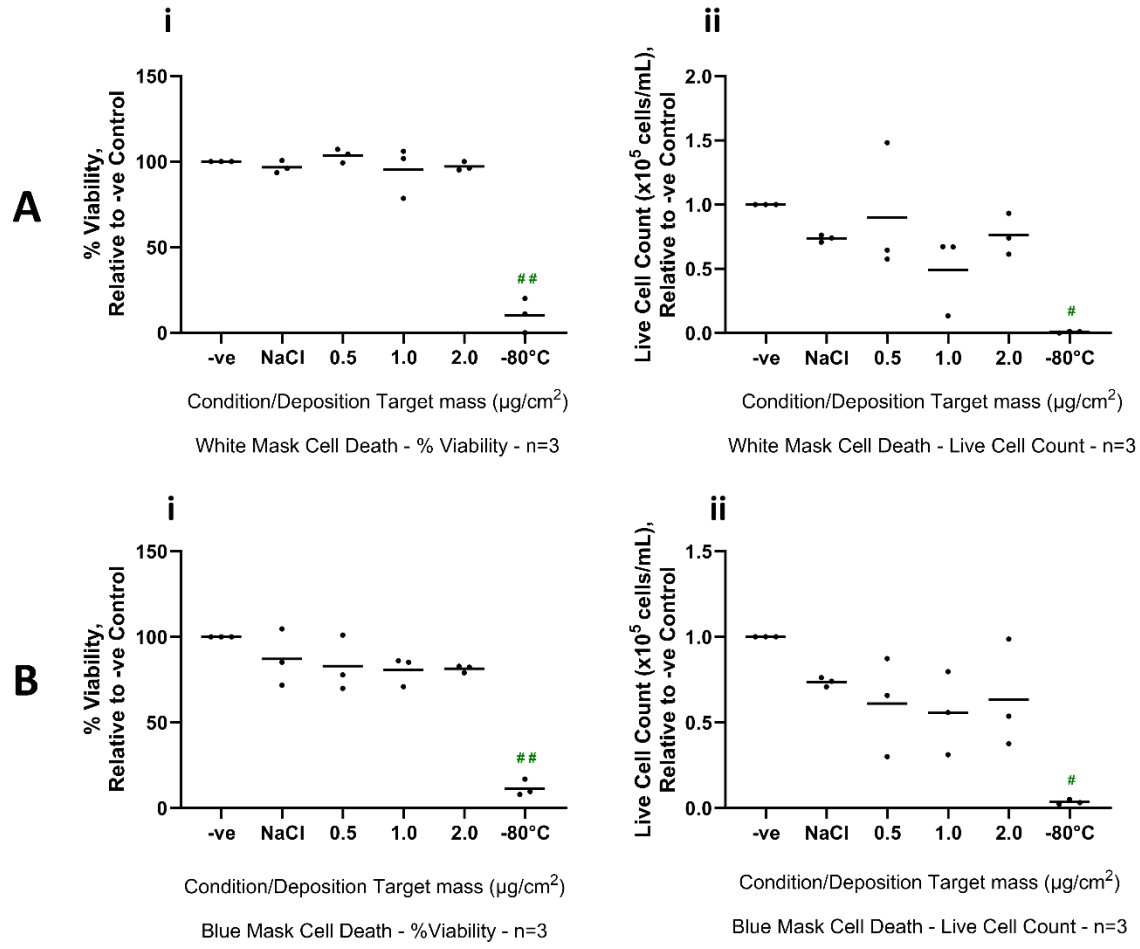

Figure 4.24 - % Viability (i) and live cell count (ii) of NCI-H441 cells following 24-hours exposure to White Mask MNPs (A) and Blue Mask MNPs (B). Data presented as each replicate (points) and mean average between replicates (bar) within each concentration.

- significance to -ve control, * - significance between concentrations.

Number of symbols determines level of significance: 1x symbol = $p \leq 0.05$, 2x symbols = $p \leq 0.001$

Neither % viability or live cell count for white mask indicated any statistically significant changes, except for the +ve controls seen in figure 4.16A(i) and 4.16A(ii).

No statistically significant changes were observed after blue mask exposure either in figure 4.16B(i) and 4.16B(ii) except for the +ve controls, although an average viability decrease of 10.42% was recorded between the -ve control and 2.0 µg/cm^2.

Biologically, there is no significance from these results. White showed no effect at any concentration, and whilst blue did present a viability decrease compared to the negative control, when compared to the NaCl vehicle control, there was no observed effect.

4.3.3.2 Membrane Integrity – Dextran Blue Assay

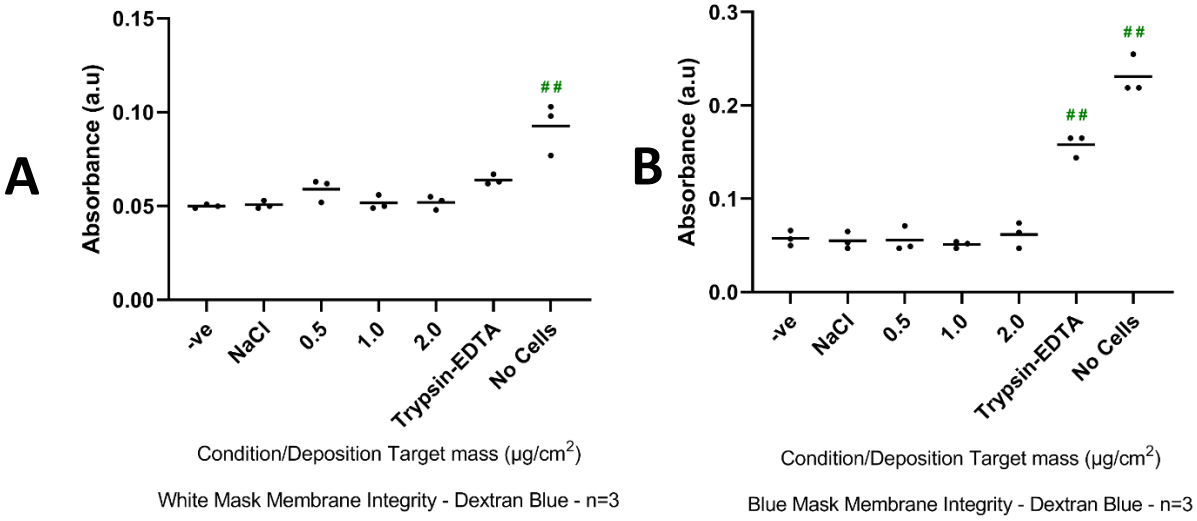

Figure 4.30 - Absorbance of basal well media of NCI-H441 cells following 24-hours exposure to White Mask (Left) and Blue Mask (Right), and two hours of Dextran Blue solution diffusion. Data presented as each replicate (points) and mean average between replicates (bar) within each concentration.

- significance to -ve control, * - significance between concentrations.

Number of symbols determines level of significance: 1x symbol = $p \leq 0.05$, 2x symbols = $p \leq 0.001$

Neither white mask in figure 4.17A, or blue mask in figure 4.17B displayed any effect to monolayer permeability, all tested conditions and concentrations held consistent results within each other and against each other, with absorbance readings rarely straying above 0.05-0.06. Only the +ve controls displayed any changes ($p \leq 0.001$) across both samples, except for Trypsin-EDTA +ve control for white mask. Therefore, both materials were not statistically or biologically significant.

4.3.3.3 Genotoxicity – Mononucleated Micronucleus

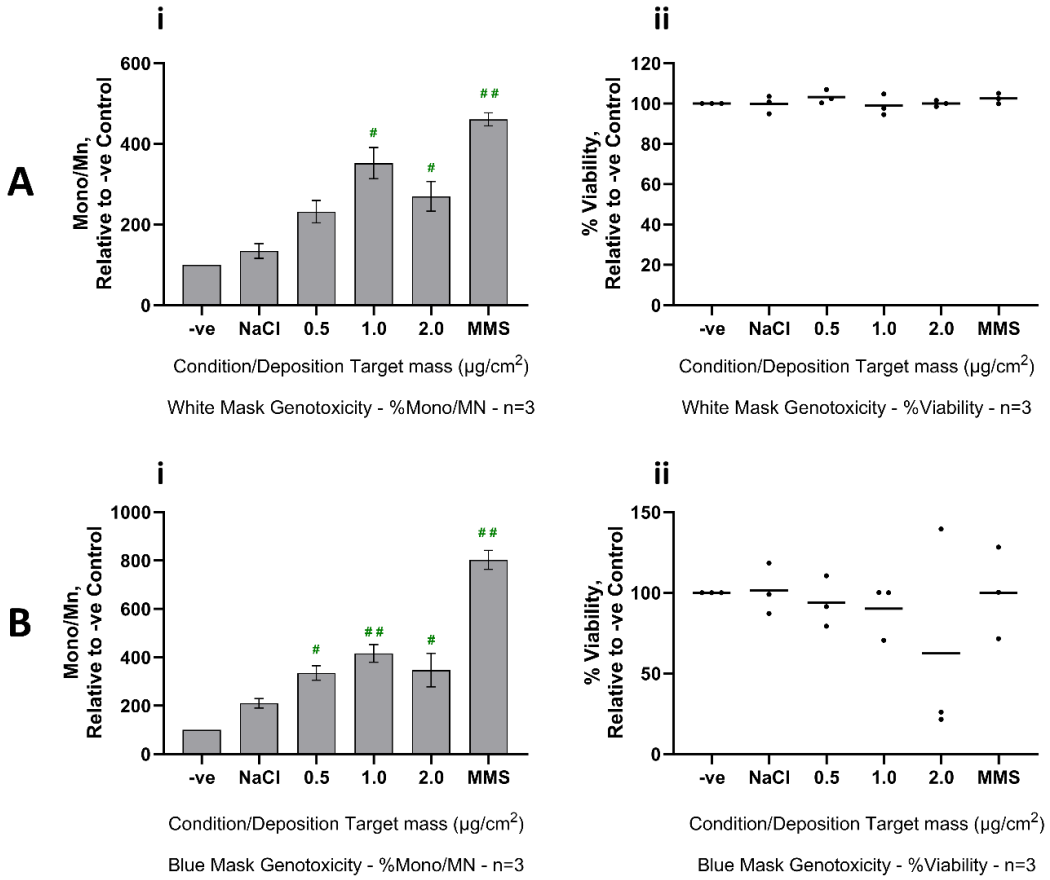

Figure 4.38 - % Mononucleated micronucleus formation (i) and % viability (ii) of NCI-H441 cells following 24-hours exposure to Carbon Black (A), C-PP (B), and R-PP (C). Data presented as mean average MN formation ± standard error of the mean (i), and as each replicate (points) and mean average between replicates (bar) (ii).

- significance to -ve control, * - significance between concentrations.

Number of symbols determines level of significance: 1x symbol = $p \leq 0.05$, 2x symbols = $p \leq 0.001$

The mononucleated-micronucleus (Mono/MN) prevalence trend observed in both mask samples figure 4.18A(i) and 4.18B(i), is similar to that also seen in figure 3.14C(i), following R-PP exposure, increasing in frequency up to 1.0 µg/cm^2 and decreasing at top concentration of 2.0 µg/cm^2. Despite both mask samples following this trend, in figure 4.18B(i) blue mask boasts greater statistical significance, demonstrated at every MNP concentration ($p \leq 0.05$ at 0.5 and 2.0 µg/cm^2, then $p \leq 0.001$ at 1.0 µg/cm^2), compared to white mask in figure 4.18A(i) ($p \leq 0.05$ at 1.0 and 2.0 µg/cm^2) and is not significant at 0.5 µg/cm^2. White mask demonstrates no effect to accompanying viability, maintaining consistent and steady 92.72%±6.33% viability across every data point in figure 4.18A(ii). On the other hand, blue mask accompanying % viability in figure 4.18B(ii), appears to follow a similar trend to R-PP seen in figure 3.14C(ii), having much greater variation than white mask, and a large outlier result at 2.0 µg/cm^2. These data suggest that all concentrations are biologically significant, considering the great difference compared to both the negative control and NaCl control.

4.3.3.4 Pro-inflammatory Response – ELISAs – IL-1β, IL-6, IL-8

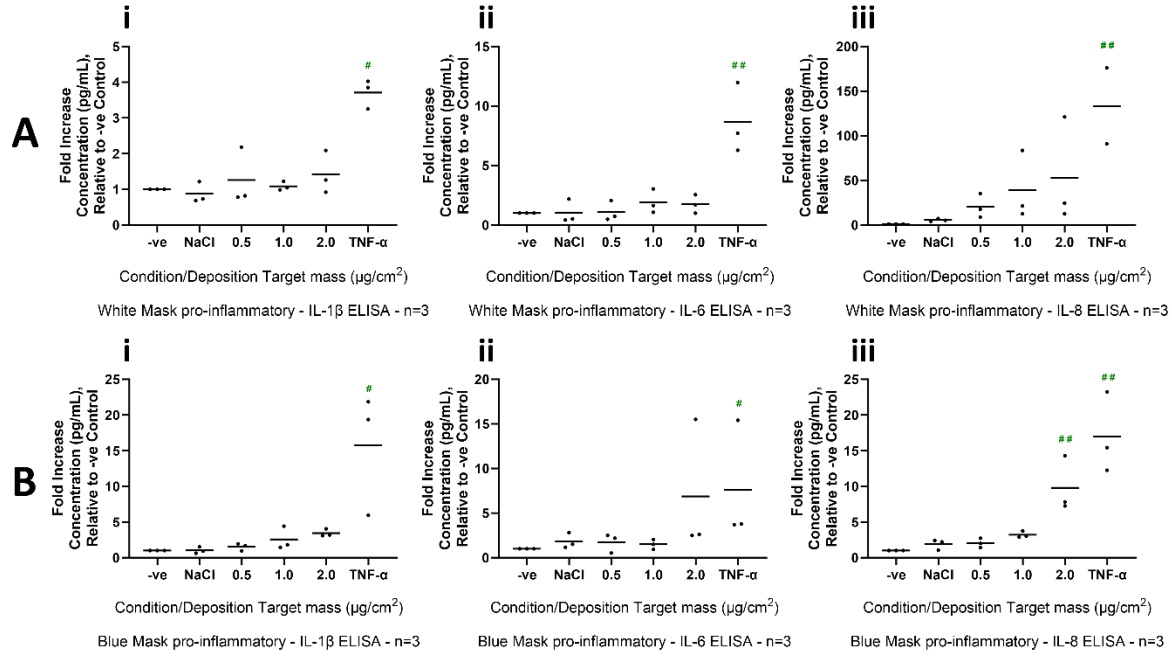

Figure 4.39 - Pro-inflammatory IL-1β (i) and IL-6 (ii) cytokine and IL-8 (iii) chemokine production from NCI-H441 cells, following 24-hours exposure to White Mask MNPs (A) and Blue Mask MNPs (B). Data presented as each replicate (points) and mean average between replicates (bar) within each concentration.

- significance to -ve control, * - significance between concentrations.

Number of symbols determines level of significance: 1x symbol = $p \leq 0.05$, 2x symbols = $p \leq 0.001$

Little-to-no IL-1β or IL-6 production was detected following white mask exposure seen in figures 4.19A(i and ii), with only the +ve controls displaying significance ($p \leq 0.05$ for IL-1β, and $p \leq 0.001$ for IL-6). The IL-8 production in figure 4.19A(iii), however, displays a dose-dependent increase, becoming significant at 2.0 µg/cm^2 ($p \leq 0.05$) and the +ve control ($p \leq 0.001$).

The same trends with both IL-1β and IL-6 production in figures 4.19B(i and ii) were seen in blue mask also, showing little-to-no effect, with only the +ve controls again demonstrating significance (both $p \leq 0.05$). There was also a reading for IL-6 at 2.0 µg/cm^2 which could be deemed anomalous. IL-8 production in figure 4.19C(iii) was the only cytokine to follow a dose-dependent increase and display any significance, starting at 1.0 µg/cm^2 ($p \leq 0.05$ at 1.0 µg/cm^2, then $p \leq 0.001$ at 2.0 µg/cm^2 and +ve control).

Only the top concentration of IL-8 in the blue sample can be deemed biologically significant. Despite the steady dose-dependent increase for blue IL-1β, the increase was not significant, and for the white IL-8 increases, due to two points for both 1.0 and 2.0 µg/cm^2 showing minimal effect.

4.4 Discussion

4.4.1 Introductory

The two batches of MNPs procured for this chapter are both derived from commercially-available Type-IIR face masks, purchased from high-street pharmacist stores. As previously mentioned in the introduction to this chapter, these masks were developed into two batches; White, containing the innermost layer only, to simulate the direct inhalation of shed MNPs, and Blue, the entire mask, to simulate the indirect inhalation as a product of disposal degradation, summarised in figure 4.20 (Han *et al*., 2021. Morgana *et al*., 2021).

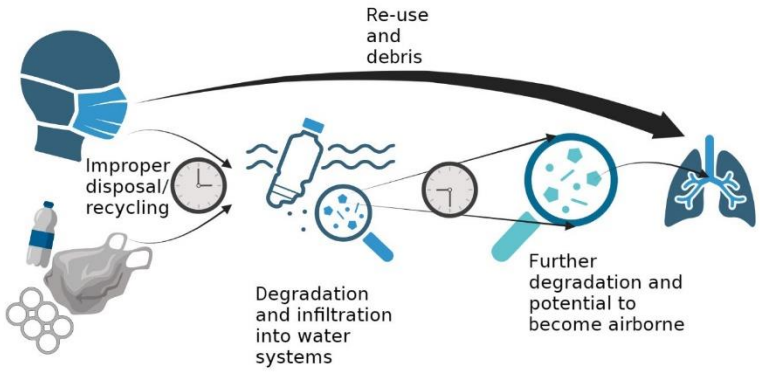

Figure 4.40 - Depiction of the routes of how mask MNPs can potentially be inhaled by humans (created by myself, using Biorender.com)

PP is listed to be the main plastic component of these masks. However, they are known to contain additives for a range of additional properties as discussed previously, such as TiO_2, which may have an effect on the adverse responses. Current research into the mask manufacturing process states that the closest layer to the respiratory system and the outermost blue layer are both made *via* spunbonded PP, which consist of coarser fibres and contribute the rigidity of the entire structure – 20 g/m^2 – in contrast to the central layer which is designed to conduct the most filtration and is synthesized *via* melt-blowing PP – 25 g/m^2 (Henneberry and Rossettie *et al*., 2020).

The cryomilling technique adopted for the commercial PP as discussed in section 3.2.1, was not suitable for the masks, the mass yield was poor, with the cut mask sections being mostly intact by the end of the process, and the extracts were laden with steel fragment contamination from the vials and milling balls. The reasons for the poor degradation could be due to overpacking of the mask, and the limited space of which the milling balls could access. The exact density of the masks is not currently known; however, it is estimated that each layer is 20-25 g/m^2 (Henneberry and Rossettie *et al*., 2020), whilst the density of the C-PP powder is 0.90-0.91 g/cm^3 according to the product datasheet. Therefore, an alternative novel technique was adopted utilising the cryostat, to efficiently maximise the chance of each particle, in at least one orientation, was less than the median mass aerodynamic diameter (MMAD) diameter of the Vitrocell Cloud12 nebuliser head pores.

4.4.2 Characterisation

Increasing the temperature of suspension increased the PDI and both temperatures were within the acceptable limit for particle homogeneity acceptance (ISO 22412:2017, 2017). Also, the negative zeta potential of both mask samples at both temperatures supports the same observed effect of agglomeration and the loss of material when handling, from the contacting with surfaces as previously discussed in section 3.4 leading to inefficient material deposition and input concentrations being practically lower than their theoretical calculations.

STEM-EDX HAADF imagery also suggests that the electric double-layer theory (Nauruzbayeva *et al*., 2020) has taken effect, as discussed in section 3.4. The deposited artefacts should be presenting as mostly carbon but are mostly signalling as sodium and chlorine, which could mislead analysis as a false negative result for the presence of carbon. Additionally, the material present on the white mask images on both SEM and TEM are more angular than blue mask, which appears more rounded and molten in shape. This suggests that the melt-blown central layer has a lower melting point of 121°C to 128.8°C (Kamin *et al*., 2020) than the spunbond external layers. An exact melting point for spunbond PP cannot be found, but literature states values between 139.3°C and 186.2°C (Kamin *et al*., 2020. Yamada *et al*., 2003) for PP fibres. However, exposure to these temperatures is not possible during the cryotome process of milling, so the cause of why the blue mask MNPs appear to be melted could be due to the intensity of electron beams when observed in TEM and SEM, which can reach 150°C at the surface of materials (Science Learning Hub, 2021). Furthermore, based on the pyro-GC-MS results, there is support for the melt-merging of the blue mask, as these MNPs consistently eluted to a lower number of unique compounds than the white mask MNPs across both the thermal desorption and pyrolysis temperatures. This also suggests that there may be additives in the central melt-blown layer and/or the outer blue mask layer, which also form different unique compounds when compared to the innermost layer alone.

4.4.3 Cellular Endpoints

Both of the mask samples were statistically significant at top concentration, and blue mask also at 1.0 μg/cm^2, in the production of IL-8. Production of IL-1β and IL-6 did not present any significant changes. No significant cell viability decreases were observed across either white or blue mask MNPs, although the overall viability was lower from the blue mask exposures. However, cell viability following exposure to the NaCl vehicle control alone was lower for the blue mask set than white mask, so this may suggest the cells cultured for the blue set were more predisposed to adverse effects at the time, despite this difference not being statistically significant.

The mononucleated micronucleus assay presented a similar trend to R-PP, where MN formation peaks at 1.0 μg/cm^2 and then decreases again at 2.0 μg/cm^2 concentration, whilst still retaining statistical significance against the negative control at both. However, the difference is the greater drop in accompanying cell viability at the top concentration in blue mask, which mimics the trend from the R-PP data unlike the white mask, although none of the three MNP exposures presented a statistically significant decrease in viability. This drop of mono/MN

formation at top concentration could be justified by the accompanying decrease in cell viability, however this is not supported from the white mask data, and further genotoxic investigation must ensue. The reason as to why cell viability decreased in both R-PP and blue mask, but not white mask is unknown.

4.4.4 Limitations

The same practical limitations as discussed in section 3.4, also apply here regarding material handling, confocal LSM and mononucleated micronucleus assay.

Any form of the micronucleus assay is not currently optimised for NCI-H441 cells. The use of NCI-H441 cells in the binucleated assay is ineffective, due to their long population doubling time of 58 hours (Meldrum *et al*., 2022), which was demonstrated initially in this project, and the reason of conversion to the mononucleated adaptation. However, the mononucleated adaptation has not been conducted before using NCI-H441 cells, also as previously discussed, and therefore these genotoxicity results are not strong enough on their own to dictate whether mask MNPs do induce deoxyribose nucleic acid (DNA) damage. The negative control results from the white and blue mask exposures were more consistent than those from CB, C-PP and R-PP in section 3, having a range of 0.82% for white, and 0.54% for blue, but this is still not enough to validate the genetic stability of the cell line.

From the use of pyro-GC-MS and STEM-EDX in this project, it is still not possible to determine the full chemical profile of the masks, or all of the materials used in their manufacture. For example, from the STEM-EDX analysis, Titanium and Oxygen was detected in all MNP images, at greatest density in the surrounding hazy areas to the main artefacts, but with sporadic signals detected across the whole image. The use of titanium dioxide (TiO_2) in the manufacture of all of these plastics could be an explanation for this, which is used as a white colourant in applications such as paints, ink, cosmetics, food, as white food colourant E171, and plastics (Haider *et al*., 2019). Its use in masks is noted in patent filings as previously discussed. Two inhalation exposure studies documented that TiO_2 increased both benign and malignant lung cancer prevalence in rats at high doses, but three additional studies on mice and rats opposed this, presenting no increase to prevalence (IARC, 2010), so the consumption of E171 was allowed to continue. In 2017, the European Chemical Agency proposed TiO_2 as a Category 2 carcinogen upon inhalation (CfRAR ECHA, 2017), although many more recent studies disagree on the toxicity of TiO_2 on other organs (Urrutia-Ortega *et al*., 2016. Blevins *et al*., 2019. Brand *et al*., 2020). TiO_2 is not observable from the pyro-GC-MS findings due to the boiling temperature of TiO_2 being unobtainable with the protocol and equipment, requiring nearly 3000°C (OSHA, 2021).

4.4.5 Knowledge Gaps and Future Direction

Time and amount of mask MNPs were limited in this project, and the largest focus was on the *in vitro* toxicity responses, so it was not possible to address every angle of the material analysis, so a separate material sciences study should be conducted on the mask MNPs to fulfil this. Additional methods could also be incorporated in future study, such as Raman spectroscopy,

which is a non-destructive elemental analysis, could be adopted. This approach uses light to determine the chemical composition of the samples (HORIBA Scientific), with the additional benefit of not melting the MNPs unlike pyro-GC-MS and triggering the of the merging layers. This would also be used to assist the other two means of elemental analysis to support or contradict their findings.

To assist the STEM-EDX analysis, additional assessment using dry-powder dropcast MNP samples could be conducted prior to their aerosolisation, which would prevent interference from NaCl, and the double electric-layer from forming, which blocks the elemental signals from the material underneath. Furthermore, the assessment of each mask layer individually could help pinpoint the exacerbation in responses from the blue mask sample in comparison to the white mask exposures, as this would also prevent the melt-merging effect observed in the blue mask MNPs and allow for a more detailed understanding of composition. Future investigation into a more detailed analysis of the chemical composition of the masks and additives will be necessary, as the complete assessment of this was beyond the scope of the project, although developing an insight was necessary.

Determining the oxidative stress responses is also imperative to investigate, to further understand the mechanisms of how the increases to IL-8 and mono/MN productions are triggered. For example, oxidative stress responses are known to instigate both a pro-inflammatory response *via* NF-κB signalling pathways (MacNee, 2001. Hoshino & Mishima, 2008) and oxidative DNA damage (Valko *et al*., 2004) leading to cancers in the respiratory system.

4.4.6 Realism

Fully understanding the constituent materials in the masks will help pave the way to develop solutions for the use of more sustainable, safer alternatives in their manufacture. For example, a suitable biodegradable alternative to PP could be developed based upon materials similar to polylactic acid, which is currently used in food and beverage containment, but also has applications in medicine in tissue engineering, regenerative medicine, and some medical equipment (DeStefano *et al*., 2020). Given further research and understanding, it could be possible to implement biodegradable plastics into the manufacture of more items. Patents grant insight into the potential materials used to construct the masks, but quantifying them requires further research to develop a hazard profile.

From the increasing use of biodegradable plastics, instead of non-biodegradable single-use plastics, the resulting annual wastage of single-use plastics should decrease in theory. Therefore, reducing the rate of which these MNPs are leaching into the environment. Reducing the rate of which MNPs leach into the environment, would allow MNP removal processes to become more effective such as coagulation (Ma *et al*., 2019), membrane bioreactor separation (Poerio *et al*., 2019), and MNP biodegradation (Rai *et al*., 2021), because the replacement rate of MNPs into the environment would decrease. Despite the initial promise that biodegradable plastic-like polymers may possess, they are more limited in functionality, they have even less toxicity understanding than commodity plastics, and at present, the representation of their ability to degrade is misleading. Polylactic Acid for example, is a common 'biodegradable' plastic-like polymer, which is often used as a food packaging. Its ability to degrade is regulated within the European Standard of BS EN 13432:2000 (European Standards, 2007). However, this standard only applies to polylactic acid used in food packaging, and its potential to degrade with the intervention of industrial composting, where conditions are consistently >60°C with continuous airflow and humidity. In the environment, polylactic acid products are estimated to degrade from between 30 years (Narancic et al., 2018. Chamas et al., 2020) to as little as 1% in 100 years (Narancic & O'Connor, 2019), depending on the composition. For masks specifically, an alternative such as polylactic acid may not be suitable for purpose, due to the heat and humidity generated by exhalation, contributing to premature degradation.

4.4.7 Conclusion

Table 4.2 - Summary of white and blue mask MNP endpoint significance. Darker shades of yellow-orange arbitrarily depict greater mean average difference, in comparison to the negative control, following exposure response. Statistical significance depicted by '#'. Absence of '#' depicts no statistical significance. (#) depicts statistical significance for accompanying dataset – [live cell count] in Cell Death, and [% viability] in Mono/MN.

= p<0.05, ## = p<0.001

Material / Assessment	White Mask			Blue Mask		
Mass Target (μg/cm^2)	0.5	1.0	2.0	0.5	1.0	2.0
Cell Death						
Barrier Int.						
Mono/MN		#	#	#	##	#
IL-1β						
IL-6						
IL-8			#		#	##

In conclusion, table 4.2 summarises the significant effects induced as a result of the simulated inhalation of mask MNPs on type-II alveolar epithelial cells cultured at the ALI. The findings from the inhalation of the blue mask MNPs supports the hypothesis, however based upon the elemental analysis and characterisation data, it is not possible to yet determine exactly why this is. Additives to the construction of masks cannot be elucidated from this data cannot yet be identified due to the merging of the mask layers and the double electric-layer of NaCl following aerosolisation.

Chapter 5 - General Discussion

5.1 Introductory

This project aimed to identify potential toxic adverse effects, if any, to NCI-H441 alveolar type-II epithelial cell-line cells, cultured at the ALI, following a 24-hour exposure to aerosolised PP of respirable and non-respirable diameters, and MNPs derived from level-2 surgical face masks *in vitro*. Very limited research exists into the inhalation of MNPs, and therefore exposure concentrations of PP or mask MNPs were unable to be obtained from current quantification data and therefore preventing conversion into an *in vitro* relative. Preliminary mass depositions were decided based upon *in vitro* conversion masses derived from carbon black exposures from an industrial setting (Søs Poulsen, *et al.*, 2013), although these deposition values were adjusted in this project for two reasons: material yield from milling was limited, especially from the masks; and in practice, the deposition of the MNPs was inefficient and it was unachievable to reach 3.1μg/cm^2 without compromising the cellular models outside of incubation (Meldrum, *et al.*, 2019).

R-PP samples were used as a representative control particle against the mask MNPs. There are no previous studies covering the same endpoints, using the same models, or the same exposure systems for C-PP or R-PP, hence the purpose of their initial assessment against CB as their positive particle control. Against the mask MNPs, R-PP (or pure PP MNPs of similar, relevant size) may be considered a comparative particle, and so any observed differences to adverse effects in the mask MNPs should be due to the additives within the masks. So overall, C-PP and R-PP may act as a representative control particle against the mask MNPs, but the scope of this project was not to establish a suitable PP control particle.

5.2 Milling, Handling and Characterisation

MNPs are difficult to handle due to the electrostatic charge they possess (Shao, *et al.*, 2015), and is supported by the zeta potential findings from this project. They attract to many surfaces, namely plastics or glass, which constitutes most surfaces the MNPs come into contact within laboratory practice. Material adhered to each contacted surface and resulted in a loss every time a transferral occurs.

Both of the novel milling approaches used for MNPs synthesis are not currently standardised, so the ability to compare these MNPs between other studies is difficult to accomplish. However, each approach was successful in forming suitable quantities of R-PP and mask MNPs at respirable diameters (Thakur, *et al.*, 2020), to total masses which could be carried across all exposures. But as the two different approaches were necessary to produce MNPs from the different plastic sources, it is not possible to determine if one is more effective than the other.

SEM and TEM imagery of R-PP and white mask MNPs appeared generally angular, however, blue mask particles appeared melted, with rounded morphology. The reason why the blue mask MNPs appeared this way is not confirmed, but could be due to the lower melting temperature of the melt-blown central layer of the mask; 121°C to 128.8°C (Kamin *et al.*, 2020), compared to the external spunbond layers; 139.3°C to 186.2°C (Kamin *et al.*, 2020. Yamada *et al.*, 2003), melting by the heat generated by the electron beams of the electron microscopes, which are expected to reach around 150°C at the surface of observed materials (Science Learning Hub, 2021). Pyro-GC-MS also suggests the possibility of this occurring, because the blue mask

sample eluted into a lower number of unique compounds than white mask, so an amalgam of the three layers could have formed, and therefore separated into a lower number of compounds.

5.3 Cellular Endpoints

Existing studies do not investigate PP on NCI-H441 cells cultured at the ALI, most studies that investigate toxicity of MNPs use polystyrene particles usually in the with micro-scale on intestinal models (Paul *et al*., 2020). These studies however, suggest pro-inflammatory, ROS production leading to oxidative stress and genotoxicity (González-Acedo *et al*., 2021).

IL-8 production and micronucleus formation (genotoxicity) presented the greatest significance in this project, which supports general findings from other MNP toxicity studies, which do not investigate inhalation or PP, indicating a pro-inflammatory response and potential to cause genotoxicity. Whereas there were little-to-no response from any other endpoints, as summarised in table 5.1, which suggests further assessment into oxidative stress-induced genotoxicity is necessary. The micronucleus assay is not widely used as a genotoxicity assessment, and its use has not been recorded on NCI-H441 cells prior to this project, except from its notation by Meldrum *et al* (2022), who stated this cell cycle replicates too slowly (58 hours) and is therefore not suitable for use with cytochalasin-b and the cytokinesis-block variation of the assay, so the mononucleate variation was adopted, which does not use cytochalasin-b (OECD, 2023). Additionally due to the limited assessment on this cell line, it is not possible to yet determine whether the cell line is genetically stable enough to be suitable for this assay. In general, blue mask MNPs instigated the most significant results across the MNP toxicity tests, which supports the hypothesis of this project.

Table 5.1 - Summary of endpoint statistical significance. Darker shades of yellow-orange depict greater mean average difference, in comparison to the negative control, following exposure response. Statistical significance depicted by '#'. Absence of '#' depicts no statistical significance. (#) depicts statistical significance for accompanying dataset – [live cell count] in Cell Death, and [% viability] in Mono/MN. Data not applicable for 1.0 and 2.0 µg/cm^2 for C-PP due to methodological limitations.

= $p<0.05$, ## = $p<0.001$

Material / Assessment	CB			C-PP			R-PP			White Mask			Blue Mask		
Mass Target (µg/cm^2)	0.5	1.0	2.0	0.5	1.0	2.0	0.5	1.0	2.0	0.5	1.0	2.0	0.5	1.0	2.0
Cell Death		#	##	#	N/A	N/A									
Barrier Int.		#	#		N/A	N/A									
Mono/MN	#	##	##(#)		N/A	N/A		#	#		#	#	#	##	#
IL-1β					N/A	N/A									
IL-6					N/A	N/A									
IL-8	#	##	##		N/A	N/A						#		#	##

5.4 Realism

The two distinct batches of mask material were representative of the two routes of which mask-derived MNPs could be inhaled. The direct route of inhalation was represented by the white mask sample and consisted of the innermost layer only. The theory behind the white mask MNPs was to replicate those from the improper use of masks, referring to the repeated or excessive long-term use of these masks, despite being single-use only. It has also been theorised by Klimek *et al*. (2020) that the shortage of PPE available during the pandemic caused the outsourcing of non-CE certified equipment with poor safety and manufacturing standards, degrade more easily and could additionally be responsible for the increase of the occupational-worker patients assessed throughout that study.

On the other hand, the blue mask MNP batch, is intended to represent the indirect route of inhalation and the more environmentally-inclined of the two mask MNPs. This material represents the improper disposal and wastage of the masks, their degradation in landfill and bodies of water, and release of MNPs into the atmosphere which are inhaled. Due to the addition of two more layers in comparison to the white mask MNPs, it was expected that blue mask MNPs would instigate a greater toxic response in general, when compared to white mask MNPs (Han *et al*., 2021). However, as the constituents of masks are not fully understood or known, the extent of potential impact could not be predicted based upon toxicity of other known materials.

Product descriptions pass over the constructive material(s) of masks fully, other than being 'mostly polypropylene'. Absence of material and chemical naming could cause issues, but it is not necessary to list on labelling in some cases. The UK Government states that all information does not have to be included on every type of labelling, but if information is included, it cannot be 'misleading' (Gov.UK, 2015). There are only three essential requirements that packaging must adhere to at the very minimum: package volume and weight; packaging must permit the reuse or recovery depending on the specific requirements; and that the use of noxious or hazardous substances should be kept to minimum (Trade, 2015).

TiO_2 particles have been found within face masks (Verleysen *et al*., 2022), which is typically used as a white colourant, even in foods as E171, and was approved by the FDA in 1966, prior to the discovery of potential genotoxicity risks (Blaznik *et al*., 2021). STEM-EDX conducted in this project did detect signals of both titanium and oxygen which could support Verleysen's *et al*., (2022) statement of TiO_2 presence of in masks, however, the pyro-GC-MS findings in this study disputed this theory, as no compounds eluted contained titanium.

5.5 Knowledge Gaps and Future Direction

It is too early to fully determine how these adverse effects could be translated into human lung impact, there is not enough research in this field to investigate every toxicity assessment for type of MNP. MNP material research for efficient toxicity assessment is novel and ongoing, and largely absent with *in vitro* inhalation models, but developing the optimisation and standardisation of processes to produce consistent MNPs will improve their accessibility to conduct research.

Evaluating the production of ROS and the impact of oxidative stress is an imperative next step for the development of this research as it has already been identified from existing MNP and $PM_{2.5}$ toxicity research (Hu & Palić, 2020), and its association with adverse outcome pathways such a s those associated with $PM_{2.5}$ inhalation on secondary cardiotoxicity (Yu et al., 2022). ROS assessment was unfortunately not conducted in this project due to limited sample number due to material quantity, and the resulting mRNA for use in PCR. Furthermore, the timing of when this assessment was to be conducted was late in the timeframe of the project, so it was necessary to prioritise thesis writing. A small number of qRT-PCR plates were run in trial, using the *SOD1* gene of interest, but due to the very limited number of which were run, it was not possible to draw strong statistical conclusions.

Additional future developments, should investigate the physicochemical analysis of MNPs, especially MNPs derived from non-pure sources, which may contain additives, such as the masks used throughout this project. The use of STEM-EDX, pyro-GC-MS, and Raman spectroscopy are methods which should be capable of generating a complete chemical map of assessed materials and the identification of additives.

As MNPs in general are difficult to handle due to their electrostatic attraction to many laboratory surfaces, additional developments should be focussed here to minimise material lost, with the aim to improve the accuracy of input concentration-deposition mass. This is important to improve as this is a key to implementing the translation between *in vivo* and *in vitro* exposure reliably.

5.6 Conclusion

This project was successful in its aim to determine a potential picture of how PP and mask-derived MNPs impact *in vitro* NCI-H441 monocultures. It is too early to determine the exact translation into *in vivo* studies, such as the exposure concentrations, but it is an indicator as to what effects should be expected. There is still much research to be done surrounding MNP inhalation *in vitro*, as there are so many different MNPs which humans are exposed to, but their effective production and implementation to *in vitro* analysis requires development.

References

Ahmed, M. H., Ghatge, M. S., & Safo, M. K. (2020). Hemoglobin: Structure, Function and Allostery. *Sub-cellular biochemistry*, 94, 345–382.

Air Quality Guidelines: Global Update 2005. (2006). WHO Regional Office for Europe.

Alabduladhem, T., & Bordoni, B. (2021). Physiology, Krebs Cycle. Ncbi.nlm.nih.gov. Retrieved 4 December 2021, from https://www.ncbi.nlm.nih.gov/books/NBK556032/.

Amann, A., Zwierzina, M., Gamerith, G., Bitsche, M., Huber, J. M., Vogel, G. F., Blumer, M., Koeck, S., Pechriggl, E. J., Kelm, J. M., Hilbe, W., & Zwierzina, H. (2014). Development of an innovative 3D cell culture system to study tumour - stroma interactions in non-small cell lung cancer cells. *PLoS ONE*. doi: 10.1371/journal.pone.0092511

Amato-Lourenço, L. F., Carvalho-Oliveira, R., Júnior, G., dos Santos Galvão, L., Ando, R., & Mauad, T. (2021). Presence of airborne microplastics in human lung tissue. *Journal Of Hazardous Materials*. doi:10.1016/j.jhazmat.2021.126124

Amato-Lourenço, L. F., de Souza Xavier Costa, N., Dantas, K. C., Dos Santos Galvão, L., Moralles, F. N., Lombardi, S., Júnior, A. M., Lindoso, J., Ando, R. A., Lima, F. G., Carvalho-Oliveira, R., & Mauad, T. (2022). Airborne microplastics and SARS-CoV-2 in total suspended particles in the area surrounding the largest medical centre in Latin America. *Environmental pollution*. doi: 10.1016/j.envpol.2021.118299

An, R., Wang, X., Yang, L., Zhang, J., Wang, N., Xu, F., Hou, Y., Zhang, H., & Zhang, L. (2021). Polystyrene microplastics cause granulosa cells apoptosis and fibrosis in ovary through oxidative stress in rats. *Toxicology*. doi:10.1016/j.tox.2020.152665

Analytik. (2020, May 29). Zeta potential – what is it and how can it be characterised?. Analytik Ltd. https://analytik.co.uk/zeta-potential-what-is-it-and-how-can-it-be-characterised/#:~:text=Zeta%20potential%20is%20the%20charge,stability%20of%20a%20colloidal%20dispersion.

Andersen, A., Wilbroe, P., & Moghimi, S. (2012). Perspectives on carbon nanotube-mediated adverse immune effects. *Advanced Drug Delivery Reviews.*

Arnida, Janat-Amsbury, M., Ray, A., Peterson, C., & Ghandehari, H. (2011). Geometry and surface characteristics of gold nanoparticles influence their biodistribution and uptake by macrophages. *European Journal of Pharmaceuticals and Biopharmaceutics*. doi:10.1016/j.ejpb.2010.11.010

ATCC. American Type Culture Collection. (accessed September 2023). NCI-H441 [H441] - CRM-HTB-174 https://www.atcc.org/products/crm-htb-174

Azizi, P. M., Zyla, R. E., Guan, S., Wang, C., Liu, J., Bolz, S.-S., Heit, B., Klip, A., & Lee, W. L. (2015). Clathrin-dependent entry and vesicle-mediated exocytosis define insulin transcytosis across microvascular endothelial cells. Molecular Biology of the Cell, 26(4), 740–750. https://doi.org/10.1091/mbc.e14-08-1307

Bai, L., Wang, J., Ma, X., & Lu, H. (2018). Are pollution forecasts: an overview. International Journal of *Environmental Research and Public Health*. doi:10.3390/ijerph15040780

Ball, M., Hossain, M., & Padalia, D. (2021). Anatomy, Airway. Ncbi.nlm.nih.gov. Retrieved 2 December 2021, from https://www.ncbi.nlm.nih.gov/books/NBK459258/.

Bannuscher, A., Schmid, O., Drasler, B., Rohrbasser, A., Braakhuis, H. M., Meldrum, K., Zwart, E. P., Gremmer, E. R., Birk, B., Rissel, M., Landsiedel, R., Moschini, E., Evans, S. J., Kumar, P., Orak, S., Doryab, A., Erdem, J. S., Serchi, T., Vandebriel, R. J., … Rothen-Rutishauser, B. (2022). An inter-laboratory effort to harmonize the cell-delivered *in vitro* dose of aerosolized materials. *NanoImpact*. doi:10.1016/j.impact.2022.100439

Barasova, H., & Rothen-Rutihauser, B. (2019, July 26). Guidance Document for ENMs Aerosolization using VITROCELL® Cloud System . Retrieved September 4, 2023,.

Bateman, J., Doak, S. H., & Clift, M. J. (2023). 26 an advanced triple cell co-culture of the alveolar epithelial barrier for inhalation hazard assessment *in vitro*. *Annals of Work Exposures and Health*. doi: 10.1093/annweh/wxac087.191

Batenburg, J. J. & Haagsman, H. P. (1998) The lipids of pulmonary surfactant: dynamics and interactions with proteins. *Prog Lipid Res*, 37, 235– 76.

Betts, G. J., Young, K. A., Wise, J. A., Johnson, E., Poe, B., Kruse, D. G., Korol, O., Johnson, J. E., Womble, M., & DeSaix, P. (2022). The Lungs. *In Anatomy and Physiology 2e (2nd ed.). essay, OpenStax*.

Blaznik, U., Krušič, S., Hribar, M., Kušar, A., Žmitek, K., & Pravst, I. (2021). Use of food additive titanium dioxide (E171) before the introduction of regulatory restrictions due to concern for genotoxicity. *Foods*. doi:10.3390/foods10081910

Blevins, L. K., Crawford, R. B., Bach, A., Rizzo, M. D., Zhou, J., Henriquez, J. E., Khan, D. M., Sermet, S., Arnold, L. L., Pennington, K. L., Souza, N. P., Cohen, S. M., & Kaminski, N. E. (2019). Evaluation of immunologic and intestinal effects in rats administered an E 171-containing diet, a food grade titanium dioxide (TIO2). *Food and Chemical Toxicology*. doi:10.1016/j.fct.2019.110793

Blic (2005). BLIC Annual Report 2004-2005.

Boggaram, V., Loose, D. S., Gottipati, K. R., Natarajan, K., & Mitchell, C. T. (2016). Gene expression profiling of the effects of organic dust in lung epithelial and thp-1 cells reveals inductive effects on inflammatory and immune response genes. Physiological Genomics, 48(4), 281–289. https://doi.org/10.1152/physiolgenomics.00096.2015

Boholm, M., & Arvidsson, R. (2016). A definition of framework for the terms nanomaterial and nanoparticle. *Nanoethics*. doi:10.1007/s11569-015-0249-7

Bond, T., Doherty, S., Fahey, D., Forster, P., Berntsen, T., & DeAngelo, B. (2013). Bounding the role of black carbon in the climate system: a scientific assessment. Journal of Geophysical Research: Atmospheres. doi:10.1002/jgrd.50171

Bourouiba, L., Dehandschoewercker, E., & Bush, J. W. M. (2014). Violent expiratory events: on coughing and sneezing. Cambridge: *Cambridge University Press*. doi: 10.1017/jfm.2014.88

Brand, W., Peters, R. J., Braakhuis, H. M., Maślankiewicz, L., & Oomen, A. G. (2020). Possible effects of titanium dioxide particles on human liver, intestinal tissue, spleen and kidney after oral exposure. *Nanotoxicology*. doi:10.1080/17435390.2020.1778809

Brody, J. S. & Williams, M. C. (1992) Pulmonary alveolar epithelial cell differentiation. *Annu Rev Physiol*, 54, 351– 71.

Brown, D. M., Wilson, M. R., MacNee, W., Stone, V., & Donaldson, K. (2001). Size-dependent proinflammatory effects of ultrafine polystyrene particles: A role for surface area and oxidative stress in the enhanced activity of ultrafines. Toxicology and Applied Pharmacology, 175(3), 191–199. https://doi.org/10.1006/taap.2001.9240

Bustamante-Marin, X. M., & Ostrowski, L. E. (2016). Cilia and mucociliary clearance. *Cold Spring Harbor Perspectives in Biology*. doi:10.1101/cshperspect.a028241

Bustamante-Marin, X. M., & Ostrowski, L. E. (2016). Cilia and mucociliary clearance. *Cold Spring Harbor Perspectives in Biology*. doi:10.1101/cshperspect.a028241

Carslaw, K., Boucher, O., Spracklen, D., Mann, G., Rae, J., Woodward, S., & Kulumala, M. (2010). a review of natural aerosol interactions and feedbacks within the earth system. *Atmospheric Chemistry and Physics*. doi:10.5194/acp-10-1701-2010

Castranova, V., Rabovsky, J., Tucker, J. H., & Miles, P. R. (1988). The alveolar type II epithelial cell: A multifunctional pneumocyte. *Toxicology and Applied Pharmacology*. doi: 10.1016/0041-008x(88)90051-8

CfRAR, E. C. H. A. (2017). Opinion proposing harmonised classification and labelling at EU level of Titanium dioxide. EC Number: 236-675-5 CAS Number: 13463-67-7 CLH-O-0000001412-86-163/F.

Chamas, A., Moon, H., Zheng, J., Qiu, Y., Tabassum, T., Jang, J. H., Abu-Omar, M., Scott, S. L., & Suh, S. (2020). Degradation rates of plastics in the environment. ACS Sustainable Chemistry & Engineering, 8(9), 3494–3511. https://doi.org/10.1021/acssuschemeng.9b06635

Chander, A., Reicherter, J. & Fisher, A. B. (1987) Degradation of dipalmitoyl phosphatidylcholine by isolated rat granular pneumocytes and reutilization for surfactant synthesis. *J Clin Invest*, 79, 1133– 8.

Chaudhry, R., & Bordoni, B. (2021). Anatomy, Thorax, Lungs. Ncbi.nlm.nih.gov. Retrieved 2 December 2021, from https://www.ncbi.nlm.nih.gov/books/NBK470197/.

Cheng, W., Zhang, W., Xia, X., Zhang, J., Wang, M., Li, Y., Li, X., Zheng, Y., Liu, J., Zhang, R., & Tang, J. (2023). The domino effect in inhaled carbon black nanoparticles triggers blood brain barrier disruption via altering circulatory inflammation. Nano Today, 48, 101721. https://doi.org/10.1016/j.nantod.2022.101721

Connolly, E., Fuller, G., Baker, T., & Willis, P. (2013). Update on inplementation of the Daily Air Quality Index. Department for Environment, Food and Rural Affairs. Retrieved from https://uk-air.defra.gov.uk/assets/documents/reports/cat14/1304251155_Update_on_Implementation_of_the_DAQI_April_2013_Final.pdf.

Costa, A., de Souza Carvalho-Wodarz, C., Seabra, V., Sarmento, B., & Lehr, C.-M. (2019). Triple co-culture of human alveolar epithelium, endothelium and macrophages for studying the interaction of nanocarriers with the air-blood barrier. *Acta Biomaterialia*. doi: 10.1016/j.actbio.2019.04.037

Danto, S. I., Zabski, S. M. & Crandall, E. D. (1992) Reactivity of alveolar epithelial cells in primary culture with type I cell monoclonal antibodies. *Am J Respir Cell Mol Biol*, 6, 296– 306.

Debbage, P., & Jaschke, W. (2008). Molecular imaging with nanoparticles: Giant roles for dwarf actors. Histochemistry and Cell Biology, 130(5), 845–875. https://doi.org/10.1007/s00418-008-0511-y

de Boer, A. H., Bridges, P. A., Clark, A. R., Hindle, M., John, W., McCallion, O. N. M., Niven, R. W., Asking, L., Brindley, A., Byron, P. R., Davies, P. J., & Edwards, D. A. (2002, October 23). Characterization of inhalation aerosols: A critical evaluation of cascade impactor analysis and laser diffraction technique. International Journal of Pharmaceutics. https://www.sciencedirect.com/science/article/pii/S0378517302005264?via%3Dihub

DeCarlo, P. F., Slowik, J. G., Worsnop, D. R., Davidovits, P., & Jimenez, J. L. (2004). Particle morphology and density characterization by combined mobility and aerodynamic diameter measurements. part 1: Theory. Aerosol Science and Technology, 38(12), 1185–1205. https://doi.org/10.1080/027868290903907

de Goede, P., Wefers, J., Brombacher, E., Schrauwen, P., & Kalsbeek, A. (2018). Circadian rhythms in mitochondrial respiration. *Journal of Molecular Endocrinology*. doi: 10.1530/jme-17-0196

Demerjian, K. L., & Mohnen, V. A. (2008). Synopsis of the temporal variation of particulate matter composition and size. Journal of the Air & Waste Management Association, 58(2), 216–233. https://doi.org/10.3155/1047-3289.58.2.216

DeStefano, V., Khan, S., & Tabada, A. (2020). Applications of PLA in modern medicine. *Engineered Regeneration*. doi:10.1016/j.engreg.2020.08.002

Di, M., & Wang, J. (2018). Microplastics in surface waters and sediments of the Three Gorges Reservoir, China. *Science of The Total Environment*. doi:10.1016/j.scitotenv.2017.10.150

Diem, K., Fauler, M., Fois, G., Hellmann, A., Winokurow, N., & Schumacher, S. *et al*. (2020). Mechanical stretch activates piezo1 in caveolae of alveolar type I cells to trigger ATP release and paracrine stimulation of surfactant secretion from alveolar type II cells. *The FASEB Journal*. doi: 10.1096/fj.202000613rrr

Ding, Y., Zhang, R., Li, B., Du, Y., Li, J., Tong, X., Wu, Y., Ji, X., & Zhang, Y. (2021). Tissue distribution of polystyrene nanoplastics in mice and their entry, transport, and cytotoxicity to GES-1 cells. *Environmental Pollution*. doi:10.1016/j.envpol.2021.116974

Dobbs, L. G., Williams, M. C. & Gonzalez, R. (1988) Monoclonal antibodies specific to apical surfaces of rat alveolar type I cells bind to surfaces of cultured, but not freshly isolated, type II cells. *Biochim Biophys Acta*, 970, 146– 56.

Dominici, F., Wang, Y., Correia, A. W., Ezzati, M., Pope, C. A., & Dockery, D. W. (2015). Chemical composition of Fine Particulate Matter and Life Expectancy. Epidemiology, 26(4), 556–564. https://doi.org/10.1097/ede.0000000000000297

dos Santos, T., Varela, J., Lynch, I., Salvati, A., & Dawson, K. A. (2011). Effects of transport inhibitors on the cellular uptake of carboxylated polystyrene nanoparticles in different cell lines. *PLoS ONE*. doi:10.1371/journal.pone.0024438

Dugdale, D. (2020). Breathing - Health Video: MedlinePlus Medical Encyclopedia. Medlineplus.gov. Retrieved 4 December 2021, from https://medlineplus.gov/ency/anatomyvideos/000018.htm.

European Chemicals Agnecy. (2019, August 22). ANNEX XV RESTRICTION REPORT PROPOSAL FOR A RESTRICTION. Helsinki.

European Commission. (2022, February 7). Guidance on regulatory requirements for medical face masks - public health. https://health.ec.europa.eu/system/files/2020-06/md_guidance-reg-req-med-face-masks_0.pdf

European Union: Titanium Dioxide banned as a food additive in the EU. USDA Foreign Agricultural Service. (2022, March 3). https://fas.usda.gov/data/european-union-titanium-dioxide-banned-food-additive-eu

Epithelix. (2006). MucilAirTM is an in vitro cell model of the human upper airway epithelium cultured at the air liquid interface. Epithelix. https://www.epithelix.com/products/mucilair

Fadare, O. O., & Okoffo, E. D. (2020). Covid-19 face masks: A potential source of microplastic fibers in the environment. Science of The Total Environment, 737, 140279. doi: 10.1016/j.scitotenv.2020.140279

Fadare, O. O., Wan, B., Guo, L.-H., & Zhao, L. (2020). Microplastics from consumer plastic food containers: Are we consuming it? Chemosphere. doi: 10.1016/j.chemosphere.2020.126787

Favi, P. M., Gao, M., Johana Sepúlveda Arango, L., Ospina, S. P., Morales, M., Pavon, J. J., & Webster, T. J. (2015). Shape and surface effects on the cytotoxicity of nanoparticles: Gold nanospheres versus Gold Nanostars. Journal of Biomedical Materials Research Part A, 103(11), 3449–3462. https://doi.org/10.1002/jbm.a.35491

Fenech, M. (2006). Commentary on the SFTG International Collaborative Study on the in vitro micronucleus test: To cyt-B or not to cyt-B? Mutation Research/Genetic Toxicology and Environmental Mutagenesis, 607(1), 9–12. https://doi.org/10.1016/j.mrgentox.2006.04.009

Fenech, M., Chang, W. P., Kirsch-Volders, M., Holland, N., Bonassi, S., & Zeiger, E. (2003). Humn project: Detailed description of the scoring criteria for the cytokinesis-block micronucleus assay using isolated human lymphocyte cultures. Mutation Research/Genetic Toxicology and Environmental Mutagenesis, 534(1–2), 65–75. https://doi.org/10.1016/s1383-5718(02)00249-8

Ferrario, M. (2021, June 7). The 7 different types of plastic
. Plastics For Change. https://www.plasticsforchange.org/blog/different-types-of-plastic

Firdessa, R., Oelschlaeger, T. A., & Moll, H. (2014). Identification of multiple cellular uptake pathways of polystyrene nanoparticles and factors affecting the uptake: Relevance for Drug Delivery Systems. European Journal of Cell Biology, 93(8–9), 323–337. https://doi.org/10.1016/j.ejcb.2014.08.001

Fournier, S. B., D'Errico, J. N., Adler, D. S., Kollontzi, S., Goedken, M. J., Fabris, L., Yurkow, E. J., & Stapleton, P. A. (2020). NANOPOLYSTYRENE Translocation and Fetal Deposition after Acute Lung Exposure during Late-Stage Pregnancy. doi:10.21203/rs.3.rs-39676/v2

Frost, T. S., Jiang, L., Lynch, R. M., & Zohar, Y. (2019, August 13). Permeability of epithelial/endothelial barriers in Transwells and microfluidic bilayer devices. MDPI. https://www.mdpi.com/2072-666X/10/8/533

Fulcher, M. L., & Randell, S. H. (2012). Human nasal and tracheo-bronchial respiratory epithelial cell culture. Methods in Molecular Biology. doi: 10.1007/978-1-62703-125-7_8

Furlow, P., & Mathisen, D. (2018). Surgical anatomy of the trachea. Annals of Cardiothoracic Surgery. doi: 10.21037/acs.2018.03.01

Fuzzi, S., Baltensperger, U., Carslaw, K., Decesari, S., Denier van der Gon, H., & Faccini, M. (2015). Particulate matter, air quality and climate: lessons learned and future needs. Atmospheric Chemistry and Physics. doi:10.5194/acp-15-8217-2015

Galloway, T., & Lewis, C. (2016). Marine microplastics spell big problems for future generations. Proceedings of the National Academy of Sciences.

Galloway, T., Bergmann, M., Gutow, L., & Klages, M. (2015). Marine Anthropogenic Litter (pp. 343-366). Springer Open.

García, J. E., Rodríguez, F. M., de Cabo, M. R., Salgado, M. J., Losada, J. P., Villarón, L. G., López, A. J., & Arellano, J. L. (1999). Evaluation of inflammatory cytokine secretion by human alveolar macrophages. Mediators of Inflammation, 8(1), 43–51. https://doi.org/10.1080/09629359990711

Geyer, R., Jambeck, J., & Law, K. (2017). Production, use, and fate of all plastics ever made. Science Advances. doi:10.1126/sciadv.1700782

Gomperts, B. N. & Strieter, R. M. (2007) Annu Rev Med, 58, 285– 298.

González-Acedo, A., García-Recio, E., Illescas-Montes, R., Ramos-Torrecillas, J., Melguizo-Rodríguez, L., & Costela-Ruiz, V. J. (2021). Evidence from in vitro and in vivo studies on the potential health repercussions of micro- and nanoplastics. Chemosphere. doi:10.1016/j.chemosphere.2021.130826

Goodman, K. E., Hare, J. T., Khamis, Z. I., Hua, T., & Sang, Q.-X. A. (2021). Exposure of human lung cells to polystyrene microplastics significantly retards cell proliferation and triggers morphological changes. Chemical Research in Toxicology, 34(4), 1069–1081. https://doi.org/10.1021/acs.chemrestox.0c00486

Goonvean Fibres. Polypropylene fibre (2023). https://goonveanfibres.com/products-services/polypropylene/

Gray, C. A., & Muranko, H. (2006). Studies of robustness of industrial aciniform aggregates and agglomerates???Carbon Black and amorphous silicas: A review amplified by New Data. Journal of Occupational and Environmental Medicine, 48(12), 1279–1290. https://doi.org/10.1097/01.jom.0000251477.40643.2a

Greim, H., Do, K., Schins, R., & Borm, P. (2001). Toxicity of fibers and PARTICLES?REPORT of the workshop held in Munich, Germany, 26?27 October 2000. Inhalation Toxicology, 13(9), 737–754. https://doi.org/10.1080/08958370118273

Griffiths, M. J., Bonnet, D. & Janes, S. M. (2005) Stem cells of the alveolar epithelium. Lancet, 366, 249– 60.

Gruber, E. S., Stadlbauer, V., Pichler, V., Resch-Fauster, K., Todorovic, A., Meisel, T. C., Trawoeger, S., Hollóczki, O., Turner, S. D., Wadsak, W., Vethaak, A. D., & Kenner, L. (2022). To waste or not to waste: Questioning potential health risks of micro- and Nanoplastics with a focus on their ingestion and potential carcinogenicity. Exposure and Health. doi: 10.1007/s12403-022-00470-8

Guyenet, P., & Bayliss, D. (2015). Neural Control of Breathing and CO2 Homeostasis. Neuron. doi: 10.1016/j.neuron.2015.08.001

Hagen, H., Boersma, J., & van Koten, G. (2002). Homogeneous vanadium-based catalysts for the Ziegler–natta polymerization of α-olefins. Chem. Soc. Rev., 31(6), 357–364. https://doi.org/10.1039/b205238e

Haider, A. J., Jameel, Z. N., & Al-Hussaini, I. H. M. (2019). Review on: Titanium dioxide applications. Energy Procedia. doi:10.1016/j.egypro.2018.11.159

Hallman, M. & Teramo, K. (1981) Measurement of the lecithin/sphingomyelin ratio and phosphatidylglycerol in aminotic fluid: an accurate method for the assessment of fetal lung maturity. Br J Obstet Gynaecol, 88, 806– 13.

Han, J., & He, S. (2021). Need for assessing the inhalation of micro(nano)plastic debris shed from face masks, respirators, and home-made face coverings during the COVID-19 pandemic. Environmental pollution. doi:10.1016/j.envpol.2020.115728

Hassan, M. S., & Lau, R. W. (2009). Effect of particle shape on dry particle inhalation: Study of flowability, Aerosolization, and deposition properties. AAPS PharmSciTech, 10(4). https://doi.org/10.1208/s12249-009-9313-3

Henneberry, B. (n.d.). How surgical masks are made, tested and used. Tested and Used. https://www.thomasnet.com/articles/other/how-surgical-masks-are-made/#_How_are_Surgical

Hernández-Fernández, J., Puello-Polo, E., & Castro-Suarez, J. R. (2023). Characterization of the morphological and chemical profile of different families of microplastics in samples of Breathable Air. Molecules. doi:10.3390/molecules28031042

Hiemstra, P. S., Grootaers, G., van der Does, A. M., Krul, C. A. M., & Kooter, I. M. (2018). Human Lung epithelial cell cultures for analysis of inhaled toxicants: Lessons learned and Future Directions. Toxicology in vitro. doi: 10.1016/j.tiv.2017.11.005

Hodgetts, L., Meldrum, K., Bateman, J., Auyang, E., Levermore, J., Vogel, U., Doak, S., Wright, S., & Clift, M. (2023). 122 elucidating the impact of inhaled micro-, nanoplastics (MNPs) from surgical face masks in vitro. Annals of Work Exposures and Health. doi:10.1093/annweh/wxac087.162

Hopkins, E., Sanvictores, T., & Sharma, S. (2021). Physiology, Acid Base Balance. Ncbi.nlm.nih.gov. Retrieved 4 December 2021, from https://www.ncbi.nlm.nih.gov/books/NBK507807/.

Hoshino, Y., & Mishima, M. (2008). Redox-based therapeutics for lung diseases. Antioxidants & Redox Signaling. doi:10.1089/ars.2007.1961

Hu, M., & Palić, D. (2020). Micro- and nano-plastics activation of oxidative and inflammatory adverse outcome pathways. Redox Biology, 37, 101620. https://doi.org/10.1016/j.redox.2020.101620

Hui Li, A. S., Sathishkumar, P., Selahuddeen, M. L., Asyraf Wan Mahmood, W. M., Zainal Abidin, M. H., Wahab, R. A., Mohamed Huri, M. A., & Abdullah, F. (2022). Adverse environmental effects of disposable face masks due to the excess usage. Environmental Pollution, 308, 119674. doi: 10.1016/j.envpol.2022.119674

Hwang, J., Choi, D., Han, S., Choi, J., & Hong, J. (2019). An assessment of the toxicity of polypropylene microplastics in human derived cells. Science of The Total Environment. doi:10.1016/j.scitotenv.2019.05.071

International Agency for Research on Cancer. (2010). Titanium Dioxide. In Carbon Black, titanium dioxide, and talc (Vol. 93). essay.

Ivleva, N. P. (2021). Chemical analysis of microplastics and nanoplastics: Challenges, advanced methods, and Perspectives. Chemical Reviews. doi: 10.1021/acs.chemrev.1c00178

Jacobson, M. (2012). Air pollution and global warming. Cambridge University Press.

Ji, Y., Wang, Y., Shen, D., Kang, Q., & Chen, L. (2021). Mucin Corona delays intracellular trafficking and alleviates cytotoxicity of nanoplastic-benzopyrene combined contaminant. Journal of Hazardous Materials. doi:10.1016/j.jhazmat.2020.124306

Jia, R., Han, J., Liu, X., Li, K., Lai, W., Bian, L., Yan, J., & Xi, Z. (2023). Exposure to polypropylene microplastics via oral ingestion induces colonic apoptosis and intestinal barrier damage through oxidative stress and inflammation in mice. Toxics. doi: 10.3390/toxics11020127

Johnston, H., Hutchinson, G., Christensen, F., Peters, S., Hankin, S., Aschberger, K., & Stone, V. (2010). A criticla review of the biological mechanisms underlying the in vivo and in vitro toxicity of carbon nanotubes: the contribution of physico-chemical characteristics. Nanotoxicology. doi:10.3109/17435390903569639

Juelicher, S. (2022, January 18). Health and Food Safety - Goodbye E171: The EU bans titanium dioxide as a food additive. https://ec.europa.eu/newsroom/sante/items/732079/en

Kamin, Z., Abdulrahim, N., Misson, M., Chel Ken, C., Sarbatly, R., Krishnaiah, D., & Bono, A. (2020). Melt blown polypropylene nanofiber template for homogenous pore channels monoliths. IOP Conference Series: Materials Science and Engineering. doi:10.1088/1757-899x/736/5/052006

Kernchen, S., Löder, M., Fischer, F., Fischer, D., Moses, S., & Georgi, C. et al. (2022). Airborne microplastic concentrations and deposition across the Weser River catchment. Science Of The Total Environment. doi: 10.1016/j.scitotenv.2021.151812

Kia'i, N., & Bajaj, T. (2021). Histology, Respiratory Epithelium. Ncbi.nlm.nih.gov. Retrieved 2 December 2021, from https://www.ncbi.nlm.nih.gov/books/NBK541061/.

Kihara, S., Ashenden, A., Kaur, M., Glasson, J., Ghosh, S., van der Heijden, N., Brooks, A. E., Mata, J. P., Holt, S., Domigan, L. J., Köper, I., & McGillivray, D. J. (2021). Cellular interactions with polystyrene nanoplastics—the role of particle size and protein Corona. Biointerphases, 16(4). https://doi.org/10.1116/6.0001124

Kikkawa, Y. & Yoneda, K. (1974) The type II epithelial cell of the lung. I. Method of isolation. Lab Invest, 30, 76– 84.

Kirchsteiger, B., Materić, D., Happenhofer, F., Holzinger, R., & Kasper-Giebl, A. (2023). Fine micro- and nanoplastics particles (PM2.5) in Urban Air and their relation to polycyclic aromatic hydrocarbons. Atmospheric Environment, 301, 119670. https://doi.org/10.1016/j.atmosenv.2023.119670

Kirsch-Volders, M. (2001). Inclusion of micronuclei in non-divided mononuclear lymphocytes and necrosis/apoptosis may provide a more comprehensive cytokinesis block micronucleus assay for biomonitoring purposes. Mutagenesis, 16(1), 51–58. https://doi.org/10.1093/mutage/16.1.51

Klemeš, J.J., Fan, Y.V., Tan, R.R., Jiang, P. (2020). Minimising the present and future plastic waste, energy and environmental footprints related to covid-19. Renewable and Sustainable Energy Reviews, 127, p. 109883. doi:10.1016/j.rser.2020.109883.

Kletting, S. (2017). Co-culture of human alveolar epithelial (haelvi) and macrophage (THP-1) cell lines. ALTEX. doi: 10.14573/altex.1607191

Klimek, L., Huppertz, T., Alali, A., Spielhaupter, M., Hörmann, K., Matthias, C., & Hagermann, J. (2020). A new form of irritant rhinitis to filtering facepiece particle (FFP) masks (FFP2/N95/KN95 respirators) during COVID-19 pandemic. World Allergy Organisation Journal. doi:10.1016/j.waojou.2020.100474

Knudsen, L., & Ochs, M. (2018). The micromechanics of lung alveoli: structure and function of surfactant and tissue components. Histochemistry And Cell Biology. doi: 10.1007/s00418-018-1747-9

Koester, V. (2022). What are face masks made of? ChemViews. doi: 10.1002/chemv.202200005

Kuhn, D. A., Vanhecke, D., Michen, B., Blank, F., Gehr, P., Petri-Fink, A., & Rothen-Rutishauser, B. (2014). Different endocytotic uptake mechanisms for nanoparticles in epithelial cells and macrophages. Beilstein Journal of Nanotechnology. doi:10.3762/bjnano.5.174

Kühn, S., van Oyen, A., Booth, A. M., Meijboom, A., & van Franeker, J. A. (2018). Marine microplastic: Preparation of relevant test materials for laboratory assessment of ecosystem impacts. Chemosphere. doi: 10.1016/j.chemosphere.2018.09.032

Kutz, M., & Grotberg, J. B. (2021). Ventilation. In Biomedical Engineering Fundamentals (3rd ed.). essay, McGraw Hill.

Kwak, J., Kim, H., Lee, J., & Lee, S. (2013). Characterization of non-exhaust coarse and fine particles from on-road driving and laboratory measurements. Science of The Total Environment, 458–460, 273–282. https://doi.org/10.1016/j.scitotenv.2013.04.040

Lawal, O., Knobel, H., Weda, H., Bos, L. D., Nijsen, T. M., Goodacre, R., & Fowler, S. J. (2018). Volatile organic compound signature from co-culture of lung epithelial cell line with pseudomonas aeruginosa. The Analyst. doi: 10.1039/c8an00759d

Lee, J., Ju, J., Kim, B., Pak, P., Choi, E.-K., Lee, H.-S., & Chung, N. (2014). Rod-shaped iron oxide nanoparticles are more toxic than sphere-shaped nanoparticles to murine macrophage cells. Environmental Toxicology and Chemistry. doi:10.1002/etc.2735

Lehmann, A. D., Daum, N., Bur, M., Lehr, C.-M., Gehr, P., & Rothen-Rutishauser, B. M. (2011). An in vitro triple cell co-culture model with primary cells mimicking the human alveolar epithelial barrier. European Journal of Pharmaceutics and Biopharmaceutics. doi: 10.1016/j.ejpb.2010.10.014

Lehner, R., Weder, C., Petri-Fink, A., & Rothen-Rutishauser, B. (2019). Emergence of nanoplastic in the environment and possible impact on human health. Environmental Science & Technology, 53(4), 1748–1765. https://doi.org/10.1021/acs.est.8b05512

Lei, L., Wu, S., Lu, S., Liu, M., Song, Y., Fu, Z., Shi, H., Raley-Susman, K. M., & He, D. (2018). Microplastic particles cause intestinal damage and other adverse effects in zebrafish danio rerio and nematode caenorhabditis elegans. Science of The Total Environment. doi:10.1016/j.scitotenv.2017.11.103

Leslie, H. A., van Velzen, M. J. M., Brandsma, S. H., Vethaak, A. D., Garcia-Vallejo, J. J., & Lamoree, M. H. (2022). Discovery and quantification of plastic particle pollution in human blood. Environment International. doi: 10.1016/j.envint.2022.107199

Li, J., Li, W., Bai, C., & Song, Y. (2017). Particulate matter-induced epigenetic changes and lung cancer. The Clinical Respiratory Journal. doi:10.1111/crj.12389

Li, J., Liu, H., & Paul Chen, J. (2018). Microplastics in freshwater systems: A review on occurrence, environmental effects, and methods for microplastics detection. Water Research. doi:10.1016/j.watres.2017.12.056

Lillehoj, E. R., & Kim, K. C. (2002). Airway mucus: its components and function. Archives of pharmacal research. doi: 10.1007/BF02976990

Liu, S., Geng, G., Xiao, Q., Zheng, Y., Liu, X., Cheng, J., & Zhang, Q. (2022). Tracking daily concentrations of PM2.5 chemical composition in China since 2000. Environmental Science & Technology, 56(22), 16517–16527. https://doi.org/10.1021/acs.est.2c06510

Liu, X., Driskell, R. R. & Engelhardt, J. F. (2006) Stem cells in the lung. Methods Enzymol, 419, 285– 321.

Long, C. M., Nascarella, M. A., & Valberg, P. A. (2013). Carbon Black vs. Black Carbon and other airborne materials containing elemental carbon: Physical and chemical distinctions. Environmental Pollution, 181, 271–286. https://doi.org/10.1016/j.envpol.2013.06.009

Lowry, G. V., Hill, R. J., Harper, S., Rawle, A. F., Hendren, C. O., Klaessig, F., Nobbmann, U., Sayre, P., & Rumble, J. (2016, August 30). Guidance to improve the scientific value of Zeta-potential measurements in nanoehs. Environmental Science: Nano. https://pubs.rsc.org/en/content/articlepdf/2016/en/c6en00136j

Loxham, M., & Nieuwenhuijsen, M. (2019). Health effects of particulate matter air pollution in underground railway systems - a critical review of the evidence. Particle and Fibre Toxicology. doi:10.1186/s12989-019-0296-2

Lundin, C. (2005). Methyl methanesulfonate (MMS) produces heat-labile DNA damage but no detectable in vivo DNA double-strand breaks. Nucleic Acids Research, 33(12), 3799–3811. https://doi.org/10.1093/nar/gki681

Luo, D., Chu, X., Wu, Y., Wang, Z., Liao, Z., Ji, X., Ju, J., Yang, B., Chen, Z., Dahlgren, R., Zhang, M., & Shang, X. (2024). Micro- and nano-plastics in the atmosphere: A review of occurrence, properties and human health risks. Journal of Hazardous Materials, 465, 133412. https://doi.org/10.1016/j.jhazmat.2023.133412

Ma, B., Xue, W., Hu, C., Liu, H., Qu, J., & Li, L. (2019). Characteristics of microplastic removal via coagulation and ultrafiltration during drinking water treatment. Chemical Engineering Journal. doi:10.1016/j.cej.2018.11.155

MacNee, W. (2001). Oxidative stress and lung inflammation in airways disease. European Journal of Pharmacology. doi:10.1016/s0014-2999(01)01320-6

Marshall, E., Cottingham, J., Davies, A., Ward, N., & Mouatt, A. (2023). Emissions of air pollutants in the UK - Summary. Department for Environment, Food and Rural Affaris. Retrieved from https://www.gov.uk/government/statistics/emissions-of-air-pollutants/emissions-of-air-pollutants-in-the-uk-summary.

Mason, R. J., Williams, M. C., Moses, H. L., Mohla, S. & Berberich, M. A. (1997) Stem cells in lung development, disease, and therapy. Am J Respir Cell Mol Biol, 16, 355– 63.

Matthews, S., Mai, L., Jeong, C.-B., Lee, J.-S., Zeng, E. Y., & Xu, E. G. (2021). Key mechanisms of micro- and nanoplastic (MNP) toxicity across taxonomic groups. Comparative Biochemistry and Physiology Part C: Toxicology & Pharmacology. doi:10.1016/j.cbpc.2021.109056

Mbachu, O., Jenkins, G., Pratt, C., & Kaparaju, P. (2020). A new contaminant superhighway? A review of sources, measurement techniques and fate of atmospheric microplastics. Water, air and soil pollution. doi:10.1007/s11270-020-4459-4

McDonough, J. E., Yuan, R., Suzuki, M., Seyednejad, N., Elliott, W. M., Sanchez, P. G., Wright, A. C., Gefter, W. B., Litzky, L., Coxson, H. O., Paré, P. D., Sin, D. D., Pierce, R. A., Woods, J. C., McWilliams, A. M., Mayo, J. R., Lam, S. C., Cooper, J. D., & Hogg, J. C. (2011). Small-airway obstruction and emphysema in chronic obstructive pulmonary disease. New England Journal of Medicine. doi: 10.1056/nejmoa1106955

Meldrum, K., Evans, S. J., Vogel, U., Tran, L., Doak, S. H., & Clift, M. J. (2022). The influence of exposure approaches to in vitro lung epithelial barrier models to assess engineered nanomaterial hazard. Nanotoxicology. doi:10.1080/17435390.2022.2051627

Meldrum, K., Mitchell, S. M., Doak, S. H., & Clift, M. J. D. (2019, July 4). Guidance Document for cell culture of lung epithelial cell-line (NCI-H441) (SOP_PATROLS_NCI-H441). Retrieved September 4, 2023,.

Mieczkowski, B., & Seavey, B. (2021). Anatomy, Head and Neck, Trachea. Retrieved 2 December 2021, from https://www.ncbi.nlm.nih.gov/books/NBK448070/.

Miyamoto, K., Taga, H., Akita, T., & Yamashita, C. (2020). Simple method to measure the aerodynamic size distribution of porous particles generated on lyophilizate for dry powder inhalation. Pharmaceutics, 12(10), 976. https://doi.org/10.3390/pharmaceutics12100976

Moebs, W., Ling, S. J., & Sanny, J. (n.d.). 14.1 fluids, density, and pressure - university physics volume 1. OpenStax. https://openstax.org/books/university-physics-volume-1/pages/14-1-fluids-density-and-pressure

Morgana, Silvia, Casentini, B., & Amalfitano, S. (2021). Uncovering the Release of Micro/Nanoplastics from Disposable Face Masks at Times of Covid-19. doi: 10.26434/chemrxiv.14483517

Mossman, B. T., Borm, P. J., Castranova, V., Costa, D. L., Donaldson, K., & Kleeberger, S. R. (2007). Mechanisms of action of inhaled fibers, particles and nanoparticles in lung and cardiovascular diseases. Particle and Fibre Toxicology, 4(1), 4. https://doi.org/10.1186/1743-8977-4-4

Narancic, T., & O'Connor, K. E. (2019). Plastic waste as a global challenge: Are biodegradable plastics the answer to the plastic waste problem? Microbiology, 165(2), 129–137. https://doi.org/10.1099/mic.0.000749

Narancic, T., Verstichel, S., Reddy Chaganti, S., Morales-Gamez, L., Kenny, S. T., De Wilde, B., Babu Padamati, R., & O'Connor, K. E. (2018). Biodegradable plastic blends create new possibilities for end-of-life management of plastics but they are not a panacea for plastic pollution. Environmental Science & Technology, 52(18), 10441–10452. https://doi.org/10.1021/acs.est.8b02963

Nauruzbayeva, J., Sun, Z., Gallo, A., Ibrahim, M., Santamarina, J. C., & Mishra, H. (2020). Electrification at water–hydrophobe interfaces. Nature Communications. doi:10.1038/s41467-020-19054-8

NHS. (2021, November). COVID-19 waste management standard operating procedure. NHS choices. https://www.england.nhs.uk/coronavirus/documents/covid-19-waste-management-standard-operating-procedure/

Niranjan, R., & Thakur, A. K. (2017). The toxicological mechanisms of environmental soot (black carbon) and carbon black: Focus on oxidative stress and inflammatory pathways. Frontiers in Immunology. doi:10.3389/fimmu.2017.00763

Niwa, Y., Hiura, Y., Sawamura, H., & Iwai, N. (2008). Inhalation exposure to carbon black induces inflammatory response in rats. Circulation Journal, 72(1), 144–149. https://doi.org/10.1253/circj.72.144

Nobbmann, U. (2021, January 8). Polydispersity – what does it mean for DLS and chromatography?. Materials Talks. https://www.materials-talks.com/polydispersity-what-does-it-mean-for-dls-and-chromatography/

Occupational Safety and Health Administration. Titanium dioxide. (2021, January 13). https://www.osha.gov/chemicaldata/246

OECD (2023), Test No. 487: In Vitro Mammalian Cell Micronucleus Test, OECD Guidelines for the Testing of Chemicals, Section 4, OECD Publishing, Paris, https://doi.org/10.1787/9789264264861-en.

Olin, S. S. (2000). The relevance of the rat lung response to particle overload for human risk assessment: A workshop consensus report. Inhalation Toxicology. doi: 10.1080/08958370050029725

Orru, H., Ebi, K., & Forsberg, B. (2017). The interplay of climate change and air pollution on health. Current Environmental Health Reports. doi:10.1007/s40572-017-0168-6

Paine, R., 3rd & Simon, R. H. (1996) Expanding the frontiers of lung biology through the creative use of alveolar epithelial cells in culture. Am J Physiol, 270, L484– 6.

Paine, R., Ben-Ze'ev, A., Farmer, S. R. & Brody, J. S. (1988) The pattern of cytokeratin synthesis is a marker of type 2 cell differentiation in adult and maturing fetal lung alveolar cells. Dev Biol, 129, 505– 15.

Parker, L. A., Höppener, E. M., Amelrooij, E. F., Henke, S., Kooter, I. M., Grigoriadi, K., Nooijens, M. G. A., Brunner, A. M., & Boersma, A. (2023). Protocol for the Production of Micro- and Nanoplastic Test Materials. doi: 10.21203/rs.3.rs-2404784/v1

Paul, M. B., Stock, V., Cara-Carmona, J., Lisicki, E., Shopova, S., Fessard, V., Braeuning, A., Sieg, H., & Böhmert, L. (2020). Micro- and nanoplastics – current state of knowledge with the focus on oral uptake and toxicity. Nanoscale Advances. doi:10.1039/d0na00539h

Pauluhn, J. (2011). Poorly soluble particulates: Searching for a unifying denominator of nanoparticles and fine particles for DNEL estimation. Toxicology. doi: 10.1016/j.tox.2010.10.009

Pease, J. E., & Sabroe, I. (2002). The role of interleukin-8 and its receptors in inflammatory lung disease. American Journal of Respiratory Medicine, 1(1), 19–25. https://doi.org/10.1007/bf03257159

Petersson, J., & Glenny, R. (2014). Gas exchange and ventilation–perfusion relationships in the lung. European Respiratory Journal. doi: 10.1183/09031936.00037014

Pezzulo, A. A., Starner, T. D., Scheetz, T. E., Traver, G. L., Tilley, A. E., Harvey, B.-G., Crystal, R. G., McCray, P. B., & Zabner, J. (2011). The air-liquid interface and use of primary cell cultures are important to recapitulate the transcriptional profile of in vivo airway epithelia. American Journal of Physiology-Lung Cellular and Molecular Physiology. doi: 10.1152/ajplung.00256.2010

PlasticsEurope;. (2019). An analysis of European plastics production, demand and waste data. Plastics - The Facts.

Poerio, T., Piacentini, E., & Mazzei, R. (2019). Membrane processes for microplastic removal. Molecules. doi:10.3390/molecules24224148

Prata, J. (2018). Airborne microplastics: Consequences to human health?. Environmental Pollution. doi: 10.1016/j.envpol.2017.11.043

Prata, J. C., da Costa, J. P., Lopes, I., Duarte, A. C., & Rocha-Santos, T. (2020). Environmental exposure to microplastics: An overview on possible human health effects. Science of The Total Environment. doi: 10.1016/j.scitotenv.2019.134455

Putaud, J.-P., Van Dingenen, R., Alastuey, A., Bauer, H., Birmili, W., Cyrys, J., Flentje, H., Fuzzi, S., Gehrig, R., Hansson, H. C., Harrison, R. M., Herrmann, H., Hitzenberger, R., Hüglin, C., Jones, A. M., Kasper-Giebl, A., Kiss, G., Kousa, A., Kuhlbusch, T. A. J., … Raes, F. (2010). A European aerosol phenomenology – 3: Physical and chemical characteristics of particulate matter from 60 rural, urban, and Kerbside sites across Europe. Atmospheric Environment, 44(10), 1308–1320. https://doi.org/10.1016/j.atmosenv.2009.12.011

Pytlak, A., Szafranek-Nakonieczna, A., Goraj, W., Śnieżyńska, I., Krążała, A., Banach, A., . . . Stępniewska, Z. (2021). A survey of greenhouse gases production in central European lignites. Science of the Total Environment. doi:10.1016/j.scitotenv.2021.149551

Radiom, M., Sarkis, M., Brookes, O., Oikonomou, E., Baeza-Squiban, A., & Berret, J. (2020). Pulmonary surfactant inhibition of nanoparticle uptake by alveolar epithelial cells. Scientific Reports. doi: 10.1038/s41598-020-76332-7

Rai, P., Mehrotra, S., Priya, S., Gnansounou, E., & Sharma, S. K. (2021). Recent advances in the sustainable design and applications of biodegradable polymers. Bioresource Technology. doi:10.1016/j.biortech.2021.124739

Raval, N., Maheshwari, R., Kalyane, D., Youngren-Ortiz, S. R., Chougule, M. B., & Tekade, R. K. (2019). Importance of physicochemical characterization of nanoparticles in pharmaceutical product development. Basic Fundamentals of Drug Delivery, 369–400. https://doi.org/10.1016/b978-0-12-817909-3.00010-8

Ren, H., Birch, N. P., & Suresh, V. (2016). An optimised human cell culture model for alveolar epithelial transport. PLOS ONE. doi: 10.1371/journal.pone.0165225

Reynolds, S. D., Giangreco, A., Hong, K. U., McGrath, K. E., Ortiz, L. A. & Stripp, B. R. (2004) Airway injury in lung disease pathophysiology: selective depletion of airway stem and progenitor cell pools potentiates lung inflammation and alveolar dysfunction. Am J Physiol Lung Cell Mol Physiol, 287, L1256– 65.

Richter, F. (January 12, 2023). Global Mask Sales Surged 30-Fold During the Pandemic [Digital image]. Retrieved July 03, 2023, from https://www.statista.com/chart/29100/global-face-mask-sales/

Rincon, M., & Irvin, C. G. (2012). Role of IL-6 in asthma and other inflammatory pulmonary diseases. International Journal of Biological Sciences, 8(9), 1281–1290. https://doi.org/10.7150/ijbs.4874

Rooney, S. A., Young, S. L. & Mendelson, C. R. (1994) Molecular and cellular processing of lung surfactant. Faseb J, 8, 957– 67.

Ryan, U. S., Ryan, J. W. & Smith, D. S. (1975) Alveolar type II cells: studies on the mode of release of lamellar bodies. Tissue Cell, 7, 587–99.

Salvati, A., Åberg, C., dos Santos, T., Varela, J., Pinto, P., Lynch, I., & Dawson, K. A. (2011). Experimental and theoretical comparison of intracellular import of polymeric nanoparticles and small molecules: Toward models of uptake kinetics. Nanomedicine: Nanotechnology, Biology and Medicine, 7(6), 818–826. https://doi.org/10.1016/j.nano.2011.03.005

Schauer, J. J., Fraser, M. P., Cass, G. R., & Simoneit, B. R. (2002). Source reconciliation of atmospheric gas-phase and particle-phase pollutants during a severe photochemical smog episode. Environmental Science & Technology, 36(17), 3806–3814. https://doi.org/10.1021/es011458j

Schnurr, R. E. J., Alboiu, V., Chaudhary, M., Corbett, R. A., Quanz, M. E., Sankar, K., Srain, H. S., Thavarajah, V., Xanthos, D., & Walker, T. R. (2018). Reducing marine pollution from single-use plastics (SUPS): A Review. Marine Pollution Bulletin. doi: 10.1016/j.marpolbul.2018.10.001

Schymanski, E. (2019). Mapping exercise – plastic additives initiative. ECHA. https://echa.europa.eu/mapping-exercise-plastic-additives-initiative

Science Learning Hub – Pokapū Akoranga Pūtaiao. (2021). Preparing samples for the electron microscope. Retrieved from https://www.sciencelearn.org.nz/resources/500-preparing-samples-for-the-electron-microscope

Service, G. D. (2015, July 9). Product labelling: The law. GOV.UK. https://www.gov.uk/product-labelling-the-law

Shao, X.-R., Wei, X.-Q., Song, X., Hao, L.-Y., Cai, X.-X., Zhang, Z.-R., Peng, Q., & Lin, Y.-F. (2015). Independent effect of polymeric nanoparticle zeta potential/surface charge, on their cytotoxicity and affinity to cells. Cell Proliferation. doi: 10.1111/cpr.12192

Shukla, S., Khan, R., Saxena, A., & Sekar, S. (2022). Microplastics from face masks: A potential hazard post covid-19 pandemic. Chemosphere. doi: 10.1016/j.chemosphere.2022.134805

Sipos, A., Kim, K.-J., Sioutas, C., & Crandall, E. D. (2019). Evidence for nanoparticle-induced lysosomal dysfunction in lung adenocarcinoma (A549) cells. International Journal of Molecular Sciences, 20(21), 5253. https://doi.org/10.3390/ijms20215253

Song, K. A., & Zhu, X. (2020, July 20). Cryopreservation of cells: Dos and don'ts. Corning. https://www.corning.com/worldwide/en/products/life-sciences/resources/stories/at-the-bench/the-dos-and-donts-of-cryopreservation.html#:~:text=For%20instance%2C%20if%20cells%20are,just%20to%20name%20a%20few.

Søs Poulsen, S., Jacobsen, N. R., Labib, S., Wu, D., Husain, M., Williams, A., Bøgelund, J. P., Andersen, O., Købler, C., Mølhave, K., Kyjovska, Z. O., Saber, A. T., Wallin, H., Yauk, C. L., Vogel, U., & Halappanavar, S. (2013). Transcriptomic analysis reveals novel mechanistic insight into murine biological responses to multi-walled carbon nanotubes in lungs and cultured lung epithelial cells. PLoS ONE. doi:10.1371/journal.pone.0080452

Srinivasan, B., Kolli, A. R., Esch, M. B., Abaci, H. E., Shuler, M. L., & Hickman, J. J. (2015, April). Teer measurement techniques for in vitro barrier model systems. Journal of laboratory automation. https://www.ncbi.nlm.nih.gov/pmc/articles/PMC4652793/

Standards, E. (2007, May 31). BS EN 13432:2000 packaging. requirements for packaging recoverable through composting and biodegradation. test scheme and evaluation criteria for the final acceptance of packaging. standard.eu. https://www.en-standard.eu/bs-en-13432-2000-packaging.-requirements-for-packaging-recoverable-through-composting-and-biodegradation.-test-scheme-and-evaluation-criteria-for-the-final-acceptance-of-packaging/

Stapleton, P. A. (2021). Microplastic and nanoplastic transfer, accumulation, and toxicity in humans. Current Opinion in Toxicology. doi:10.1016/j.cotox.2021.10.001

Sullivan, G. L., Delgado-Gallardo, J., Watson, T. M., & Sarp, S. (2021). An investigation into the leaching of micro and nano particles and chemical pollutants from disposable face masks - linked to the COVID-19 pandemic. Water Research. doi: 10.1016/j.watres.2021.117033

Sultana, S., Ali, R., Talegaonkar, S., Ahmad, F. J., Mittal, G., & Bhatnagar, A. (2013). In vivo lung deposition and sub-acute inhalation toxicity studies of nano-sized alendronate sodium as an antidote for inhaled toxic substances in Sprague Dawley rats. Environmental Toxicology and Pharmacology. doi: 10.1016/j.etap.2013.05.016

Sun, M., Ding, R., Ma, Y., Sun, Q., Ren, X., Sun, Z., & Duan, J. (2021). Cardiovascular toxicity assessment of polyethylene nanoplastics on developing zebrafish embryos. Chemosphere. doi:10.1016/j.chemosphere.2021.131124

Tanaka, K., Kuramochi, H., Maeda, K., Takahashi, Y., Osako, M., & Suzuki, G. (2023). Size-controlled preparation of polyethylene nanoplastic particles by nanoprecipitation and insights into the underlying mechanisms. ACS Omega. doi: 10.1021/acsomega.2c08233

Tanaka, K., Takahashi, Y., Kuramochi, H., Osako, M., Tanaka, S., & Suzuki, G. (2021). Preparation of nanoscale particles of five major polymers as potential standards for the study of Nanoplastics. Small. doi: 10.1002/smll.202105781

Tang, P., Chan, H.-K., & Raper, J. A. (2004). Prediction of aerodynamic diameter of particles with rough surfaces. Powder Technology, 147(1–3), 64–78. https://doi.org/10.1016/j.powtec.2004.09.036

Tantra, R. (Ed.). (2016). Nanomaterial characterization : an introduction. John Wiley & Sons.

Taylor, T. (2021). Respiratory System | Interactive Anatomy Guide. Innerbody Research. Retrieved 2 December 2021, from https://www.innerbody.com/anatomy/respiratory.

Thakur, A., Kaundle, B., & Singh, I. (2020). Targeting Chronic Inflammatory Lung Diseases Using Advanced Drug Delivery Systems (pp. 475-491. Chapter 22 - Mucoadhesive drug delivery systems in respiratory diseases). Academic Press.

Thomas, A., Wang, S., Sohrabi, S., Orr, C., He, R., Shi, W., & Liu, Y. (2017, March 3). Characterization of vascular permeability using a biomimetic microfluidic blood vessel model. AIP Publishing. https://pubs.aip.org/aip/bmf/article/11/2/024102/150597

Tidy, D. (2021). The respiratory system | Lung Function and Chest Anatomy. Retrieved 30 November 2021, from https://patient.info/news-and-features/the-respiratory-system

Uhal, B. D. (1997) Cell cycle kinetics in the alveolar epithelium. Am J Physiol, 272, L1031– 45.

UK Government - Department for Environment, Food and Rural Affairs. (2022). Emissions of air pollutants in the UK. Retrieved from https://www.gov.uk/government/statistics/emissions-of-air-pollutants

Urrutia-Ortega, I. M., Garduño-Balderas, L. G., Delgado-Buenrostro, N. L., Freyre-Fonseca, V., Flores-Flores, J. O., González-Robles, A., Pedraza-Chaverri, J., Hernández-Pando, R., Rodríguez-Sosa, M., León-Cabrera, S., Terrazas, L. I., van Loveren, H., & Chirino, Y. I. (2016). Food-grade titanium dioxide exposure exacerbates tumor formation in colitis Associated Cancer Model. Food and Chemical Toxicology. doi:10.1016/j.fct.2016.04.014

U.S. National Library of Medicine. (2005a, February 5). Potassium 3-(phenylsulfonyl)benzenesulfonate. National Center for Biotechnology Information. PubChem Compound Database. https://pubchem.ncbi.nlm.nih.gov/compound/Potassium-3-_phenylsulfonyl_benzenesulfonate

U.S. National Library of Medicine. (2005b, March 27). Bis(2,2,6,6-tetramethyl-4-piperidyl) sebacate. National Center for Biotechnology Information. PubChem Compound Database. https://pubchem.ncbi.nlm.nih.gov/compound/Bis_2_2_6_6-tetramethyl-4-piperidyl_-sebacate

U.S. National Library of Medicine. (2005c, March 27). Pentaerythritol tetrakis(3-(3,5-di-tert-butyl-4-hydroxyphenyl)propionate). National Center for Biotechnology Information. PubChem Compound Database. https://pubchem.ncbi.nlm.nih.gov/compound/Irganox-1010

U.S. National Library of Medicine. (2005d, August 8). 2,4,6-tris(2,4,6-tribromophenoxy)-1,3,5-triazine. National Center for Biotechnology Information. PubChem Compound Database. https://pubchem.ncbi.nlm.nih.gov/compound/91820

U.S. National Library of Medicine. (2015, April 28). 2-[2-methoxy-5-(1,1,3,3-tetramethylbutyl)phenyl]-2h-benzotriazole. National Center for Biotechnology Information. PubChem Compound Database. https://pubchem.ncbi.nlm.nih.gov/compound/91739821

Valko, M., Izakovic, M., Mazur, M., Rhodes, C. J., & Telser, J. (2004). Role of oxygen radicals in DNA damage and cancer incidence. Molecular and Cellular Biochemistry. doi:10.1023/b:mcbi.0000049134.69131.89

Varela, J. A., Bexiga, M. G., Åberg, C., Simpson, J. C., & Dawson, K. A. (2012). Quantifying size-dependent interactions between fluorescently labeled polystyrene nanoparticles and mammalian cells. Journal of Nanobiotechnology, 10(1), 39. https://doi.org/10.1186/1477-3155-10-39

Vasilescu, D., Phillion, A., Kinose, D., Verleden, S., Vanaudenaerde, B., & Verleden, G. et al. (2020). Comprehensive stereological assessment of the human lung using multiresolution computed tomography. Journal Of Applied Physiology. doi: 10.1152/japplphysiol.00803.2019

Veldhuizen, E. J. A., & Haagsman, H. P. (2000). Role of pulmonary surfactant components in Surface Film Formation and dynamics. Biochimica et Biophysica Acta (BBA) - Biomembranes. doi: 10.1016/s0005-2736(00)00256-x

Verleden, S. E., Vasilescu, D. M., Willems, S., Ruttens, D., Vos, R., Vandermeulen, E., Hostens, J., McDonough, J. E., Verbeken, E. K., Verschakelen, J., Van Raemdonck, D. E., Rondelet, B., Knoop, C., Decramer, M., Cooper, J., Hogg, J. C., Verleden, G. M., & Vanaudenaerde, B. M. (2014). The site and nature of airway obstruction after lung transplantation. American Journal of Respiratory and Critical Care Medicine. doi: 10.1164/rccm.201310-1894oc

Verleysen, E., Ledecq, M., Siciliani, L., Cheyns, K., Vleminckx, C., Blaude, M.-N., De Vos, S., Brassinne, F., Van Steen, F., Nkenda, R., Machiels, R., Waegeneers, N., Van Loco, J., & Mast, J. (2022). Titanium dioxide particles frequently present in face masks intended for general use require regulatory control. Scientific Reports. doi:10.1038/s41598-022-06605-w

Verleysen, E., Waegeneers, N., Brassinne, F., De Vos, S., Jimenez, I. O., Mathioudaki, S., & Mast, J. (2020). Physicochemical characterization of the pristine E171 food additive by standardized and validated methods. Nanomaterials, 10(3), 592. https://doi.org/10.3390/nano10030592

Vianello, A., Jensen, R., Liu, L., & Vollertsen, J. (2019). Simulating human exposure to indoor airborne microplastics using a Breathing Thermal Manikin. Scientific Reports. doi: 10.1038/s41598-019-45054-w

Walters, S. (2021). 7 Groundbreaking ancient civilizations that influence us today. Discover. Retrieved from https://www.discovermagazine.com/planet-earth/7-groundbreaking-ancient-civilizations-that-influence-us-today

Wang, L., Li, S., Ahmad, I. M., Zhang, G., Sun, Y., Wang, Y., Sun, C., Jiang, C., Cui, P., & Li, D. (2023). Global face mask pollution: Threats to the environment and wildlife, and potential solutions. Science of The Total Environment, 887, 164055. https://doi.org/10.1016/j.scitotenv.2023.164055

Wang, Y., Hao, W. W., Cheng, K., Zhi, G. R., Yi, P., Fan, J., & Zhang, Y. (2018). Huan jing ke xue= Huanjing kexue, 39(8), 3518–3523. https://doi.org/10.13227/j.hjkx.201801080

Watson, A. Y., & Valberg, P. A. (2001). Carbon Black and soot: Two different substances. AIHAJ - American Industrial Hygiene Association, 62(2), 218–228. https://doi.org/10.1080/15298660108984625

Weiss, D. J., Berberich, M. A., Borok, Z., Gail, D. B., Kolls, J. K., Penland, C. & Prockop, D. J. (2006) Adult stem cells, lung biology, and lung disease. NHLBI/Cystic Fibrosis Foundation Workshop. Proc Am Thorac Soc, 3, 193– 207.

Wen, X., Wang, Y., Gong, J., Liu, J., Tian, N., Wang, Y., Jiang, Z., Qiu, J., & Tang, T. (2012). Thermal and flammability properties of polypropylene/carbon black nanocomposites. Polymer Degradation and Stability, 97(5), 793–801. https://doi.org/10.1016/j.polymdegradstab.2012.01.031

Williams, M. C. (1984) Endocytosis in alveolar type II cells: effect of charge and size of tracers. Proc Natl Acad Sci U S A, 81, 6054– 8.

Withers, C. (2019). HM20/70P Product data sheet. Retrieved from Goonvean Fibres Ltd.

Wlasits, P. J., Konrat, R., & Winkler, P. M. (2023). Heterogeneous nucleation of supersaturated water vapor onto sub-10 NM nanoplastic particles. Environmental Science & Technology. doi:10.1021/acs.est.2c07643

Woo, J.-H., Seo, H. J., Lee, J.-Y., Lee, I., Jeon, K., Kim, B., & Lee, K. (2023). Polypropylene nanoplastic exposure leads to lung inflammation through p38-mediated $NF-$KB pathway due to mitochondrial damage. Particle and Fibre Toxicology. doi:10.1186/s12989-022-00512-8

World Health Organisation. (2021a). Air Pollution. Retrieved from https://www.who.int/health-topics/air-pollution#tab=tab_1

World Health Organisation. (2021b). Particulate matter (PM2.5 and PM10), ozone, nitrogen dioxide, sulfur dioxide and carbon monoxide. Global Air Quality Guidelines. Retrieved from https://www.who.int/publications/i/item/9789240034228

Wright, S., & Kelly, F. (2017). Plastic and human health: a micro issue? Environmental Science and Technology. doi:10.1021/acs.est.7b00423

Xu, D., Ma, Y., Han, X., & Chen, Y. (2021). Systematic toxicity evaluation of polystyrene nanoplastics on mice and molecular mechanism investigation about their internalization into Caco-2 cells. Journal of Hazardous Materials. doi:10.1016/j.jhazmat.2021.126092

Xu, J.-L., Lin, X., Wang, J. J., & Gowen, A. A. (2022). A review of potential human health impacts of micro- and nanoplastics exposure. Science of The Total Environment. doi: 10.1016/j.scitotenv.2022.158111

Xu, M., Halimu, G., Zhang, Q., Song, Y., Fu, X., Li, Y., Li, Y., & Zhang, H. (2019). Internalization and toxicity: A preliminary study of effects of nanoplastic particles on human lung epithelial cell. Science of The Total Environment, 694, 133794. https://doi.org/10.1016/j.scitotenv.2019.133794

Yaghi, A., & Dolovich, M. (2016). Airway Epithelial Cell Cilia and Obstructive Lung Disease. Cells. doi: 10.3390/cells5040040

Yamada, K., Hikosaka, M., Toda, A., Yamazaki, S., & Tagashira, K. (2003). Equilibrium melting temperature of Isotactic polypropylene with high tacticity: 1. determination by differential scanning calorimetry. Macromolecules. doi:10.1021/ma021206i

Yu, Y., Sun, Q., Li, T., Ren, X., Lin, L., Sun, M., Duan, J., & Sun, Z. (2022). Adverse outcome pathway of fine particulate matter leading to increased cardiovascular morbidity and mortality: An integrated perspective from Toxicology and Epidemiology. Journal of Hazardous Materials, 430, 128368. https://doi.org/10.1016/j.jhazmat.2022.128368

Yuan, R., Nagao, T., Paré, P., Hogg, J., Sin, D., & Elliott, M. et al. (2010). Quantification of lung surface area using computed tomography. Respiratory Research. doi: 10.1186/1465-9921-11-153

Yuan, X., Zhang, X., Sun, L., Wei, Y., & Wei, X. (2019). Cellular toxicity and immunological effects of carbon-based nanomaterials. Particle and Fibre Toxicology, 16(1). https://doi.org/10.1186/s12989-019-0299-z

Zauner, W., Farrow, N. A., & Haines, A. M. R. (2001). In vitro uptake of polystyrene microspheres: Effect of particle size, cell line and cell density. Journal of Controlled Release, 71(1), 39–51. https://doi.org/10.1016/s0168-3659(00)00358-8

Zhai, X., Zheng, H., Xu, Y., Zhao, R., Wang, W., & Guo, H. (2023). Characterization and quantification of microplastics in indoor environments. Heliyon. doi:10.1016/j.heliyon.2023.e15901

Zhang, Q., Xu, E. G., Li, J., Chen, Q., Ma, L., Zeng, E. Y., & Shi, H. (2020). A review of microplastics in table salt, drinking water, and air: Direct human exposure. Environmental Science and Technology. doi: 10.1021/acs.est.9b04535

Zhang, R., Dai, Y., Zhang, X., Niu, Y., Meng, T., Li, Y., Duan, H., Bin, P., Ye, M., Jia, X., Shen, M., Yu, S., Yang, X., Gao, W., & Zheng, Y. (2014). Reduced pulmonary function and increased pro-inflammatory cytokines in nanoscale carbon black-exposed workers. Particle and Fibre Toxicology, 11(1). https://doi.org/10.1186/s12989-014-0073-1

Zhu, C., Maharajan, K., Liu, K., & Zhang, Y. (2021). Role of atmospheric particulate matter exposure in COVID-19 and other health risks in humans: a review. Environmental research. doi:10.1016/j.envres.2021.111281

Ziajahromi, S., Kumar, A., Neale, P.A., Leusch, F.D.L. (2017). Impact of microplastic beads and fibers on waterflea (ceriodaphnia dubia) survival, growth, and reproduction: Implications of single and mixture exposures. Environmental Science & Technology, 51(22), pp. 13397–13406. doi:10.1021/acs.est.7b03574.